Appendix B

Report - Application of UAM-V for the Houston/Galveston and Beaumont/Port Arthur Nonattainment Areas for Two Multiday Ozone Episodes

BEAUMONT/PORT ARTHUR ATTAINMENT DEMONSTRATION

October 1999 Revision

SYSAPP-95/054

Technical Report

APPLICATION OF UAM-V FOR THE HOUSTON/GALVESTON AND BEAUMONT/ PORT ARTHUR NONATTAINMENT AREAS FOR TWO MULTIDAY OZONE EPISODES

Volume I: UAM-V Input Preparation

ICF KAISER

Systems Applications International

September 1995

Technical Report

APPLICATION OF UAM-V FOR THE HOUSTON/GALVESTON AND BEAUMONT/PORT ARTHUR NONATTAINMENT AREAS FOR TWO MULTIDAY OZONE EPISODES

Volume I: UAM-V Input Preparation

30 September 1995

SYSAPP-95/054

Prepared for

Texas Natural Resource Conservation Commission
12100 Park 35 Circle, Mail Stop 164
Austin, Texas 78753

(TNRCC Contract P.O. 582-5-32107)

Prepared by

Nina K. Lolk
Zitian Guo
Hans P. Deuel
Jay L. Haney
Sharon G. Douglas

Systems Applications International
101 Lucas Valley Road
San Rafael, California 94903

Contents

List of Figures iv
List of Tables vii

1 INTRODUCTION 1-1
Background 1-1
Overview of the Study 1-1
Modeling Grid Specification 1-2
Simulation Periods 1-4

2 CHARACTERIZATION OF METEOROLOGY AND AIR QUALITY FOR THE MODELING EPISODES 2-1
Meteorological Conditions 2-1
Air Quality 2-16

3 APPLICATION OF THE SAIMM 3-1
Overview of the SAIMM 3-1
Application of the SAIMM to Southeast Texas 3-2
Simulation Results for 23–25 October 1992 3-5
Simulation Result for 31 August–2 September 1993 3-11

4 INPUT PREPARATION 4-1
Meteorological Inputs 4-1
Air Quality Inputs 4-2
Other Inputs 4-5

5 TRACER SIMULATIONS 5-1
23–25 October 1992 5-1
31 August - 2 September 1993 5-2

6 SUMMARY 6-1

References R-1

Figures

1-1 Southeast Texas UAM-V modeling domain 1-2

1-2 Locations of ozone nonattainment areas in the inner nested grids 1-3

2-1 Locations of meteorological monitoring sites for the 23–25 October 1992 and 31 August–2 September 1993 episodes 2-18

2-2 Locations of air quality monitoring sites for the 23–25 October 1992 and 31 August–2 September 1993 episodes 2-22

3-1 SAIMM wind fields for the Southeast Texas area for 0400, 1000, 1600, and 2200 CST, 24 October 1992 3-16

3-2 SAIMM wind fields for the Southeast Texas area for 0400, 1000, 1600, and 2200 CST, 25 October 1992 3-32

3-3 SAIMM surface temperature fields for the Southeast Texas area for 0400, 1000, 1600 and 2200 CST, 24 October 1992 3-48

3-4 SAIMM surface temperature fields for the Southeast Texas area for 0400, 1000, 1600 and 2200 CST, 25 October 1992 3-52

3-5 SAIMM surface specific humidity fields for the Southeast Texas area for 0400, 1000, 1600 and 2200 CST, 24 October 1992 3-56

3-6 SAIMM surface specific humidity fields for the Southeast Texas area for 0400, 1000, 1600 and 2200 CST, 25 October 1992 3-60

3-7 Vertical cross section of wind and potential temperature along east-west grid cell number 75 from south-north grid cell 47 to 84 on 24 October 1992 at 0400, 1000, 1600, and 2200 CST 3-64

3-8 Vertical cross section of wind and potential temperature along east-west grid cell number 75 from south-north grid cell 47 to 84 on 25 October 1992 at 0400, 1000, 1600, and 2200 CST 3-68

3-9 Hourly mean unsigned errors for surface wind speed and wind direction for 24 and 25 October 1992 3-72

3-10 SAIMM wind fields for the Southeast Texas area for 0400, 1000, 1600, and 2200 CST on 1 September 1993 3-73

3-11 SAIMM wind fields for the Southeast Texas area for 0400, 1000, 1600, and 2200 CST on 2 September 1993 3-89

3-12 SAIMM surface temperature fields for the Southeast Texas area for 0400, 1000, 1600, and 2200 CST on 1 September 1993 3-105

3-13 SAIMM surface temperature fields for the Southeast Texas area for 0400, 1000, 1600, and 2200 CST on 2 September 1993 3-109

3-14 SAIMM surface specific humidity fields for the Southeast Texas area for 0400, 1000, 1600, and 2200 CST on 1 September 1993 3-113

3-15 SAIMM surface specific humidity fields for the Southeast Texas area for 0400, 1000, 1600, and 2200 CST on 2 September 1993 3-117

3-16 Vertical cross section of wind and potential temperature along east-west grid cell number 75 from south-north grid cell 47 to 84 on 1 September 1993 at 0400, 1000, 1600, and 2200 CST 3-121

3-17 Vertical cross section of wind and potential temperature along east-west grid cell number 75 from south-north grid cell 47 to 84 on 2 September 1993 at 0400, 1000, 1600, and 2200 CST 3-125

3-18 Hourly mean unsigned errors for surface wind speed and wind direction for 1 and 2 September 1993 3-129

4-1 SAIMM-derived vertical exchange coefficients for 1400 CST 24 October 1992 4-7

4-2 SAIMM-derived vertical exchange coefficients for 1400 CST 1 September 1993 4-11

4-3 Marine subdomain used to develop background concentrations for the modeling domain 4-15

4-4 Initial concentrations of ozone and NO_2 for 0000 CST on 23 October 1992 and 31 August 1993 4-16

4-5 Land-use distribution for the outer modeling domain 4-18

5-1 Relative contribution of the initial condition tracer at 1200 CST on 24 October 1992 5-3

5-2 Relative contribution of northern, eastern, southern, and western boundary condition tracers at 1200 CST on 24 October 1992 5-4

5-3 Relative contribution of the initial condition tracer at 1200 CST on 24 October 1992 5-8

5-4 Relative contribution of the northern, eastern, southern, and western boundary condition tracers at 1200 CST on 1 September 1993 5-9

Tables

2-1 Surface and upper-air meteorological monitoring sites for the COAST modeling domain 2-2

2-2 Surface air quality monitoring sites for the COAST modeling domain . 2-5

2-3 Data availability for the COAST modeling domain 2-7

2-4 Daily maximum ozone observations for 23–25 October 1992 2-16

2-5 Five highest ozone observations for each day of the 31 August–1 September 1993 episode 2-17

3-1 Vertical structure of the SAIMM modeling domain for application to the Texas Gulf Coast 3-3

3-2 Input parameters for application of the SAIMM to the Texas Gulf Coast 3-4

3-3 Comparison of mean simulated and observed values for 23–25 October 1992 3-9

3-4 Statistical comparison of simulated and observed values for 23–25 October 1992 3-10

3-5 Comparison of mean simulated and observed values for 31 August–2 September 1993 3-13

3-6 Statistical comparison of simulated and observed values for 31 August–2 September 1993 3-14

4-1 Marine air concentrations of CB-IV species 4-3

4-2 EPA default boundary concentrations of CB-IV species 4-3

4-3 Surface boundary concentrations for the portion of the eastern boundary located over land for the 23–25 October 1992 episode 4-4

4-4 Distribution of land-use categories used in the application of the UAM-V to the southeast Texas area 4-5

1 INTRODUCTION

BACKGROUND

As mandated by the Clean Air Act Amendments of 1990, air quality planning agencies for ozone nonattainment areas designated as serious or above must perform photochemical modeling to evaluate ozone attainment strategies and demonstrate attainment of the National Ambient Air Quality Standard (NAAQS). The Houston/Galveston area is designated "severe-17" with an attainment date of 2007, while the Beaumont/Port Arthur area is a "serious" area with an attainment date of 1999. The Texas Natural Resource Conservation Commission (TNRCC) has recently applied the current regulatory version of the Urban Airshed Model (UAM) to these areas using routinely available air quality and meteorological data for historical episodes. Because of the complex meteorological conditions influencing the production and transport of ozone in these areas, the TNRCC concluded that the current regulatory version of the model, applied using routinely collected data, was inadequate for simulating episodes for ozone planning purposes. Recognizing the need for supplemental air quality, meteorological, and emission inventory data for adequately simulating episodes in these nonattainment areas, the TNRCC sponsored a small supplemental field program in the summer of 1992 and a more comprehensive program during the summer of 1993 known as the Coastal Oxidant Assessment for Southeast Texas (COAST) program.

In addition to the efforts made in collecting supplemental air quality, meteorological, and emission inventory data for photochemical modeling, the TNRCC requested and was granted permission by the EPA to apply the variable-grid version of the UAM, known as UAM-V, for episodes occurring during 1992 and 1993, using supplemental data collected during the field programs, for the purpose of developing the State Implementation Plan (SIP) for ozone. In addition to its variable nested grid feature, the UAM-V directly accepts three dimensional meteorological fields (i.e., winds, temperatures) developed from the application of a data-assimilating prognostic meteorological model; a necessary approach for more accurately simulating the complex three-dimensional structure of the land-gulf breeze circulation patterns affecting ozone production and transport in the area. With assistance from SAI, the TNRCC is applying the UAM-V for two episodes (16–19 August 1993 and 6–11 September 1993); SAI is applying the UAM-V for two additional episodes: 23–25 October 1992 and 31 August - 2 September 1993.

OVERVIEW OF THE STUDY

The primary objective of this study is to provide the TNRCC with base-case modeling inputs for two historical ozone episodes, 23–25 October 1992 and 31 August - 2 September 1993, that can be used for future-year attainment-demonstration modeling. The overall study consists of several tasks: (1) evaluation and quality assurance of aerometric data, (2) development of meteorological and air quality inputs, and (3) application of UAM-V and model performance evaluation.

This document describes the input preparation procedures and resulting UAM-ready meteorological, air quality, and land-use inputs. The remainder of this section describes the modeling domain and simulation periods. Section 2 describes the meteorological conditions and air quality observed during the two modeling episodes. Section 3 summarizes the application of the Systems Applications International Mesoscale Model (SAIMM) and describes the resulting meteorological fields. The procedures for development of air quality and geographical inputs are outlined in Section 4. Modeling emission inventories were developed by the TNRCC; these are described in a separate document. Section 5 describes the results of inert UAM-V tracer simulations for identification of potentially important inflow and outflow modeling domain boundaries. A summary is provided in Section 6.

MODELING GRID SPECIFICATION

The UAM-V modeling domain for the southeast Texas area as illustrated in Figure 1-1 consists of multiple nested grids with varying resolution. The outer (coarse) grid

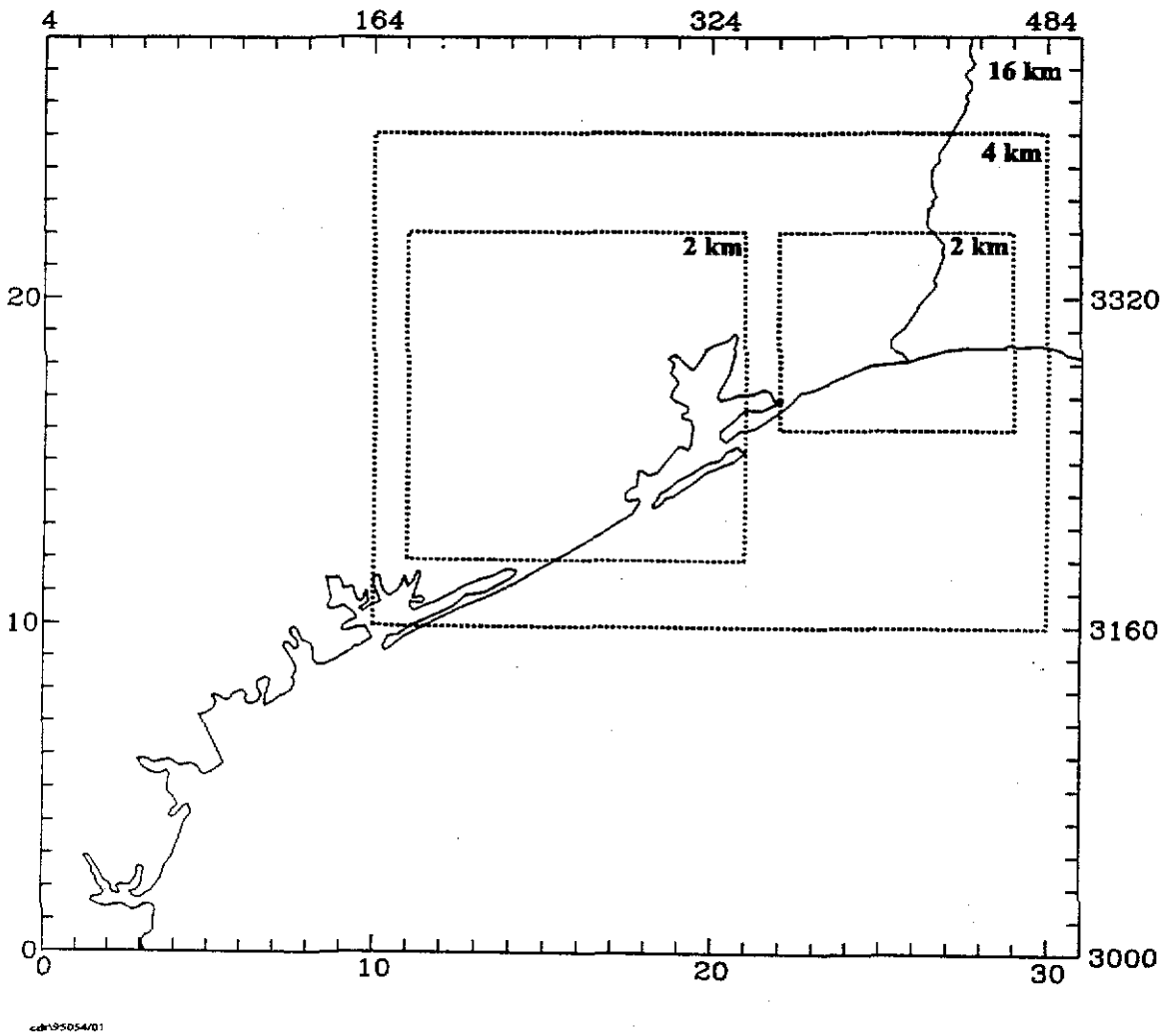

FIGURE 1-1. Southeast Texas UAM-V modeling domain. Inner boxes indicate locations of nested grids.

encompasses the Houston/Galveston and the Beaumont/Port Arthur nonattainment areas as well as the Corpus Christi, Victoria, and Austin urban areas, and a portion of southwestern Louisiana. The origin of the modeling domain is 4 km Easting and 3000 km Northing in Zone 15 Universal Transverse Mercator (UTM) coordinates. The outer grid consists of 31 grid cells in the west-east direction and 28 grid cells in the south-north direction with a horizontal resolution of 16 km. A middle domain, with 4-km resolution, encompassing the nonattainment areas and the area in between, consists of 80 grid cells in the west-east direction and 60 grid cells in the south-north direction. Two inner domains with 2 km horizontal resolution focus on the Houston/Galveston and Beaumont/Port Arthur areas, respectively (Figure 1-2). The first (Houston) consists of 80 grid cells in the west-east direction and 80 grid cells in the north-south direction and the second (Beaumont/Port Arthur) consists of 56 grid cells in the west-east direction and 48 grid cells in the south-north direction. In the vertical, the UAM-V domain comprises eight vertical layers with interfaces at 20, 80, 220, 380, 720, 1380, 2120, and 3030 meters above ground level.

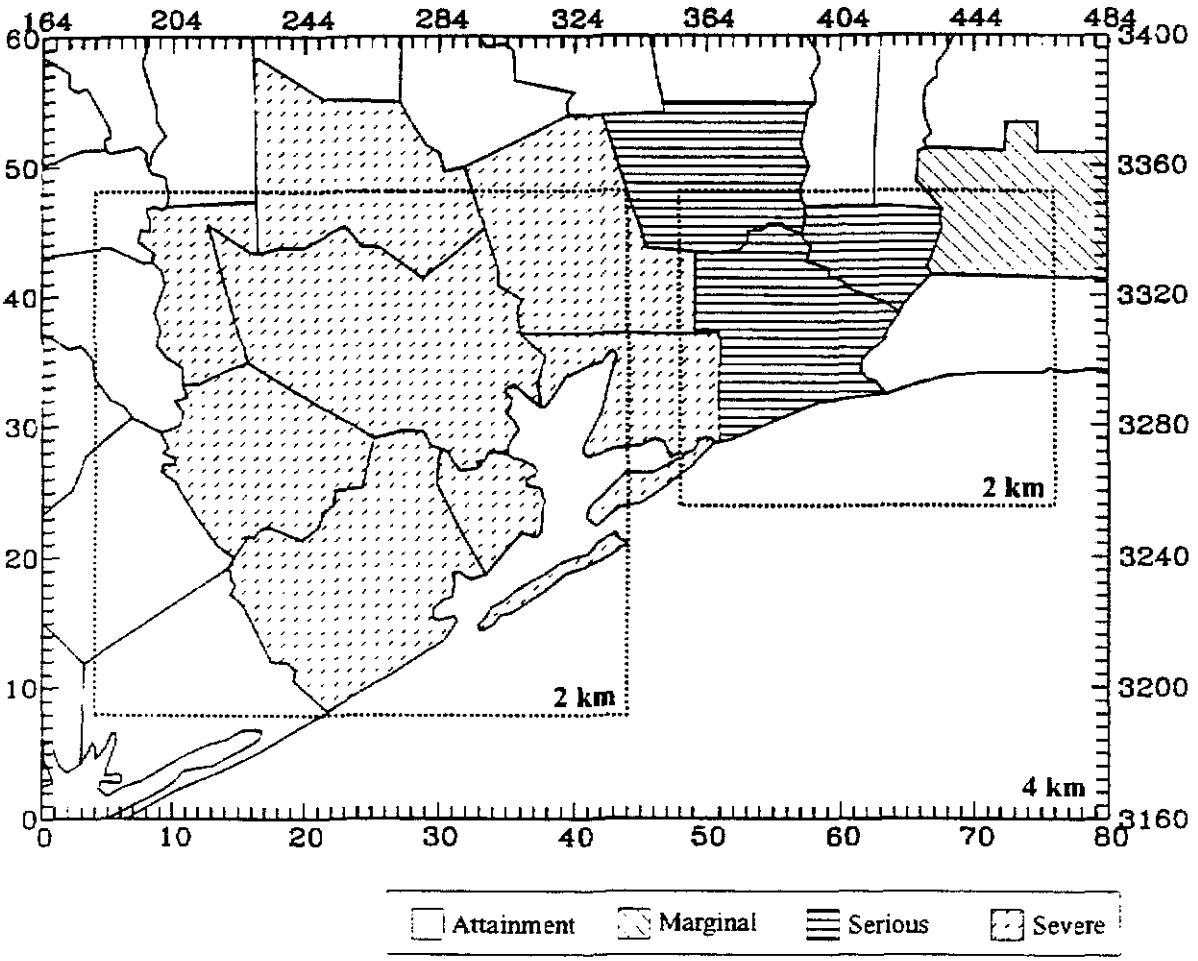

FIGURE 1-2. Locations of ozone nonattainment areas in the inner nested grids.

SIMULATION PERIODS

Two multiday ozone episodes have been selected for this application of UAM-V for the Houston/Galveston and Beaumont/Port Arthur nonattainment areas: 23–25 October 1992 and 31 August – 2 September 1993. In each case, the first day of the simulation period represents a start-up day, used to limit the influence of the initial conditions (which are not well known) on the simulation of the primary episode days. The selection of episodes from 1992 and 1993 was guided by the magnitude and temporal and spatial distribution of observed ozone concentrations as well as the availability of supplemental data.

2 CHARACTERIZATION OF METEOROLOGY AND AIR QUALITY FOR THE MODELING EPISODES

Ozone episodes in southeast Texas generally occur when the region is under the influence of a broad high pressure system and synoptic pressure gradients are weak. These conditions lead to clear skies, suppressed convection, and airflows dominated by land-sea breeze circulations (SAI et al., 1995). The meteorological conditions associated with the two Houston/Galveston and Beaumont/Port Arthur ozone episodes are described in this section. The descriptions are based on the National Meteorological Center (NMC) surface and 500 mb analyses and observed wind and temperature data.

Locations of the available surface and upper-air meteorological monitoring sites are listed in Table 2-1 and plotted in Figure 2-1. Surface air-quality monitoring sites are listed in Table 2-2 and plotted in Figure 2-2. Table 2-3 summarizes the data availability for each episode.

METEOROLOGICAL CONDITIONS

23-25 October 1992

Synoptic Meteorology

The NMC 500 mb analyses for the 23-25 October 1992 episode indicate a flat ridge over the south-central United States. On 23 October, the first day of the simulation period, a high-pressure system was located over the Texas Gulf coast. During the next two days of the episode, this high-pressure system weakened. Winds at 500 mb as measured by the Lake Charles radiosonde were northerly and wind speeds appeared to increase throughout the episode.

The NMC surface analyses for this episode indicate that the southeastern and south-central portions of the United States were influenced by a high-pressure system. For the duration of the episode, surface wind speeds in the Texas/Louisiana Gulf coast region were weak and variable. Maximum temperatures greater than 80°F were recorded; no precipitation was reported in the region.

Airflow Patterns

Surface Winds. During the early morning hours on 23 October, surface winds in the Houston and Beaumont/Port Arthur areas were weak and from the northeast. After 0800 CST, winds veered to the southeast with the onset of the daytime onshore flow. Winds

TABLE 2-1. Surface and upper-air meteorological monitoring sites for the COAST modeling domain. Sites located within 50 km of the modeling domain are included.

Monitoring Site		Site ID	UTM-northing (km)	UTM-easting (km)
GULF OF MEXICO BUOY 19		019N	3087.562	303.147
GULF COAST OIL PLTF		01TN	3112.555	362.508
GULF OF MEXICO BUOY 35		035N	3254.912	354.478
GULF COAST OIL PLTF		5R0N	3121.296	426.404
CAMERON	LA	7R5N	3294.632	471.002
ALICE / INTL AIRPORT	TX	ALIN	3077.653	3.527
AUSTIN/MUELLER MUNICIPAL	TX	AUSN	3359.364	47.729
BAYTOWN C24/HARRIS CO	TX	BAYC	3294.738	304.944
BLOOMINGTON (GLDN CRES 84)	TX	BLOG	3174.26	119.157
BEAUMONT C02/JEFFERSON CO	TX	BMTC	3323.435	396.383
PORT ARTHUR / WSO	TX	BPTN	3315.35	401.904
BROWNSVILLE INTL	TX	BRON	2871.966	55.667
BERGSTROM	TX	BSMN	3352.219	50.326
CLINTON CGC / HARRIS CO	TX	C35C	3291.222	281.628
COLLEGE STATION	TX	CLLN	3388.07	177.109
CLUTE CAMS 11/BRAZORIA CO	TX	CLTA	3211.4	266.419
COCODRIE (MMS)	LA	COCM	3238.156	728.047
CORPUS CHRISTI INTL	TX	CRPN	3079.305	56.331
CROSBY AQ/MET SITE	TX	CRSC	3314.994	299.94
DEER PARK C18/HARRIS CO	TX	DRPA	3284.937	293.783
ELLINGTON AFB	TX	EFDN	3278.096	290.199
GALVESTON AS SITE	TX	GALC	3238.387	319.626
LONGVIEW/GREGG CO.	TX	GGGN	3580.239	344.731
GALLERIA CGC SITE	TX	GLRC	3290.33	261.796
GALVESTON / SCHOLES FIELD	TX	GLSN	3238.802	318.632
ROBERT GRAY AAF	TX	GRKN	3447.219	38.965
GALVESTON RADAR PROFILER	TX	GRPC	3234.086	312.78
HRM SITE 1	TX	H01H	3289.09	281.799
HRM SITE 3	TX	H03H	3294.594	289.086
HRM SITE 4	TX	H04H	3302.197	294.015
HRM SITE 7	TX	H07H	3294.704	304.943
HRM SITE 8	TX	H08H	3281.16	300.939
HRM SITE 10	TX	H10H	3306.737	314.44
HRM SITE 11	TX	H11H	3294.184	315.304
ALDINE C8/HARRIS CO	TX	HALC	3309.92	275.405

Continued

TABLE 2-1. Continued.

Monitoring Site		Site ID	UTM-northing (km)	UTM-easting (km)
HOBBY AIRPORT RPS	TX	HBYC	3281.544	277.593
SITE T-19 CRAWFORD	TX	HCFA	3293.462	271.685
SITE T-18 CROQUET	TX	HCQA	3279.502	260.451
HIGH ISLAND PLTF 199 MMS	LA	HIPM	3223.169	383.672
SITE T-26 LANG	TX	HLAA	3302.937	258.826
FT HOOD AAF/KILLEEN	TX	HLRN	3455.632	50.184
MANCHESTER C22	TX	HMCA	3288.207	279.323
NORTHWEST HARRIS C26	TX	HNWA	3325.942	242.051
EAST C1 / HARRIS CO	TX	HOEA	3295.077	285.264
HOUSTON / (HOBBY AIRPORT)	TX	HOUN	3282.004	278.978
SWISS&MONROE / HARRIS CO	TX	HSMA	3279.202	280.502
TEXAS COMMERCE TOWER	TX	HTCC	3294.387	271.453
SITE S-13 N WAYSIDE	TX	HWAA	3301.736	279.3
HOUSTON/INTERCONTINENTAL	TX	IAHN	3317.228	273.235
JEFFERSON CO ARPRT RPS	TX	JCAC	3314.454	401.742
JEFFERSON CO ARPRT AS SITE	TX	JCSC	3314.454	401.742
KOUNTZE C85/HARDIN CO	TX	KTZA	3361.557	373.554
BRAZORIA CTY AI	TX	LBXN	3229.067	264.635
LAKE CHARLES MUNICIPAL	LA	LCHN	3331.545	479.133
LUFKIN/ANGELINA CO.	TX	LFKN	3456.593	333.327
LOUISIANA STATE UNIV. MMS	LA	LSUM	3359.937	675.156
MET 5, TEXAS CITY	TX	ME5T	3251.193	313.975
MOBILE, TEXAS CITY	TX	MOBT	3252.776	316.836
CORPUS CHRISTI NAAS	TX	NGPN	3069.298	77.397
KINGSVILLE NAS	TX	NQIN	3050.901	23.919
NORTHWEST HOUSTON AS	TX	NWHC	3315.575	254.531
PORT ARTHUR WEST C28	TX	PAWC	3307.27	404.604
POINT COMFORT (GLDN CRES 84)	TX	PCOG	3181.103	152.769
FORT POLK (ARMY)	LA	POEN	3434.959	500
PALACIOS / FAA AIRPORT	TX	PSXN	3180.754	182.493
ROCK PORT	TX	RKPN	3112.834	103.55
RANDOLPH AFB	TX	RNDN	3278.559	-12.315
SABINE PASS USGG(28T)	TX	RPEN	3285.743	408.096
SETRPC SITE 40 - Sabine Pass	TX	S40S	3287.707	413.249
SETRPC SITE 41 - West Orang Co.	TX	S41S	3327.165	425.885
SETRPC SITE 42 - Mauriceville	TX	S42S	3338.872	415.95

Continued

TABLE 2-1. Concluded.

Monitoring Site		Site ID	UTM-northing (km)	UTM-easting (km)
SETRPC SITE 43 - Jeff. Co. Airport	TX	S43S	3312.048	403.101
SAN ANTONIO INTL	TX	SATN	3279.384	-30.117
SEABROOK C20	TX	SBRC	3272.903	304.592
SEA DRIFT (GLDN CRES 82)	TX	SDRG	3148.8	135.292
STEPHENVILLE/CLARK	TX	SEPN	3576.061	11.264
KELLY AFB	TX	SKFN	3263.264	-42.253
SLIDELL	LA	SLID	3361.7	806.6
SABINE PASS AS SITE	TX	SPSC	3285.975	409.443
SMITH POINT AQ/MET SITE	TX	SPTC	3268.283	329.661
SHIP SHOAL PLTF 178A MMS	TX	SSPM	3164.689	675.386
STOWELL (WINNIE) AQ/MET	TX	STWC	3296.476	364.036
SEAWALL, TEXAS CITY	TX	SWLT	3252.776	316.836
CORPUS CHRISTI WEST C4	TX	T04A	3087.985	63.267
CORPUS CHRISTI C21	TX	T21A	3087.102	50.986
TEXAS CITY / LA MARQUE	TX	TLMC	3253.437	312.342
TEMPLE/MILLER(AWOS)	TX	TPLN	3454.449	78.813
VICTORIA CAMS 87	TX	VCTC	3196.24	109.023
VICTORIA REGIONAL	TX	VCTN	3197.501	117.806
VICTORIA (GLDN CRES 81)	TX	VICG	3185.772	118.907
WEST ORANGE CAMS 9	TX	WORA	3328.379	426.568

in the Lake Charles and Corpus Christi areas remained from the east-northeast for most of the day. Some onshore flow developed in late afternoon along the Louisiana coast. In the evening, surface winds became weak and unorganized throughout the domain.

Weak and variable winds continued over Houston during the early morning hours on 24 October. Northwesterly winds near 3–4 ms^{-1} developed first in the Beaumont/Port Arthur area around 0500 CST and several hours later in the Houston and Corpus Christi areas. The Galveston (GALC) and Clute (CLTA) wind data indicate onset of the gulf breeze along the Texas coast at 1400 CST. The gulf breeze arrived in Baytown and Deer Park around 1500 CST and in Houston around 1700 CST. In the eastern part of the domain, the wind data showed southerly flow beginning around 1600 CST at Sabine Pass and Cameron (along the coast) and at 1700 CST in Beaumont, Port Arthur, and Lake Charles. Daytime wind speeds on this day were generally between 2 and 4 ms^{-1}.

On 25 October, surface winds in the domain were weak and variable through 0700 CST. Along the Texas coast, winds were from the southwest at approximately 5 ms^{-1} for most of the afternoon. Wind data for the Houston area indicate the onset of southeasterly

TABLE 2-2. Surface air quality monitoring sites for the COAST modeling domain.

Monitoring Site		Site ID	UTM-northing (km)	UTM-easting (km)
TEXAS CITY	TX	34ST	3253.944	311.166
BEAUMONT C02/JEFFERSON CO	TX	BMTC	3323.435	396.383
CLINTON CGC / HARRIS CO	TX	C35C	3291.222	281.628
CLUTE CAMS 11/BRAZORIA CO	TX	CLTA	3211.4	266.419
CROSBY AQ/MET SITE	TX	CRSC	3314.994	299.94
DEER PARK C18/HARRIS CO	TX	DRPA	3284.937	293.783
GALVESTON AS SITE	TX	GALC	3238.387	319.626
LONGVIEW/GREGG CO. (CAMS 19)	TX	GGGC	3583.913	338.859
GALLERIA CGC SITE	TX	GLRC	3290.33	261.796
HRM SITE 1	TX	H01H	3289.09	281.799
HRM SITE 3	TX	H03H	3294.594	289.086
HRM SITE 4	TX	H04H	3302.197	294.015
HRM SITE 7	TX	H07H	3294.704	304.943
HRM SITE 8	TX	H08H	3281.16	300.939
HRM SITE 10	TX	H10H	3306.737	314.44
HRM SITE 11	TX	H11H	3294.184	315.304
ALDINE C8/HARRIS CO	TX	HALC	3309.92	275.405
SITE T-19 CRAWFORD	TX	HCFA	3293.462	271.685
SITE T-18 CROQUET	TX	HCQA	3279.502	260.451
SITE T-26 LANG	TX	HLAA	3302.937	258.826
MANCHESTER C22	TX	HMCA	3288.207	279.323
NORTHWEST HARRIS C26	TX	HNWA	3325.942	242.051
EAST C1 / HARRIS CO	TX	HOEA	3295.077	285.264
SWISS&MONROE / HARRIS CO	TX	HSMA	3279.202	280.502
TEXAS COMMERCE TOWER	TX	HTCC	3294.387	271.453
SITE S-13 N WAYSIDE	TX	HWAA	3301.736	279.3
KOUNTZE C85/HARDIN CO	TX	KTZA	3361.557	373.554
PORT ARTHUR WEST C28	TX	PAWC	3307.27	404.604
SETRPC SITE 40 - Sabine Pass	TX	S40S	3287.707	413.249
SETRPC SITE 41 - West Orang Co.	TX	S41S	3327.165	425.885
SETRPC SITE 42 - Mauriceville	TX	S42S	3338.872	415.95
SETRPC SITE 43 - Jeff. Co. Airport	TX	S43S	3312.048	403.101
SEABROOK C20	TX	SBRC	3272.903	304.592
SMITH POINT AQ/MET SITE	TX	SPTC	3268.283	329.661
STOWELL (WINNIE) AQ/MET	TX	STWC	3296.476	364.036

Continued

TABLE 2-2. Concluded.

Monitoring Site		Site ID	UTM-northing (km)	UTM-easting (km)
SEAWALL, TEXAS CITY	TX	SWLT	3252.776	316.836
CORPUS CHRISTI WEST C4	TX	T04A	3087.985	63.267
CORPUS CHRISTI (TULOSA HI. SCH.)C21	TX	T21A	3087.102	50.986
TEXAS CITY / LA MARQUE	TX	TLMC	3253.437	312.342
VICTORIA CAMS 87	TX	VCTC	3196.24	109.023
WEST ORANGE CAMS 9	TX	WORA	3328.379	426.568
CARLYSS (2201900002)	LA	LO05	3334.500	464.200
LE BLEU (2201900007)	LA	LO16	3348.700	492.000
RAGLEY (220110002)	LA	LO24	3373.100	486.400
(220190009)	LA	LO27	3344.000	444.400
(220190008)	LA	LO28	3347.600	472.700

winds near 4–5 ms^{-1} around 1400 CST. During the evening hours, winds in the Houston area veered to southwesterly again.

Upper-Air Winds. On 23 October, the Houston Hobby wind profiler (H04H) data and Lake Charles (LCHN) and Slidell (SLID) sounding data indicated easterly winds, with wind speeds near 5–10 ms^{-1}, during the first half of the day and northeasterly winds during the evening. Northeasterly winds also dominated the soundings at Corpus Christi (CRPN) and Brownsville (BRON). To the north of the domain, at Stephenville (SEPN) and Longview (GGGN), westerly winds were evident above approximately 1000 m above ground level (m agl). In the lower 1000 m agl, the sounding data showed very weak wind speeds (near 1 ms^{-1}) at GGGN and southerly winds near 4 ms^{-1}, becoming weak and southwesterly in the evening at SEPN. Between approximately 0900 and 1300 CST, southeasterly flow was evident in the H04H profiler data up to about 1200 m agl. In the HG area, strong northerly flow developed aloft after 1400 CST and the gulf breeze weakened and became confined to the lower 500 m agl. During the early evening hours, winds below about 400 m agl veered to the southwest and strong north to northeasterly winds (15–20 ms^{-1}) dominated aloft. The GALC sodar data showed easterly winds most of the day with no evidence of gulf-breeze development. After 1800 CST, winds at GALC were mostly weak and unorganized with some westerly flow developing in the lower 200 m agl late in the evening.

On 24 October, upper-air winds in the domain remained northerly and a shallow gulf breeze developed late in the day. In the evening, winds below approximately 700 m agl weakened to 1–2 ms^{-1} and became more northwesterly. Winds at BRON and CPRN were easterly in the morning, becoming more northerly in the evening; southwesterly flow was evident below 500 m agl in the CRPN evening sounding data. To the north of the domain, winds at GGGN were northwesterly all day, while winds at SEPN were predominantly from the southwest. Early morning winds in the Houston area were from the northwest near the surface and from the northeast at speeds near 15–20 ms^{-1} above 400 m agl. Winds in the lower 400 m agl at both Houston and Galveston remained from

TABLE 2-3a. Data availability for the COAST modeling domain surface monitoring sites. Available data are indicated by the symbols X, Y, Z corresponding to: 31 August - 2 September 1993 episode only, both episodes, and 23-25 October 1992 episode only, respectively.

Monitoring Site		Site ID	Source	Wind	Temper-ature	Pres-sure	Mois-ture	Ozone	NO	NO_2	CO	VOC
Gulf of Mexico Buoy 1		001N	NWS	X	X	X	X					
Gulf of Mexico Buoy 2		002N	NWS	Y	Y	Y	Y					
Gulf of Mexico Buoy 7		007N	NWS	X	X	X	X					
Gulf of Mexico Buoy 19		019N	NWS	X	X	X	X					
Gulf Coast Oil Pltf		01TN	NWS	X	X	X	X					
Gulf of Mexico Buoy 35		035N	NWS	X	X	X	X					
Texas CITY	TX	34ST	TNRCC					X	X	X		
Gulf Coast Oil Pltf		5R0N	NWS	X	X	X	X					
Cameron	LA	7R5N	NWS	Y	Y	Y	Y					
Gulf Coast Oil Pltf		7R8N	NWS	X	X	X	X					
Abilene Municipal	TX	ABIN	NWS	Z	Z	Z	Z					
Waco-Madison Cooper Field	TX	ACTN	NWS	Y	Y	Y	Y					
Alice / Intl Airport	TX	ALIN	NWS	Y	Y	Y	Y					
Amarillo	TX	AMAN	NWS	Z	Z	Z	Z					
Austin/Mueller Municipal	TX	AUSN	NWS	Y	Y	Y	Y					
Barksdale AFB	LA	BADN	NWS	X	X	X	X					
Baytown C24/Harris Co	TX	BAYC	TNRCC	Y	Y							
Bloomington (GLDN CRES 84)	TX	BLOG	TNRCC	X	X							
Beaumont C02/Jefferson	TX	BMTC	TNRCC	Y	Y			Y	Y	Y	Y	
Port Arthur / WSO	TX	BPTN	NWS	Y	Y	Y	Y					
Brownsville Intl	TX	BRON	NWS	Y	Y	Y	Y					

Continued

TABLE 2-3a. Continued.

Site	ST	Site ID	Source	Wind	Temperature	Pressure	Moisture	Ozone	NO	NO_2	CO	VOC
Bergstrom	TX	BSMN	NWS	Z	Z	Z	Z					
Clinton CGC / Harris CO	TX	C35C	TNRCC	Y	Y			Y	Y	Y	Y	
Childress	TX	CDSN	NWS	Z	Z	Z	Z					
College Station / Easterwood Fld	TX	CLLN	NWS	Y	Y	Y	Y					
Clute Cams 11/Brazoria Co	TX	CLTA	TNRCC	Y	Y			Y				
Cotulla	TX	COTN	NWS	Z	Z	Z	Z					
Corpus Christi INTL	TX	CRPN	NWS	Y	Y	Y	Y					
Crosby AQ/Met Site	TX	CRSC	COAST	X	X			X	X	X		
Dalhart	TX	DHTN	NWS	Z	Z	Z	Z					
Del Rio Laughlin AFB	TX	DLFN	NWS	Z	Z	Z	Z					
Deer Park C18/Harris Co	TX	DRPA	TNRCC	Y	Y			Z				
Del Rio	TX	DRTN	NWS	Z	Z	Z	Z					
Abilene Dyess AFB	TX	DYSN	NWS	Z	Z	Z	Z					
Ellington AFB	TX	EFDN	NWS	Y	Y	Y	Y					
El Paso	TX	ELPN	NWS	Z	Z	Z	Z					
Alexandria/Esler	LA	ESFN	NWS	X	X	X	X					
Fort Worth	TX	FTWN	NWS	Z	Z	Z	Z					
Fort Wprth Crswl AFB	TX	FWHN	NWS	Z	Z	Z	Z					
Galveston AS Site	TX	GALC	COAST	Y	Y	Z		Y	Y	Y	Y	
Guadalupe Pass	TX	GDPN	NWS	Z	Z	Z	Z					
Longview/Gregg Co. (CAMS 19)	TX	GGGC	TNRCC	X	X			X				
Longview/Gregg Co.	TX	GGGN	NWS	Y	Y	Y	Y					

Continued

TABLE 2-3a. Continued.

Site	ST	Site ID	Source	Wind	Temperature	Pressure	Moisture	Ozone	NO	NO_2	CO	VOC
Galleria CGC Site	TX	GLRC	COAST	X	X			X	X	X		
Galveston / Scholes Field	TX	GLSN	NWS	Y	Y	Y	Y					
Robert Gray AAF	TX	GRKN	NWS	Z	Z	Z	Z					
Galveston Radar Profiler	TX	GRPC	COAST	X	X	X	X					
HRM Site 1	TX	H01H	HRM	Y	Y			Y	Y	Y	Y	
HRM Site 3	TX	H03H	HRM	Y	Y			Y	Y	Y	Y	
HRM Site 4	TX	H04H	HRM	Y	Y			Y	Y	Y	Y	
HRM Site 7	TX	H07H	HRM	Y	Y			Y	Y	Y	Y	
HRM Site 8	TX	H08H	HRM	Y	Y			Y	Y	Y	Y	
HRM Site 10	TX	H10H	HRM	Y	Y			Y	Y	Y	Y	
HRM Site 11	TX	H11H	HRM	Y	Y			Y	Y	Y	Y	
Aldine C8/Harris Co	TX	HALC	TNRCC	Y	Y			Y	Y	Y	Y	
Hobby Airport RPS	TX	HBYC	COAST	X	X	X	X					
Site T-19 Crawford	TX	HCFA	TNRCC	Y	Y			Y	Y	Y	Y	
Site T-18 Croquet	TX	HCQA	TNRCC	Y	Y			Y				
Hondo Municipal	TX	HDON	NWS	Y	Y	Y	Y					
High Island PLTF 199 MMS	LA	HIPM	MMS	X	X	X	X					
Site T-26 Lang	TX	HLAA	TNRCC	Y	Y			Y	Y	Y	Y	
Ft Hood AAF/Killeen	TX	HLRN	NWS	Y	Y	Y	Y					
Manchester C22	TX	HMCA	TNRCC	Y	Y			Y				
Northwest Harris C26	TX	HNWA	TNRCC	Z	Y			Z				
East C1 / Harris Co	TX	HOEA	TNRCC	Z	Z			Z	Z	Z	Z	

Continued

TABLE 2-3a. Continued.

Monitoring Site		Site ID	Source	Wind	Temperature	Pressure	Moisture	Ozone	NO	NO_2	CO	VOC
Houston / FAA (Hobby Airport)	TX	HOUN	NWS	Y	Y	Y	Y					
Harlingen Intl Airport	TX	HRLN	NWS	Y	Y	Y	Y					
Swiss&Monroe / Harris Co	TX	HSMA	TNRCC	Y	Y			Y				
Texas Commerce Tower	TX	HTCC	COAST	X	X			X	X	X		
Site S-13 N Wayside	TX	HWAA	TNRCC	Y	X			Y				
Houston/Intercontinental	TX	IAHN	NWS	Y	Y	Y	Y					
New Iberia	LA	ARAN	NWS	Z	Z	Z	Z					
Killen	TX	ILEN	NWS	Z	Z	Z	Z					
Wink	TX	INKN	NWS	Z	Z	Z	Z					
Intracoastal City	LA	7R4N	NWS	Z	Z	Z	Z					
Junction	TX	JCTN	NWS	Z	Z	Z	Z					
Kountze C85/Hardin Co	TX	KTZA	TNRCC	X	X			X				
Lubbock	TX	LBBN	NWS	Z	Z	Z	Z					
Brazoria Cty Airport		LBXN	NWS	Z	Z	Z	Z					
Lake Charles Municipal	LA	LCHN	NWS	Y	Y	Y	Y					
Lufkin/Angelina Co.	TX	LFKN	NWS	Y	Y	Y	Y					
Lafayette	LA	LFTN	NWS	Z	Z	Z	Z					
Laredo	TX	LRDN	NWS	Z	Z	Z	Z					
Louisiana State Univ. MMS	LA	LSUM	MMS	X	X	X	X					
Midland	TX	MAFN	NWS	Z	Z	Z	Z					
Met 5, Texas City	TX	MEST	TNRCC	X	X	X	X					
McAllen/Miller Intl	TX	MFEN	NWS	Y	Y	Y	Y					

Continued

TABLE 2-3a. Continued.

Site	ST	Site ID	Source	Wind	Temperature	Pressure	Moisture	Ozone	NO	NO_2	CO	VOC
Mobile, Texas CITY	TX	MOBT	TNRCC	X								
Monroe	LA	MLUN	NWS	Z	Z	Z	Z					
Marft	TX	MRFN	NWS	Z	Z	Z	Z					
Mineral Wells	TX	MWLN	NWS	Z	Z	Z	Z					
Corpus Christi NAAS	TX	NGPN	NWS	Y	Y	Y	Y					
Kingsville NAS	TX	NQIN	NWS	Y	Y	Y	Y					
Sanderson	TX	P07N	NWS	Z	Z	Z	Z					
Port Arthur West C28	TX	PAWC	TNRCC	Y	Y			Y				
Point Comfort (Gldn Cres 84)	TX	PCOG	TNRCC	X	X							
Fort Polk (Army)	LA	POEN	NWS	X	X	X	X					
Palacios / FAA Airport	TX	PSXN	NWS	Y	Y	Y	Y					
Reese AFB	TX	REEN	NWS	Z	Z	Z	Z					
Rock Port	TX	RKPN	NWS	Y	Y	Y	Y					
Randolph AFB	TX	RNDN	NWS	Y	Y	Y	Y					
Sabine Pass USGG(28T)	TX	RPEN	NWS	Z	Z	Z	Z					
SETRPC Site 40 - Sabine Pass	TX	S40S	SETPRC	Y	Y			Y	Y	Y		
SETRPC Site 41 - West Orang Co.	TX	S41S	SETPRC	Y	Y			Y	Y	Y		
SETRPC Site 42 - Mauriceville	TX	S42S	SETPRC	Y	Y			Y	Y	Y		
SETRPC Site 43 - Jeff. Co. Airport	TX	S43S	SETPRC	Y	Y			Y	Y	Y		
San Antonio Intl	TX	SATN	NWS	Y	Y	Y	Y					
Seabrook C20	TX	SBRC	COAST	X	X			X	X	X		
Sea Drift (Gldn Cres 82)	TX	SDRG	TNRCC	X	X							

Continued

TABLE 2-3a. Concluded.

Site	ST	Site ID	Source	Wind	Temperature	Pressure	Moisture	Ozone	NO	NO_2	CO	VOC
Stephenville/Clark	TX	SEPN	NWS	Z	Z	Z	Z					
Shreveport Regional	LA	SHVN	NWS	X	X	X	X					
San Angelo	TX	SJTN	NWS	Z	Z	Z	Z					
Kelly AFB	TX	SKFN	NWS	Y	Y	Y	Y					
Wichita Falls	TX	SPSN	NWS	Z	Z	Z	Z					
Smith Point AQ/Met Site	TX	SPTC	COAST	X	X			X	X	X		
Ship Shoal Pltf 178A MMS	TX	SSPM	MMS	X	X	X	X					
Stowell (Winnie) AQ/Met	TX	STWC	COAST	X	X			X	X	X		
Seawall, Texas City	TX	SWLT	TNRCC	X					X	X		
Corpus Christi West C4	TX	T04A	TNRCC	Y	Y			Y				
Corpus Christi (Tulosa Hi. Sch.) C21	TX	T21A	TNRCC	Y	Y			Y				
Texas City / La Marque	TX	TLMC	TNRCC	Y	Y			Z				
Temple/Miller(AWOS)	TX	TPLN	NWS	Y	Y	Y	Y					
Tyler/Pounds Field	TX	TYRN	NWS	Y	Y	Y	Y					
Victoria CAMS 87	TX	VCTC	TNRCC	Y	Y			Y				
Victoria Regional	TX	VCTN	NWS	Y	Y	Y	Y					
Victoria (Gldn Cres 81)	TX	VICG	TNRCC	X	X							
West Orange CAMS 9	TX	WORA	TNRCC	Y	Y			Y	Y	Y		
Carlyss (220190002)	LA	LO05	AIRS					Z				
Le Bleu (220190007)	LA	LO16	AIRS					Z				
Ragley (220110002)	LA	LO24	AIRS					Z				
(220190009)	LA	LO27	AIRS					Z				
(220190008)	LA	LO28	AIRS					Z				

TABLE 2-3b. Data availability for the COAST modeling domain upper-air monitoring sites. Available data are indicated by the symbols X, Y, Z corresponding to: 31 August - 2 September 1993 episode only, both episodes, and 23-25 October 1992 episode only.

Site	ST	Site ID	Source	Wind	Temper-ature	Virtual Temper-ature	Pressure	Dew Point Temper-ature
Brownsville Intl	TX	BRON	NWS	Y	Y		Y	Y
Cocodrie	LA	COCM	MMS	X		X		
Corpus Christi Intl	TX	CRPN	NWS	Y	Y		Y	Y
Galveston AS Site	TX	GALC	COAST	Y				
Longview/Gregg Co.	TX	GGGN	NWS	Y	Y		Y	Y
Galveston Radar Profiler	TX	GRPC	COAST	X		X		
HRM Site 4	TX	H04H	TNRCC	Z		Z		
Hobby Airport RPS	TX	HBYC	COAST	X		X		
High Island Pltf 199 MMS	LA	HIPM	MMS	X		X		
Jefferson Co Airport RPS	TX	JCAC	COAST	X		X		
Jeffson County	TX	JCSC	COAST	X				
Lake Charles Municipal	LA	LCHN	NWS	Y	Y		Y	Y
Louisiana State Univ. MMS	LA	LSUM	MMS	X		X		
Northwest Houston	TX	NWHC	COAST	X				
Stephenville/Clark	TX	SEPN	NWS	Y	Y		Y	Y
Slidell	LA	SLID	NWS	Z	Z		Z	Z
Sabine Pass	TX	SPSC	COAST	X				
Ship Shoal Pltf 178A MMS	TX	SSPM	MMS	X		X		

the northwest until about 1200 CST. In the afternoon, the southerly flow of a late-developing gulf breeze appeared below 300 m first at Galveston at 1300 CST and later in the Houston area at 1600 CST. The gulf breeze does not appear to have developed above 500 m agl on this day.

Northerly winds continued above approximately 1500 m agl on 25 October. Within the domain, winds at Lake Charles above approximately 700 m agl were somewhat unorganized with weak wind speeds between 3 and 5 ms^{-1} most of the day. In the lower 500 m agl, winds were from the west-northwest in the morning and from the west-southwest in the evening. Winds below approximately 1000 m agl were southeasterly at CRPN and BRON and southwesterly at GGGN and SEPN. During the morning hours, the H04H and GALC data indicated northwesterly flow around 6–8 ms^{-1}. Southerly flow began in the Houston area around 1000 CST and at Galveston after 1100 CST.

The southeasterly winds in the Houston area extended to approximately 1000 m agl at 1800 CST and wind speeds were relatively strong, near 10–15 ms^{-1}. In the evening, winds in the lower 500 m agl veered to the southwest.

Temperatures

Maximum observed surface temperatures for the Beaumont (BPTN) area on 24 and 25 October were 28.9°C and 30.6°C, respectively. Observed temperatures in the Houston area were somewhat higher. Maximum temperatures of 32.2°C and 33.9°C were recorded at the HALC monitoring site on 24 and 25 October, respectively.

31 August - 2 September 1993

Synoptic Meteorology

The NMC 500 mb analyses for all three days showed a weak trough over the northern U.S. A high-pressure system developed over the Texas/Louisiana Gulf coast region during the episode as a westward extension of the Bermuda high-pressure system continued to build over the gulf. As a result, no significant upper-level synoptic forcing developed and the 500-mb upper-air winds at Lake Charles were weak and from the west-southwest throughout the episode.

The surface analyses for 31 August and 1 September showed a high-pressure system over the central U.S. and a stationary front located over Texas, northwest of the Houston area. On 2 September, the surface analysis indicated a surface trough near the Lake Charles and Beaumont/Port Arthur areas. Daily maximum temperatures exceeded 90°F. Some precipitation was reported on 31 August and 1 September along the Texas coast between Houston and Corpus Christi.

Airflow Patterns

Surface Winds. Early morning surface winds on 31 August had southerly components throughout the domain. Winds were weak and variable in the HG and BPA areas. Along the coast, wind speeds were generally near 3–4 ms^{-1}. During the rest of the day, surface winds in Southeast Texas were unorganized and variable between 1000 and 1600 CST and mostly southwesterly after 1700 CST. Throughout the day, winds from Victoria to Corpus Christi were from the south and southeast at 3–5 ms^{-1}.

At 0000 CST on 1 September, calm or very weak winds prevailed along the coast and in Corpus Christi, Victoria, Houston, and the Beaumont/Port Arthur area. Northerly winds developed from Houston and eastward after 0300 CST and continued to dominate the airflow patterns in southeast Texas until 1200 CST. Wind speeds at 1000 CST were approximately 3 ms^{-1} inland and near 5 ms^{-1} at the coastline. Southeasterly flow developed around 0900 CST over Corpus Christi and at 1300 CST near Galveston. Surface winds in the HG and BPA areas were from the west-southwest after 1300 CST and remained southwesterly for the remainder of the day.

On 2 September, early morning surface winds maintained westerly components but became weaker and more variable. After sunrise, wind speeds increased to 3–4 ms^{-1} and the wind became southwesterly in Corpus Christi, westerly in Houston, and northwesterly in the BPA area. A southerly gulf breeze was evident first at Galveston around 1200 CST, then in Texas City at 1300 CST, and in Baytown at 1400 CST. The gulf breeze appeared to pass through downtown Houston between 1600 and 1700 CST. Surface winds also became southwesterly in BPA after 1600 CST. Southerly winds persisted through the end of the day.

Upper-Air Winds. On 31 August, as indicated by the upper-air data from the CRPN and BRON soundings, winds in the southeastern portion of the domain (at all levels below 3000 m agl) were from the south to southwest all day. In north Texas, the SEPN soundings indicated northeasterly winds below 1000 m agl backing to southerly above 2000 m agl, and at GGGN, winds were weak in the morning and westerly in the evening. The LCHN upper-air sounding data were dominated by north-to-northwesterly winds with wind speeds increasing during the day. Upper-air wind patterns in the HG area were variable throughout the day. During the morning, the HBYC and GRPC radar profiler data indicated southerly winds up to approximately 3000 m agl. Between 1200 and 1500 CST, the lower 500 m agl winds over Houston became westerly with a weak northerly component near the surface. Over Galveston, winds shifted to easterly for one hour at 1400 CST. These short-duration wind shifts are consistent with variations noted in the surface wind observations. In the Beaumont/Port Arthur area, the JCAC wind profiler data showed westerly to northwesterly winds for most of the day with some southwesterly winds between 1500 and 1800 CST in the lower 500 m agl.

On 1 September, southeasterly winds continued in the southwestern portion of the domain. Wind speeds at CRPN decreased from approximately 7–8 ms^{-1} in the morning to 5 ms^{-1} or less. At GGGN, upper-air winds were from the west-southwest. The SEPN radiosonde data indicated weak flow from the northeast below 1000 m in the morning veering to southerly in the evening. Winds above approximately 1000 m were southerly all day. During the morning on this day, upper-air monitoring sites along the Texas Gulf coast and in the Houston area (GALC, JCSC, NWHC, SPSC, JCAC, GRPC, HBYC, and LCHN) showed northwesterly winds in the lower 1500 m. In the afternoon, wind speeds decreased and southerly winds developed at Galveston (as indicated by both the GRPC and GALC data) at 1200 CST, at Sabine Pass (SPSC) at 1400 CST, and in Houston after 1700 CST. The southerly flow was confined to the lower 700 m agl. The JCSC and JCAC data suggest that the gulf breeze did not extend inland to Beaumont/Port Arthur on this day.

On 2 September, the CRPN and BRON sounding data continued to show southeasterly winds. Wind speeds increased somewhat during the day to 7–8 ms^{-1}. At SEPN, winds were from the southwest with wind speeds decreasing during the day and becoming very weak in the lower 1000 m agl in the evening. In east Texas, the LCHN upper-air winds were northwesterly in the morning, backing to southwesterly below 1000 m agl in the evening, and the GGGN data showed southwesterly winds all day. In the Houston area and along the Texas coast, westerly winds prevailed in the lower 500 m agl for the first half of the day. A fairly strong gulf breeze (with wind speeds of up to 10 ms^{-1}) was evident in the GRPC and GALC data in the afternoon. Winds in Houston were from the west and southwest in the morning and from the south after 1300 CST. The NWHC

SODAR data showed southwesterly winds for most of the day until 1900 CST when winds increased and shifted to the southeast and, thus, these data suggest that the gulf breeze did not pass through Houston until late in the evening. Winds in the BPA area shifted from westerly to southwesterly in the afternoon.

Temperatures

On 1 and 2 September, maximum observed surface temperatures in the Beaumont and Houston areas were between 35°C and 36°C on both days.

AIR QUALITY

23–25 October 1992

Observed air-quality patterns during this episode were characterized by high ozone concentrations to the south of the Houston area on 24 October and in Baytown and in the Beaumont/Port Arthur area on 25 October. The top five daily maximum ozone concentrations for each episode day are summarized in Table 2-4. No exceedance of the federal ozone standard was recorded on 23 October; the highest ozone concentrations for this day were 112 ppb and 108 ppb, measured at Beaumont (BMTC) and Northwest Harris County (NWHA), respectively. The maximum observed ozone concentration for the episode was 198 ppb, observed at the Galveston (GALC) monitoring site on 24 October. On this day, an exceedance (126 ppb) was also recorded at the Texas City (TLMC) monitoring site. On 25 October, the maximum ozone concentration (157 ppb)

TABLE 2-4. Daily maximum ozone observations for 23–25 October 1992.

Site	Ozone Conc. (ppb)	>120 ppb	Date	Hour
BMTC	112		23 October	21–22
HNWA	108		23 October	16–17
WORA	94		23 October	14–15
HALC	91		23 October	14–15
S43S	83		23 October	17–18
GALC	198	*	24 October	17–18
TLMC	126	*	24 October	17–18
H08H	117		24 October	15–16
S40S	112		24 October	18–19
H07H	101		24 October	15–16
H07H	157	*	25 October	13–14
H04H	148	*	25 October	14–15
H11H	141	*	25 October	12–13
WORA	137	*	25 October	12–13
S43S	125	*	25 October	13–14

occurred in the Baytown area at the H07H monitoring site. Two additional monitoring sites in the Baytown area, H04H and H11H, recorded daily maximum ozone concentrations in excess of the federal standard on this day: 148 and 141 ppb, respectively.

In the Beaumont/Port Arthur nonattainment area, two exceedances were recorded on 25 October at the West Orange (WORA) and the Beaumont (S43S) monitoring sites. The daily maximum observed ozone concentrations for these sites were 137 and 125 ppb, respectively.

31 August - 2 September 1993

Table 2-5 summarizes the daily maximum ozone concentrations for each day of this episode. During this episode, high ozone concentrations were observed in the Baytown area, to the east-southeast of Houston in Chambers County, and in the Beaumont/Port Arthur area. No exceedances were observed on 31 August. The observed maximum ozone concentration for this episode (164 ppb) was recorded at the Baytown H11H monitoring site on 1 September. Another exceedance (137 ppb) occurred on this day at the Smith Point (SPTC) monitoring site. On 2 September, the maximum concentration was 139 ppb and was recorded at the Beaumont (S43S) monitoring site. The second highest concentration (131 ppb) was measured at the Stowell site in eastern Chambers County.

TABLE 2-5. Five highest ozone observations for each day of the 31 August–1 September 1993 episode.

Site	Ozone Conc. (ppb)	> 120 ppb	Date	Hours
H07H	96		31 August	15–16
CRSC	91		31 August	11–12
H11H	87		31 August	15–16
WORA	84		31 August	15–16
KTZA	81		31 August	17–18
H11H	164	*	1 September	15–16
SPTC	137	*	1 September	13–14
H07H	121	*	1 September	15–16
STWC	118		1 September	18–19
GGGC	114		1 September	11–12
S43S	139	*	2 September	15–16
STWC	131	*	2 September	13–14
PAWC	115		2 September	15–16
H10H	115		2 September	13–14
KTZA	111		2 September	17–18

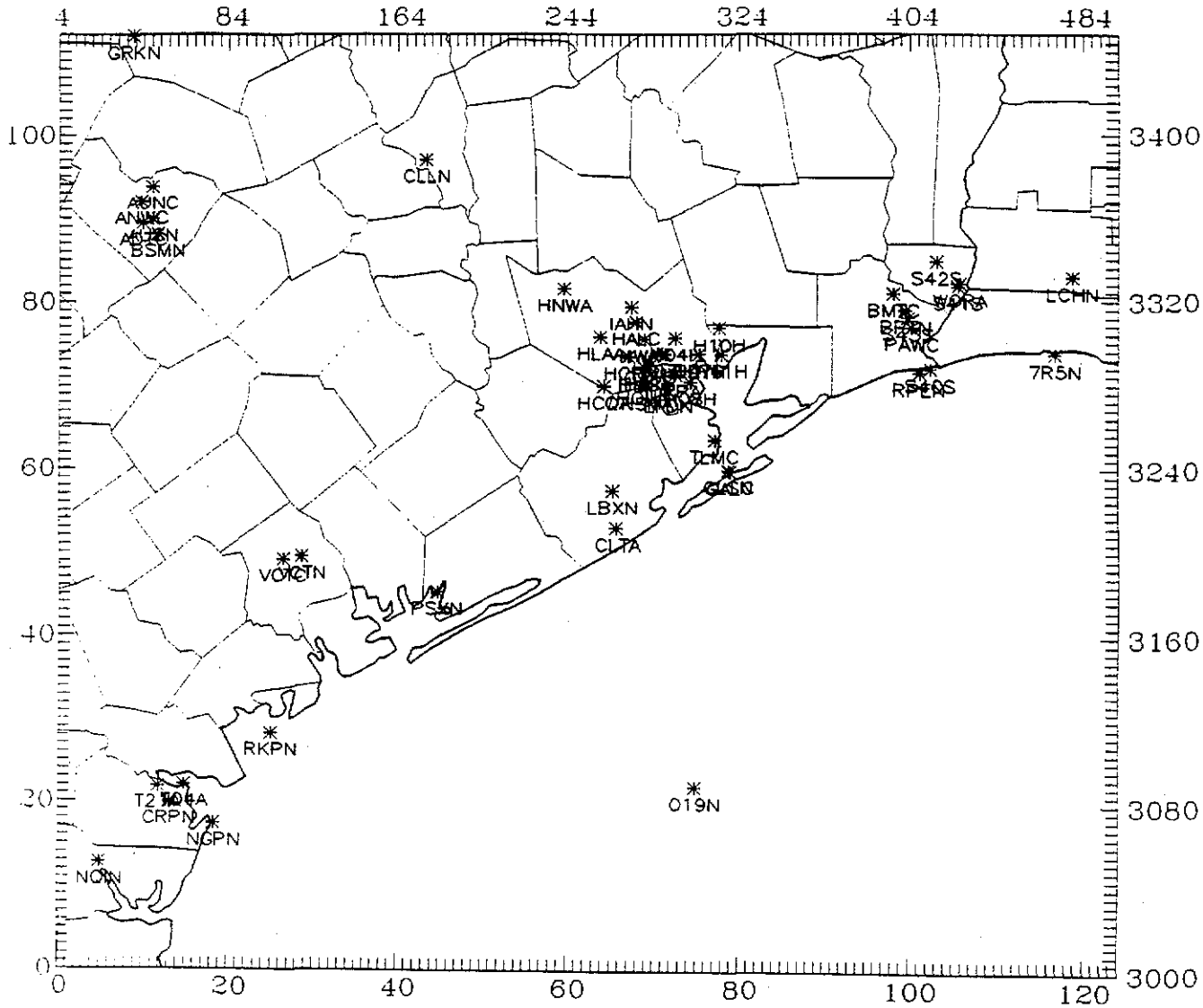

FIGURE 2-1a. Locations of meteorological monitoring sites for the 23–25 October 1992 episode in the Southeast Texas UAM-V modeling domain.

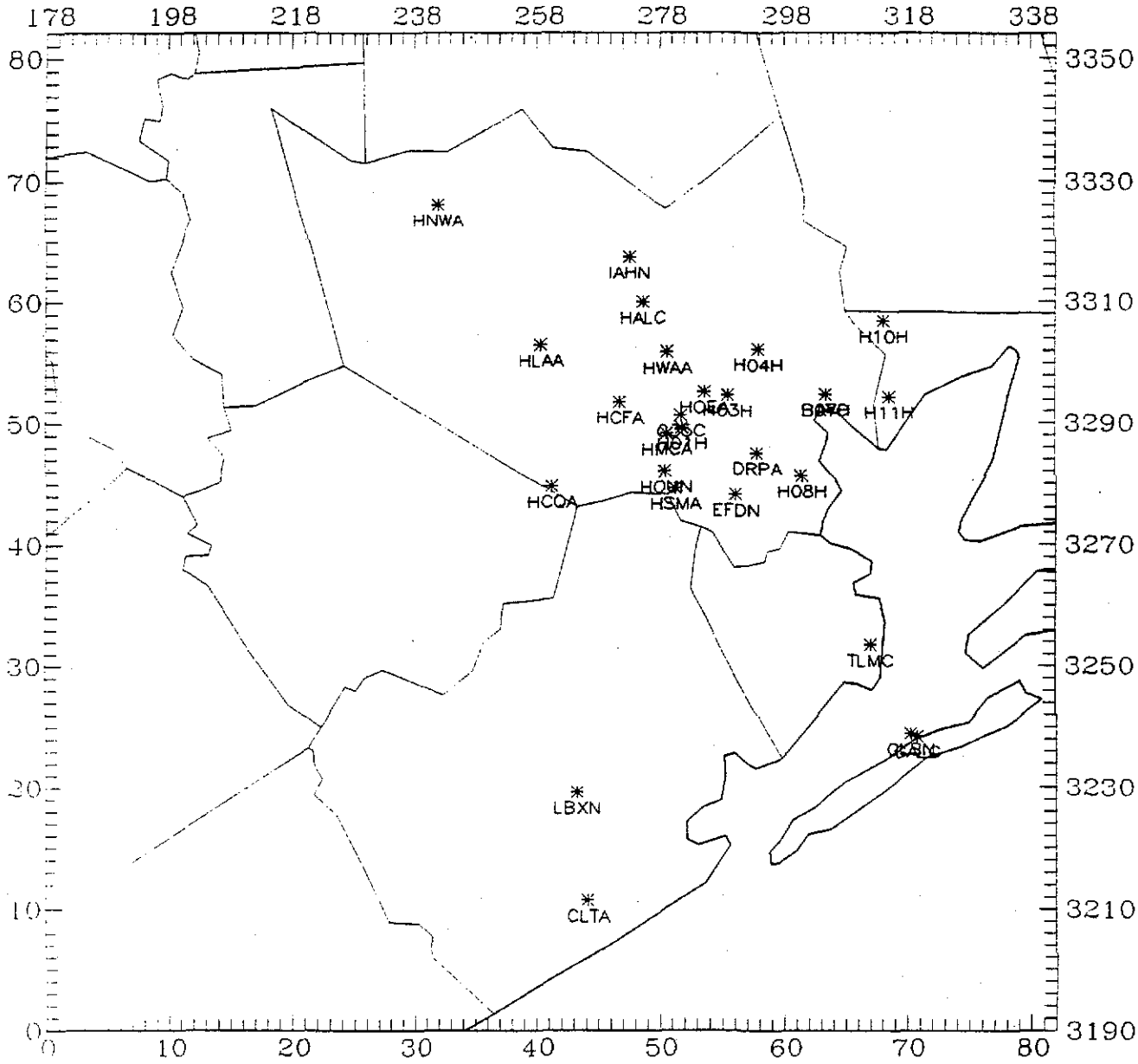

FIGURE 2-1b. Locations of meteorological monitoring sites for the 23–25 October 1992 episode in the middle (4 km) UAM-V modeling domain.

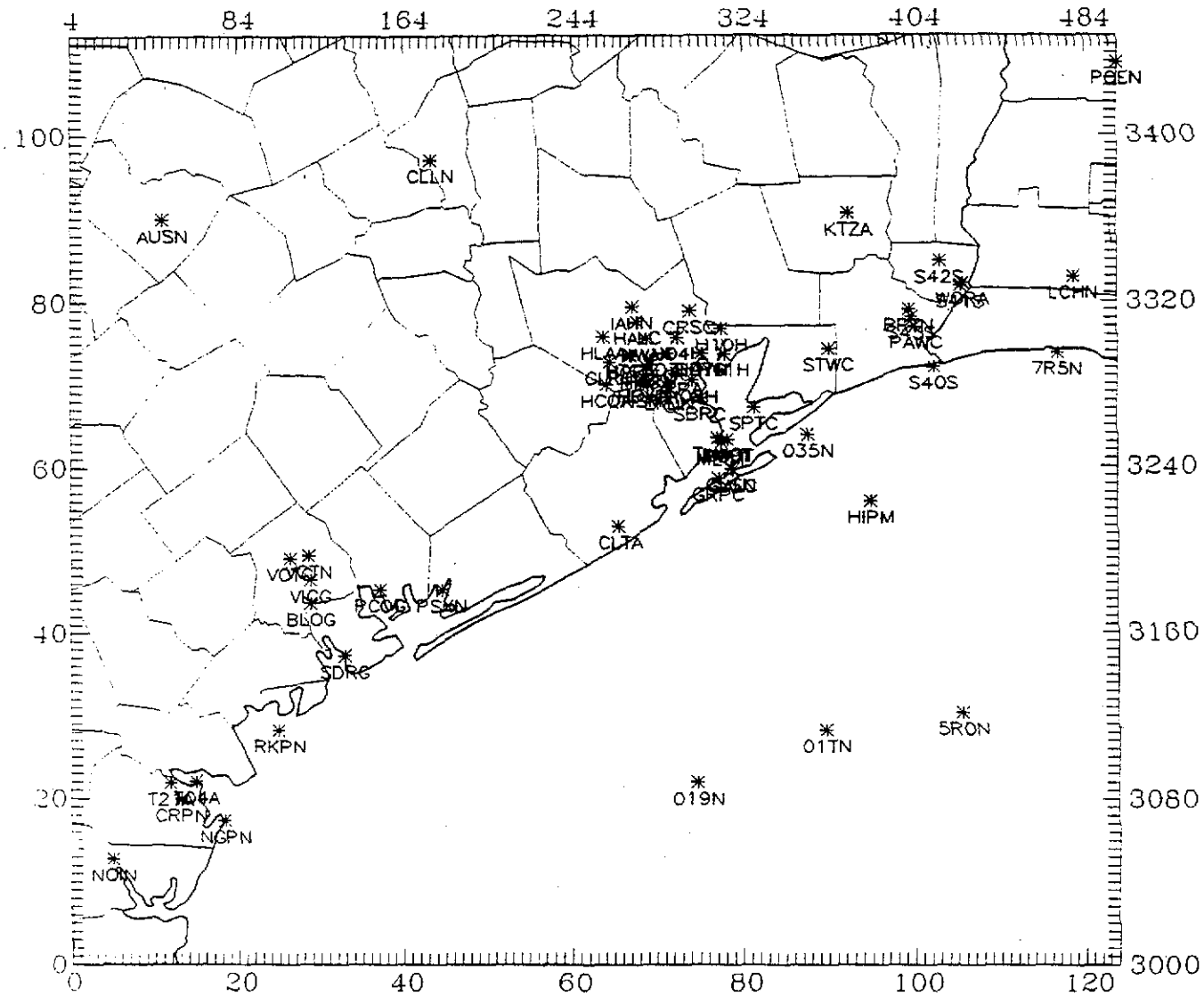

FIGURE 2-1c. Locations of meteorological monitoring sites for the 31 August – 2 September 1993 episode in the Southeast Texas UAM-V modeling domain.

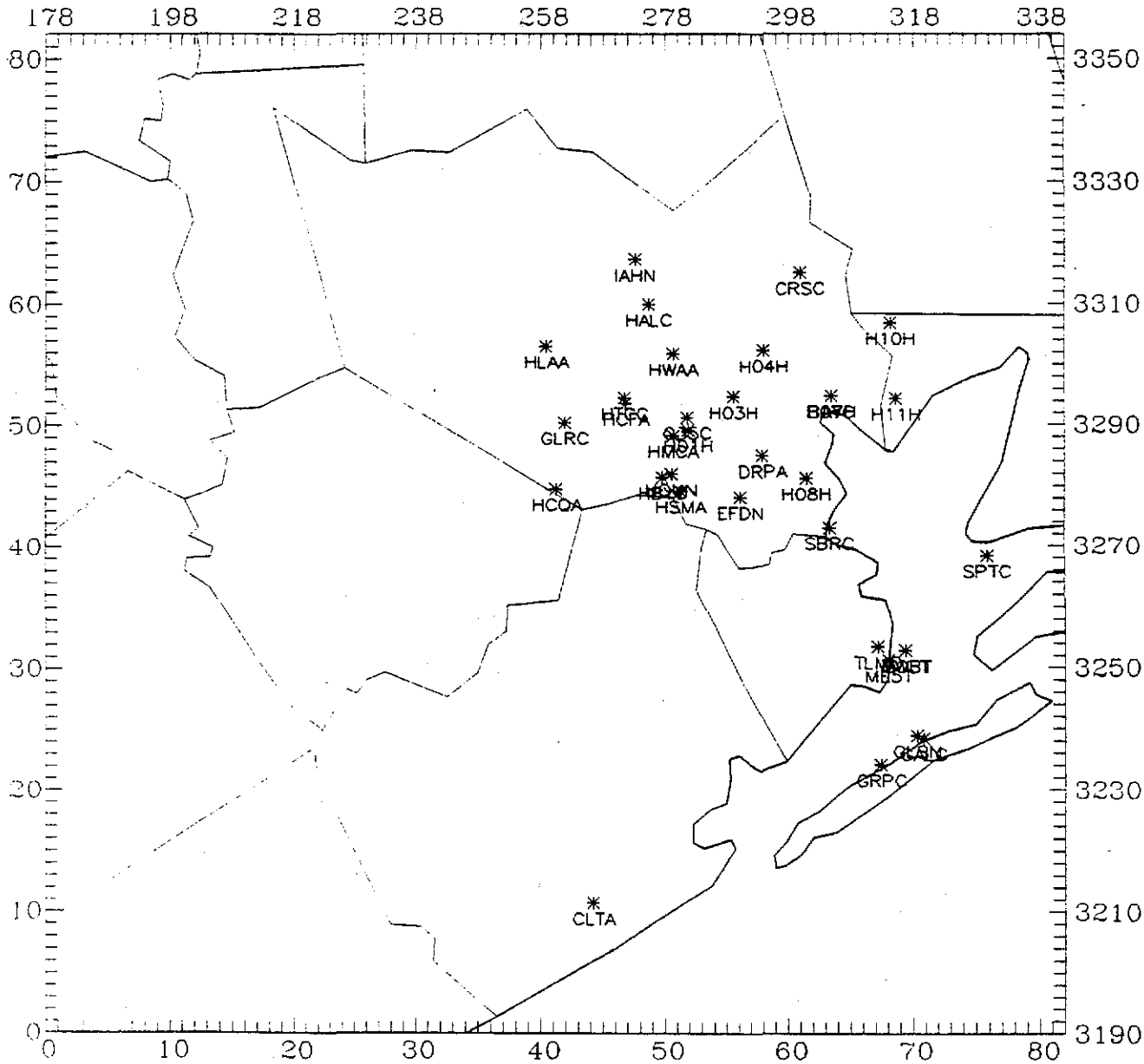

FIGURE 2-1d. Locations of meteorological monitoring sites for the 31 August - 2 September 1993 episode in the middle (4 km) UAM-V modeling domain.

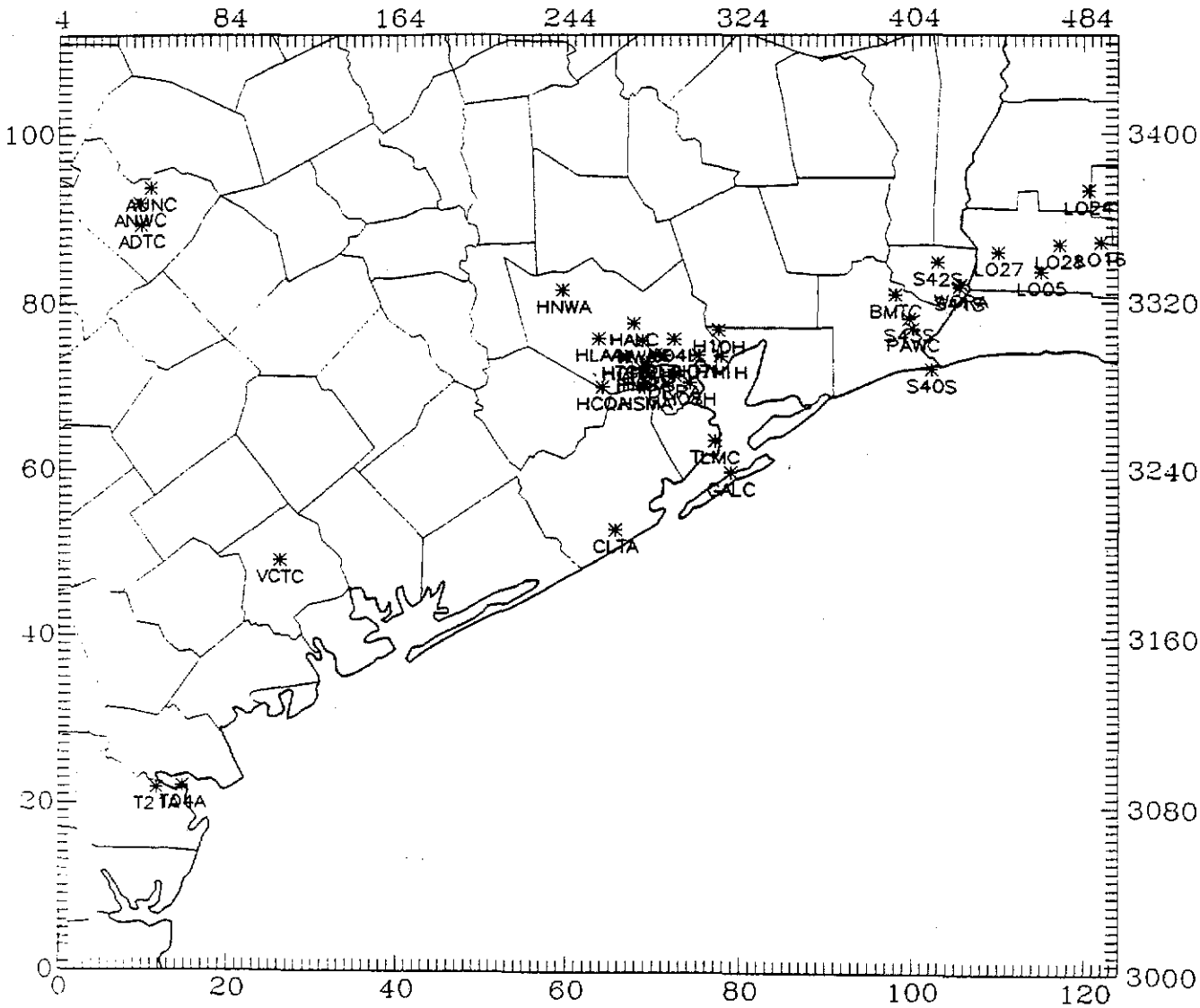

FIGURE 2-2a. Locations of air quality monitoring sites for the 23–25 October 1992 episode in the Southeast Texas UAM-V modeling domain.

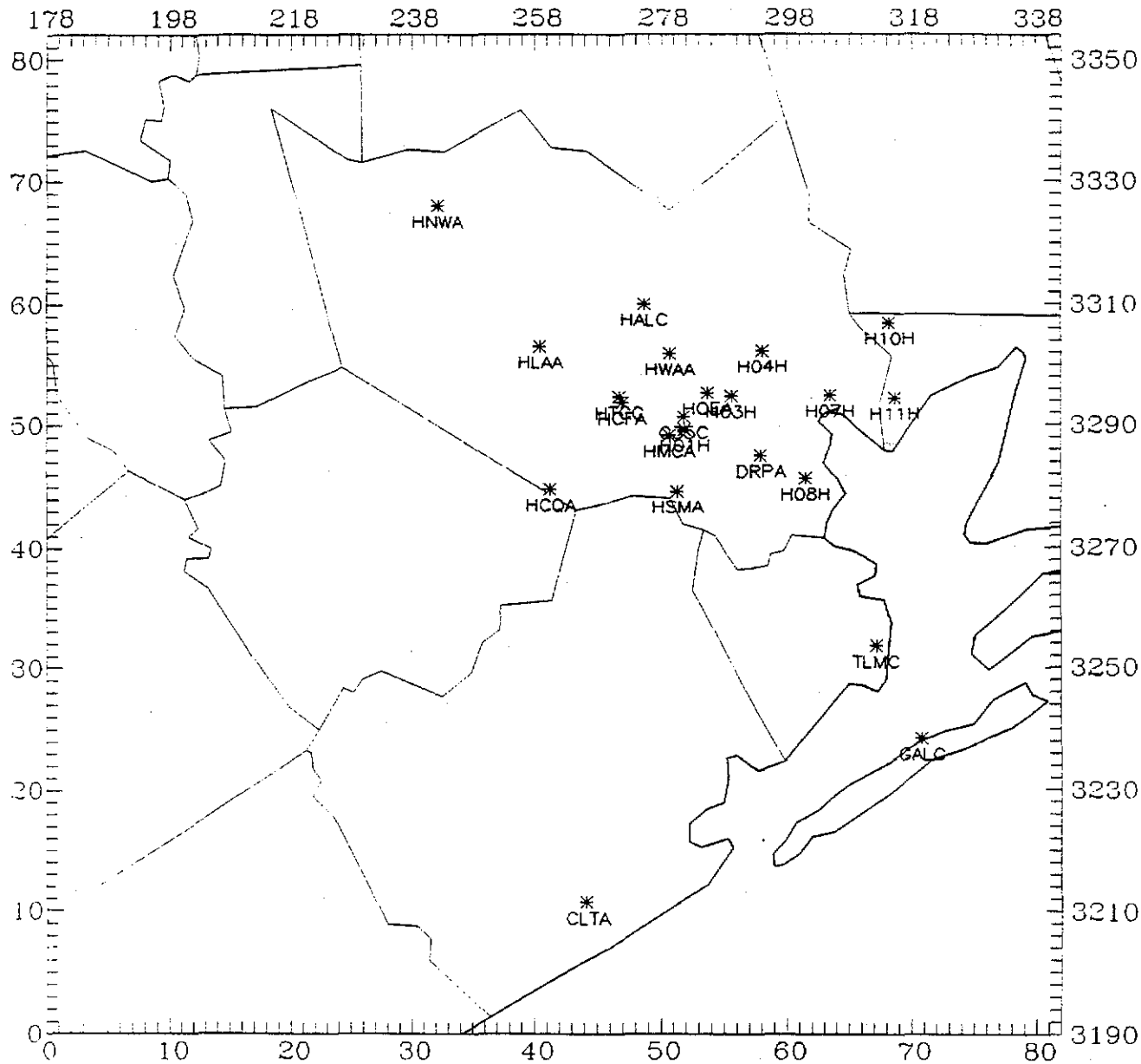

FIGURE 2-2b. Locations of air quality monitoring sites for the 23-25 October 1992 episode in the middle (4 km) UAM-V modeling domain.

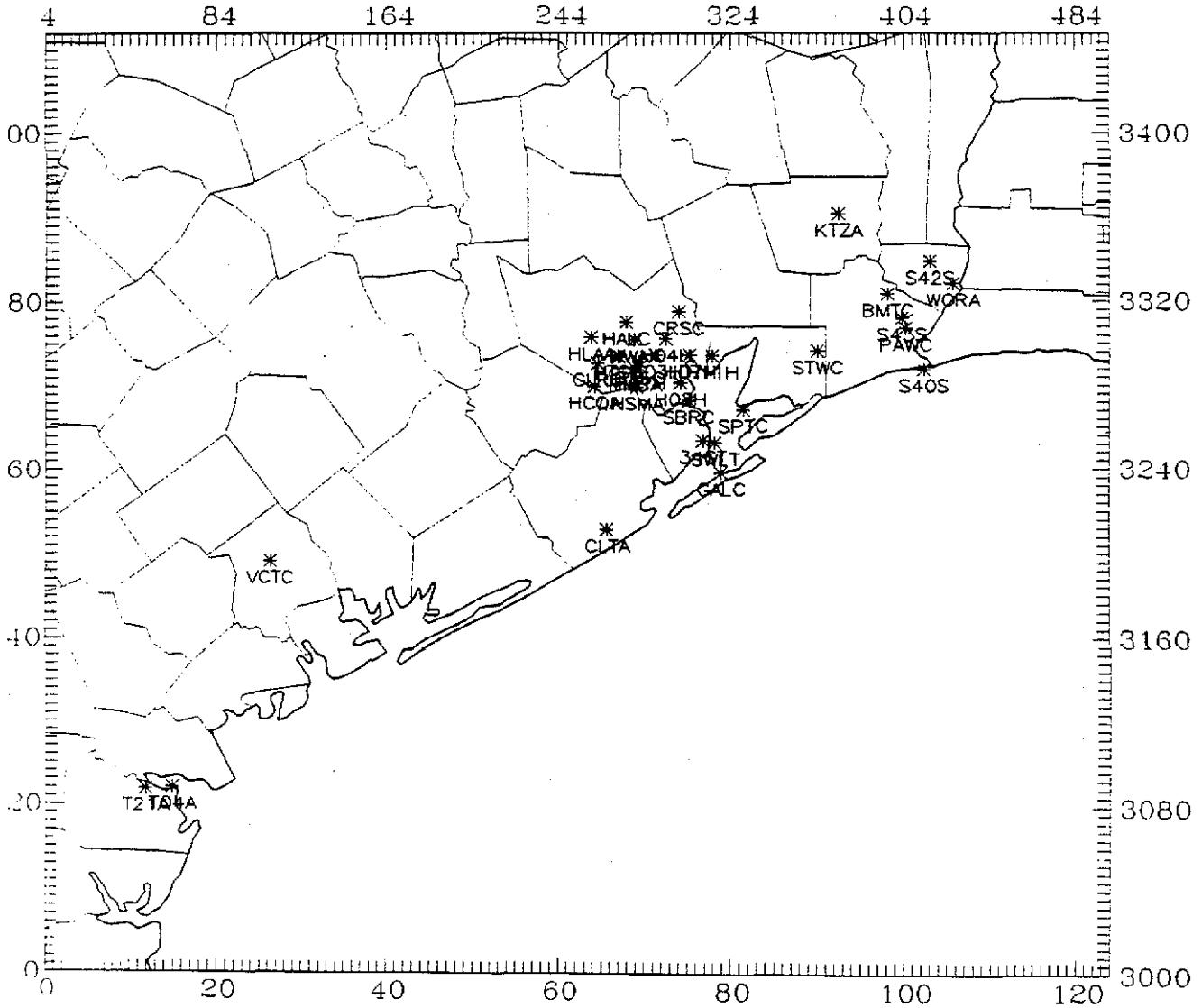

FIGURE 2-2c. Locations of air quality monitoring sites for the 31 August – 2 September 1993 episode in the Southeast Texas UAM-V modeling domain.

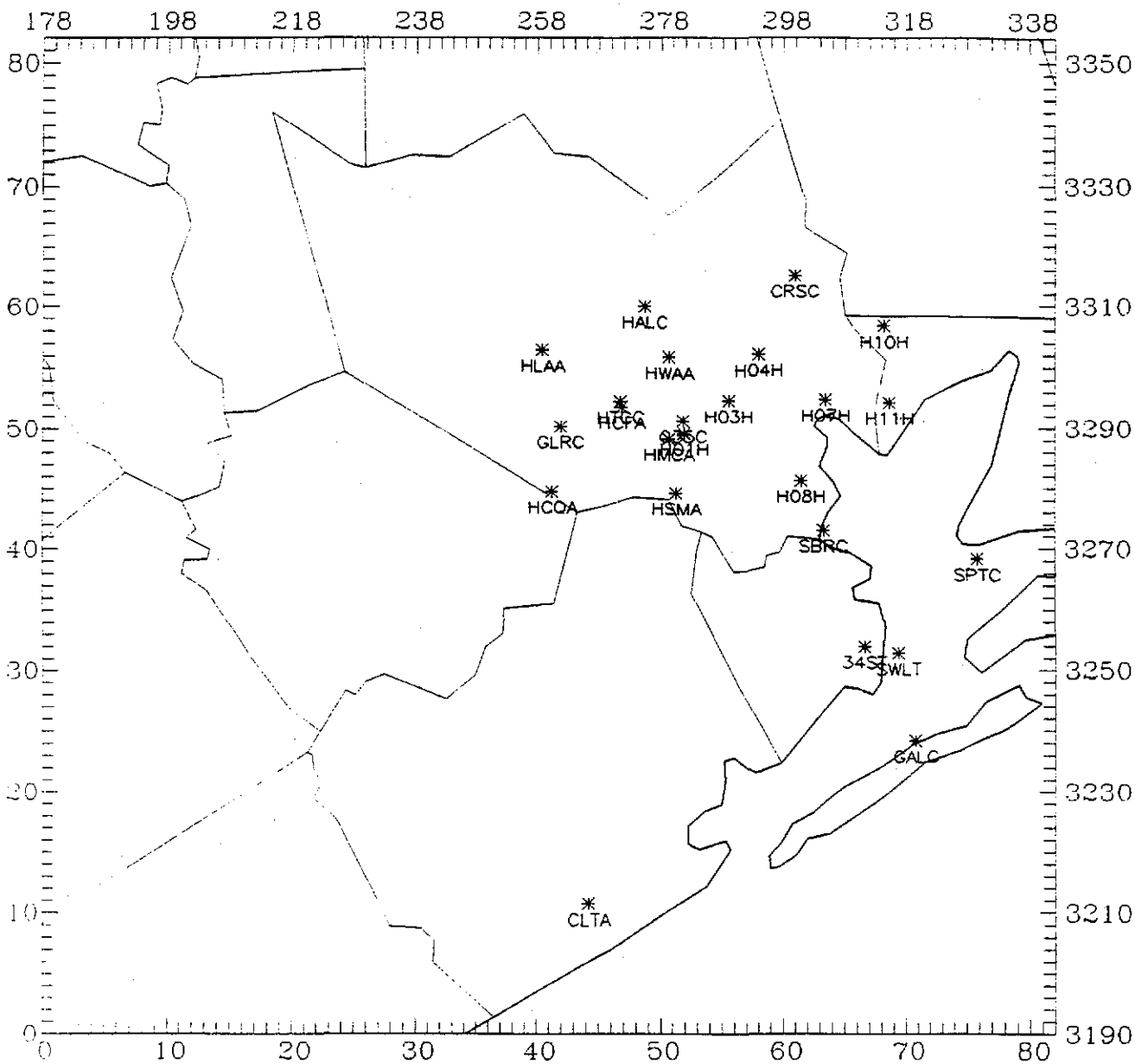

FIGURE 2-2d. Locations of air quality monitoring sites for the 31 August - 2 September 1993 episode in the middle (4 km) UAM-V modeling domain.

3 APPLICATION OF THE SAIMM

The Systems Applications International Mesoscale Model (SAIMM) (Kessler and Douglas, 1992) was used in this study to generate meteorological input fields for the application of the UAM-V for the Southeast Texas area. The SAIMM is a prognostic meteorological model; that is, beginning with a set of initial conditions that represent the state of the atmosphere at the initial simulation time, the model simulates the response of the atmosphere to differential surface heating and terrain irregularities and thus provides information on the development and evolution of mesoscale meteorological features within the modeling domain. Observed meteorological data are incorporated into the SAIMM using a four-dimensional data assimilation (FDDA) procedure. The model produces hourly, three-dimensional fields of several meteorological variables including wind, temperature, specific humidity, pressure, planetary-boundary-layer height, and vertical turbulent exchange coefficients.

The SAIMM was used for this study to accommodate (1) the lack of sufficient data to properly characterize, using interpolative and diagnostic techniques, the meteorology within the modeling domain and (2) the input requirements of the UAM-V (three-dimensional fields of wind, temperature, water-vapor concentration, pressure, and vertical diffusivities). The SAIMM has the attributes necessary to simulate the gulf/land breeze circulations that characterize the gulf coast area, and the assimilation of observed data using the FDDA procedure allows the simulation of day-specific meteorological features.

The application of the SAIMM to the Southeast Texas area is described in this section, which includes an overview of the SAIMM and a summary of the application procedures and modeling results for 23–25 October 1992 and 31 August – 2 September 1993.

OVERVIEW OF THE SAIMM

The SAIMM is a hydrostatic, incompressible, primitive-equation, prognostic meteorological model designed to simulate the mesoscale airflows generated by differential heating of the earth's surface and terrain irregularities. The SAIMM is an enhanced version of the Colorado State University Mesoscale Model (CSUMM). The basic model formulation is given by Mahrer and Pielke (1977); the numerical advection scheme (upstream interpolation of cubic splines) is described by Mahrer and Pielke (1978).

The SAIMM is formulated in the terrain-following coordinate $z^* = s(z - z_G)/(s - z_G)$, where z is height above sea level, z_G is terrain height, and s is fixed height of the model top. This model includes a surface heat budget and relatively detailed treatments of the

atmospheric surface and planetary boundary layers. Vertical exchange coefficients are based on predicted turbulent kinetic energy, as described by Ulrickson and Mass (1990).

The SAIMM is particularly well suited to the study of thermally forced mountain-valley airflow patterns, urban heat-island effects, and sea-breeze circulations with horizontal scales of 10 to 300 km. It has been used to generate meteorological inputs for air quality modeling of California's San Joaquin Valley (Morris et al., 1990), South Central Coast Air Basin (Kessler and Douglas, 1991), South Coast Air Basin (Douglas et al., 1992), Sacramento Valley (Douglas, Shepard, and Haney, 1993), Northeast United States (Douglas et al., 1995), and the Texas/Louisiana Gulf coast area (SAI, et al., 1995) as part of the Gulf of Mexico Air Quality Study (GMAQS).

The SAIMM requires external input of gridded terrain data (topographic heights, land and water coverage) and initial profiles of temperature and specific humidity. The SAIMM supports FDDA, a procedure by which observational data are incorporated into the prognostic model simulation using the Newtonian relaxation or "nudging" technique (Stauffer and Seaman, 1990; Stauffer et al., 1991). Using this methodology, one or more of the time-dependent variables are relaxed or "nudged" toward observed values during the course of the simulation. The nudging is effected by the addition of artificial tendency terms to the prognostic model equations. The general form of the prognostic equation for a variable a is

$$\frac{\partial a}{\partial t} = F(a,x,t) + G \times w_t \times w_{xyz} \times (a' - a)$$

The first term on the right-hand side of this equation, F, represents all of the model's physical processes. The second term is the nudging term. G determines the relative weight of the nudging term with respect to the model's physical processes. Typical values of G are 10^{-3} s^{-1} for strong nudging and 10^{-4} s^{-1} for moderate nudging. The variables w_t and w_{xyz} are temporal and spatial weighting functions, respectively, and the quantity a' represents the observed value.

Incorporation of observational data into the prognostic model simulation using FDDA should improve the agreement between the observations and the prognostic model results. The influence of the data may be propagated throughout the simulation and thus may also improve the simulated fields in areas removed from observations.

APPLICATION OF THE SAIMM TO SOUTHEAST TEXAS

The modeling domain encompasses the Houston metropolitan area and the Beaumont/Port Arthur area, as well as Corpus Christi, Victoria, and a portion of the Gulf of Mexico. The origin of the SAIMM domain is 6 km Easting and 3002 km Northing in Zone 15 UTM coordinates and the domain consists of 124 grid cells in the west-east direction and 112 grid cells in the south-north direction. The horizontal resolution is 4 km. Nineteen vertical levels were used. Table 3-1 summarizes the vertical resolution.

TABLE 3-1. Vertical structure of the SAIMM modeling domain for application to the Texas Gulf Coast.

Level	Height (m agl)	Level	Height (m agl)
1	10	11	1400
2	50	12	1800
3	100	13	2600
4	150	14	3400
5	200	15	4200
6	300	16	5000
7	400	17	6000
8	550	18	7000
9	800	19	8000
10	1050		

In the initial application, the SAIMM was exercised without FDDA to test the response of the model to the initial conditions, boundary conditions, and input parameters. The initial simulation also serves as a basis for evaluation of the data assimilation procedure employed in subsequent simulations. Input parameters for the initial simulation included the specification of spatially varying surface characteristics (e.g., roughness length or soil moisture availability). Results of the initial simulation were characterized by noisy temperature and humidity fields and what appeared to be a spurious, or unrealistic, eddy located over the Houston area. It was concluded that the model responded unfavorably to the somewhat noisy gridded fields of surface characteristics, and therefore, subsequent simulations used constant surface characteristics. Similarly, the input file that contains the fractional coverage of land and water was modified because it contained high-resolution information that the model is not expected to respond to (such as small bodies of water located inland).

Application of the SAIMM to Southeast Texas for the 23–25 October 1992 and 31 August – 2 September 1993 ozone episodes included (1) specification of the SAIMM input parameters, (2) preprocessing of the surface and upper-air meteorological data, (3) preparation of the FDDA analyses, (4) exercise of the SAIMM, and (5) graphical and statistical analysis of the results. Input simulation parameters include sea-surface temperature, time step, surface characteristics, and nudging coefficients. Input parameters used in this application are summarized in Table 3-2. The sea-surface temperature was based on buoy measurements for 23–25 October 1992. As no buoy data were available for the 31 August – 2 September 1993 episode, the sea surface temperature was estimated based on buoy data for the two GMAQS episodes, 17–20 August and 6–11 September 1993.

Meteorological data from several sources were used to prepare gridded fields for data assimilation and for evaluation of the meteorological fields. Wind, temperature, and humidity data were provided by TNRCC and quality-assured by SAI. The database was supplemented with data acquired from the National Climatic Data Center (NCDC).

TABLE 3-2. Input parameters for application of the SAIMM to the Texas Gulf Coast.

Parameter	Value
Time step (s)	60
Horizontal filter coefficient	0.05
Vertical filter coefficient	0.0
Sea surface temperature (°C):	
23–25 October 1992	30.8
31 August – 2 September 1993	29.8
Roughness length (cm)	50
Soil thermal diffusivity (cm^2s^{-1})	0.005
Albedo	0.2
Soil specific heat ($g^{-1}K^{-1}$)	0.25
Soil moisture availability parameter	0.25
Soil density ($g\ cm^{-3}$)	1.8
Nudging coefficients (s^{-1}):	
Wind	10^{-3}
Temperature/humidity	10^{-4}

Locations of the surface and upper-air meteorological monitoring sites are provided in Section 2.

Preparation (preprocessing) of the meteorological data for FDDA includes temporal interpolation of the data to the assimilation time interval (hourly) and vertical interpolation of the upper-air wind, temperature, and humidity data to the SAIMM levels. A temporal influence range of 3 hours was used for the surface wind data and 12 hours was used for the upper-air data. The interpolated data were plotted and examined for spatial and temporal consistency.

Upper-air virtual temperature data, measured by Radio Acoustic Sounding Systems (RASS), were converted to air temperature using surface humidity and temperature data. For each of the RASS monitoring sites, the surface virtual temperature was calculated. The difference between the virtual temperature and the observed air temperature, estimated using the surface data, was then assumed to apply throughout the mixed layer.

Gridded fields of wind, temperature, and specific humidity for FDDA were calculated using an objective analysis procedure. The scheme employs an inverse-distance-squared interpolation procedure to grid the variables at each model level for each assimilation time. The interpolation is governed by a number of user-specified parameters including the maximum radius of influence, number of stations to be used in the interpolation, and number of smoothing passes. The maximum radius of influence should be based on data representativeness (which may vary under different meteorological conditions) and should reflect the limiting influence of terrain features on the interpolation of data. The

same values of interpolation parameters are used for the entire grid. A 160-km maximum radius of influence was used for the surface wind data and 800 km was used for the upper-air data. Note that it is not necessary that every grid point be influenced by an observation. The interpolation of data to a grid point was further limited to the four nearest observation points at the surface and aloft.

Following interpolation of the data, a spatial weighting factor was assigned to each grid cell depending on data availability. This factor ranged from 1.0 at the data point to 0.0 within a user-specified radius of influence. The weighting factor determines the strength of the nudging (or data assimilation) at each grid point in the domain. The weighting coefficients are larger near the observation sites (the nudging is stronger in these cases). Moderate nudging ($G = 10^{-3}$) of the winds and weak nudging ($G = 10^{-4}$) of the temperature and moisture variables were applied.

All available meteorological data, including the surface temperature and moisture data, were assimilated into the simulation. Results of previous applications of the SAIMM to the southeast Texas area, without the incorporation of surface temperature and moisture data, suggested that the observed diurnal variation in surface temperature was not well simulated. Accurate simulation of the surface thermodynamic fields may be important for proper simulation of mesoscale circulations such as the sea breeze. Therefore, the SAIMM has recently been updated to accommodate the assimilation of surface temperature and moisture into the simulation. The surface temperature nudging technique employs the assumption that the potential temperature is constant within the planetary boundary layer (PBL) (Anthes, 1987; Garratt et al., 1982). The simulated temperatures were nudged throughout the PBL using surface potential temperature; upper-air temperature data were used above the PBL.

SIMULATION RESULTS FOR 23–25 OCTOBER 1992

The simulated meteorological fields are described in this section. The discussion focuses on 24 and 25 October 1992, the primary episode days. Horizontal cross section plots of the simulated winds for 10, 300, and 1050, and 1800 meters above ground level (m agl) at 0400, 1000, 1600, and 2200 CST are shown in Figures 3-1 and 3-2. (All figures are at the end of this section.) Observed wind vectors are overplotted in bold. Note that because the daytime maximum mixing heights for both episodes are nearly always less than 1800 m agl, this level is used to represent the wind fields above the mixed layer. Plots of the surface-layer temperature and specific humidity are shown in Figures 3-3 through 3-6.

Wind Fields

At 0400 CST on 24 October, the simulated near-surface winds are generally from the northwest at 2–3 ms^{-1} along the Texas coast (Figure 3-1a). Winds are from the west in the Houston area and light and variable in the Beaumont/Port Arthur area. Simulated upper-air winds are generally from the northeast with wind speeds of 3–5 ms^{-1} at 300 m agl and 5–7 ms^{-1} at 1050 and 1800 m agl. At 1000 CST, surface winds in the Houston

area are from the northwest and wind speeds have increased somewhat (Figure 3-1b). Surface winds in the Beaumont/Port Arthur area are from the north. Upper-layer winds at 300 m agl are from the northeast over Houston and from the north over Beaumont/Port Arthur. At 1050 and 1800 m agl, winds are northerly, with some northeasterly winds in the southwestern portion of the domain. During the afternoon, southerly components develop over the gulf and along the coast, west of Jefferson County at the surface and at 300 m agl (Figure 3-1c). As indicated by the observed wind vectors (bold), the gulf breeze does not penetrate the Houston area at 1600 CST; this feature is replicated very well in the simulated fields. Similarly, the limited inland extent of the gulf breeze in eastern Texas and southwestern Louisiana is well simulated. Northerly winds continue aloft during the afternoon and evening. Surface winds at 2200 CST are southwesterly along the coast as well as in the Houston/Galveston area while winds in the Beamont/Port Arthur area are easterly (Figure 3-1d). Strong northeasterly winds near 10-15 ms^{-1} develop at 1800 m agl.

Early morning surface winds on 25 October are from the west over most of the gulf and in the Corpus Christi area (Figure 3-2a). In Houston, surface winds are weak (near 1 ms^{-1}) and from the southwest. Some easterly components are evident in the Beaumont/Port Arthur area; a convergence zone is located northwest of Port Arthur. Winds aloft are westerly at 300 m agl and from the north-northeast at 1050 and 1800 m agl. At 1000 CST, winds from the west and southwest continue at the surface (Figure 3-2b). Although the observed surface winds are characterized by more variability than the simulated surface winds, wind speeds are generally well simulated in Houston as well as in the Beaumont/Port Arthur area. At 300 m agl, winds over Houston continue from the west while winds at 1050 and 1800 m agl are northwesterly and northerly, respectively. Surface winds at 1600 CST are characterized by onshore winds (4–6 ms^{-1}) along the entire coast (Figure 3-2c). The gulf breeze penetrates relatively far inland, affecting the Victoria, Houston, Beaumont/Port Arthur, and Lake Charles urban areas. The onshore flow is evident at 300 m agl as well. In the evening, surface winds decrease in speed and become southwesterly again (Figure 3-2d). Strong wind shear characterizes the upper-air winds over Houston, where winds at 300 m agl from the southwest near 10 ms^{-1} change to northeasterly winds at more than 15 ms^{-1} at 1800 m agl.

Temperature and Humidity Fields

In past applications of the SAIMM, simulated surface temperature fields were characterized by fairly flat spatial and temporal distributions. The updated data assimilation scheme employed in this application of the SAIMM allows for much improved replication of the observed surface temperature data.

Figure 3-3 illustrates the simulated surface temperature fields for 24 October. At 0400 CST, simulated surface temperatures are between 16 and 18°C inland and between 20 and 25°C over the gulf. The absence of a strong coastal gradient in surface temperatures for this episode is most likely due to persistent northerly flow aloft. During the day, surface temperatures inland increase to 24°C at 1000 CST and to 28°C at 1600 CST. In the evening, temperatures along the coast are between 20 and 22°C; a few degrees cooler than temperatures farther inland in areas that were not affected by the daytime onshore flow.

The diurnal variation in simulated surface temperature for 25 October is illustrated in Figure 3-4. Temperatures on this day are generally 1–2°C warmer than for the previous day. In the Houston area, surface temperatures warm up to 25°C at 1000 CST and to 30°C at 1600 CST. Afternoon temperatures are a few degrees cooler in the Beaumont/Port Arthur area. In the evening, a relatively strong temperature gradient develops along the coast.

Simulated surface specific humidities at 0400 CST on 24 October range from 9 gkg^{-1} over land to 14 gkg^{-1} over the gulf (Figure 3-5). On this day, specific humidities in the Houston and Beaumont/Port Arthur areas are between 10 and 12 gkg^{-1}. The humidity is generally higher by about 1–2 gkg^{-1} on 25 October (Figure 3-6). The relatively strong onshore flow on this day, increases humidities in the afternoon to near 15 gkg^{-1} at Galveston, Texas City, Smith Point, and in the Beaumont/Port Arthur area.

Vertical Cross-Sections of Wind and Potential Temperature

Vertical cross-sections of the simulated wind and potential temperature fields are shown in Figures 3-7 through 3-10. These plots illustrate the vertical and temporal evolution of the simulated sea breeze. The y-axis represents the vertical dimension and the x-axis represents the south-north direction (y-z section). Wind vectors represent horizontal wind components and may be interpreted similarly to the wind vectors plotted on the x-y cross-section plots; the vertical variation of potential temperature is indicated by the contours. Figure 3-7 shows a y-z section along west-east grid cell number 75; it starts over the Gulf, approximately 50 km south of Galveston Island (south-north grid cell number 47) and ends north of Baytown (south-north grid cell number 84). Approximate locations of Galveston Island, Texas City, and Baytown are indicated on Figure 3-7a. At 0400 CST on 24 October, winds are northwesterly in the lower 300 m agl and northeasterly up to 2000 m agl. The strong vertical gradients in the potential temperatures in the northern portion of the section suggests cooler temperatures over land. Figures 3-7b and 3-7c suggest that the sea breeze onset occurred between 1000 and 1600 CST. At 1600 CST, the sea breeze is evident along the entire section, up to approximately 300 m agl. At this time, wind speeds are 3 ms^{-1} over Galveston and 1 ms^{-1} in the Baytown area. The vertical extent of the onshore flow, which has become more southwesterly, increases during the evening and appears to extend up to 500 m agl at 2200 CST (Figure 3-7d).

Figure 3-8 shows the y-z sections for 25 October. On this day, sea breeze onset occurs somewhat earlier; Figure 3-8b indicates weak southwesterly components over land at 1000 CST. The vertical extent of the onshore flow is about 800 m agl at 1600 CST (Figure 3-8c). A strong wind-shear zone develops at level 10 (1050 m agl), where the southwesterly winds transition to the overlying, very strong, northerly winds aloft.

Comparison with Observed Data

Meteorological statistics are computed for quantitative examination of the simulation results. The statistics compare the mean predicted (simulated) and the mean observed values, in addition to the mean unsigned error (MUE) and the mean residual (MRES).

These values are computed for every hour of each simulation day for all SAIMM vertical levels. Additionally, cumulative statistics (over all 24 hours) are computed for each day. The MUE and the MRES are calculated with the following equations:

$$\textit{Mean Unsigned Error} = \frac{\sum_{i=1}^{N} |S_i - O_i|}{N}$$

$$\textit{Mean Residual} = \frac{\sum_{i=1}^{N} (S_i - O_i)}{N}$$

S_i is the ith simulated value, O_i is the ith observed value, and N is the number of observed values.

Statistics were calculated for all episode days and 19 vertical levels. Daily mean simulated and observed values for wind direction, wind speed, u and v components, temperature, and specific humidity for 23–25 October 1992 at SAIMM level 1 (surface), level 6 (300 m agl), level 10 (1050 m agl), and level 12 (1800 m agl) are summarized in Table 3-3. The corresponding mean residuals (MRES) and mean unsigned errors (MUE) are shown in Table 3-4. Plots of the hourly MUE for surface wind speeds and directions are illustrated in the form of barplots in (Figure 3-9).

Overall, observations are well represented in the simulated fields. Simulated mean wind speeds are somewhat weaker than observed at the surface as well as aloft. The mean residual at the surface is -0.4 ms^{-1} and -0.5 ms^{-1} on 24 and 25 October, respectively. Replication of the observed wind directions is fairly good. While comparison of the mean simulated and observed wind directions may suggest poor performance for levels 10 and 12, the errors are not large; mean unsigned errors at level 10 and 12 range from 3.5 degrees to 17.0 degrees, which is quite good. Deviations from observed wind directions at the surface are within 26 degrees for all days.

Observed temperatures aloft are well represented on all three days. Mean simulated surface temperatures are somewhat higher than observed on 24 October and lower than observed on 25 October. Mean unsigned errors are near 2°C, while mean residuals range from 1.1°C to -0.4°C. The lower residuals indicate overestimation as well as underestimation of surface temperatures. Mean simulated specific humidities are higher than observed at the surface; unsigned errors are between 1.3 and 1.6 gkg^{-1}. Errors in simulated specific humidity decrease with height, which may suggest that the soil moisture availability parameter was set too high for this episode.

Figure 3-9 illustrates the ability of the model to simulate the diurnal variations in the surface airflows for this episode. With a few exceptions, the simulated surface wind speeds are within 1 ms^{-1} of the observed wind speeds. The highest errors in wind speed occur at 0800 and 1600 CST on both days. Representation of the observed wind directions is good during the morning and evening hours and is generally less good between 1000 and 1600 CST. This is expected as this time period is associated with

TABLE 3-3. Comparison of mean simulated and observed values for 23–25 October 1992.

	Level 1, 10 m agl		Level 6, 300 m agl		Level 10, 1050 m agl		Level 12, 1800 m agl	
	Sim	Obs	Sim	Obs	Sim	Obs	Sim	Obs
23 October								
Wind direction (°)	100	108	99	95	81	83	73	74
Wind speed (m s^{-1})	2.3	2.4	5.3	5.8	6.3	6.6	6.8	7.0
U-component (m s^{-1})	−1.7	−1.6	−4.2	−4.2	−4.9	−5.0	−4.5	−4.4
V-component (m s^{-1})	0.0	−0.1	−0.3	−0.7	−0.4	−0.7	−2.6	−2.9
Temperature (°C)	22.6	21.5	22.3	22.0	16.3	16.4	11.4	11.2
Humidity (g kg^{-1})	12.7	11.4	12.0	12.0	7.1	7.2	2.9	2.8
24 October								
Wind direction (°)	205	235	153	170	170	215	81	122
Wind speed (m s^{-1})	1.6	2.0	3.2	3.6	5.4	5.9	6.3	6.4
U-component (m s^{-1})	0.3	0.7	−0.2	0.0	−1.0	−0.7	−1.7	−1.3
V-component (m s^{-1})	0.0	−0.2	−0.9	−1.3	−4.6	−5.1	−5.5	−5.7
Temperature (°C)	22.2	21.6	23.0	22.7	16.4	16.4	11.0	10.9
Humidity (g kg^{-1})	11.1	10.3	10.0	10.0	7.0	6.9	3.2	3.2
25 October								
Wind direction (°)	211	212	239	239	136	185	84	114
Wind speed (m s^{-1})	1.8	2.3	4.9	5.4	3.5	3.7	5.3	5.8
U-component (m s^{-1})	0.6	0.8	3.2	3.3	0.3	0.7	−1.9	−1.7
V-component (m s^{-1})	1.2	1.4	1.6	1.8	−2.5	−2.1	−4.5	−4.8
Temperature (°C)	22.8	23.1	23.8	23.5	17.2	17.3	11.4	11.2
Humidity (g kg^{-1})	11.5	10.2	9.9	10.0	7.3	7.4	4.9	4.8

TABLE 3-4. Statistical comparison of simulated and observed values for 23–25 October 1992.

	Level 1, 10 m agl		Level 6, 300 m agl		Level 10, 1050 m agl		Level 12, 1800 m agl	
	MRES	MUE	MRES	MUE	MRES	MUE	MRES	MUE
23 October								
Wind direction (°)	−6.5	19.3	4.0	11.5	3.5	5.2	3.7	4.3
Wind speed (m s^{-1})	−0.2	0.8	−0.5	0.8	−0.4	0.5	−0.2	0.4
U-component (m s^{-1})	−0.1	0.8	0.0	0.7	0.1	0.5	−0.2	0.5
V-component (m s^{-1})	0.1	0.6	0.4	0.7	0.4	0.5	0.4	0.4
Temperature (°C)	1.1	2.0	0.2	0.5	0.0	0.6	0.3	0.5
Humidity (g kg^{-1})	1.2	1.6	−0.0	0.5	−0.1	1.0	0.1	0.2
24 October								
Wind direction (°)	0.2	25.8	5.5	18.4	5.0	6.6	4.3	5.6
Wind speed (m s^{-1})	−0.4	0.7	−0.3	0.6	−0.6	0.8	−0.1	0.6
U-component (m s^{-1})	−0.4	0.7	−0.3	0.7	−0.3	0.9	−0.5	0.6
V-component (m s^{-1})	0.1	0.6	0.4	0.7	0.5	0.7	0.2	0.5
Temperature (°C)	0.6	2.2	0.3	0.4	0.1	0.5	0.1	0.4
Humidity (g kg^{-1})	0.8	1.3	0.0	0.5	0.1	0.3	−0.1	0.2
25 October								
Wind direction (°)	−4.8	22.6	0.6	9.1	7.1	17.0	−3.8	12.2
Wind speed (m s^{-1})	−0.5	0.8	−0.5	0.9	−0.2	0.6	−0.5	1.1
U-component (m s^{-1})	−0.2	0.7	−0.2	0.8	−0.4	0.7	−0.2	0.7
V-component (m s^{-1})	−0.2	0.8	−0.2	0.7	−0.4	0.7	0.3	1.0
Temperature (°C)	−0.4	2.1	0.3	0.5	0.0	0.5	0.1	0.6
Humidity (g kg^{-1})	1.3	1.6	−0.1	0.3	0.0	0.2	0.1	0.2

abrupt flow reversals at many monitoring sites. The highest MUE is about 45 degrees and occurs at 1600 CST on 24 October.

SIMULATION RESULT FOR 31 AUGUST - 2 SEPTEMBER 1993

Plots of the simulated winds for 10, 300, and 1050, and 1800 m agl at 0400, 1000, 1600, and 2200 CST on 1 and 2 September are shown in Figures 3-10 and 3-11, respectively. Observed wind vectors are overplotted in bold. Plots of the surface-layer temperature and specific humidity are shown in Figures 3-12 through 3-15, respectively.

Wind Fields

The simulated wind fields for this episode suggest the presence of an anticyclone centered over the Texas Gulf Coast area for the duration of the period. Early morning surface winds on 1 September are weak and from the northwest over Houston and near 2 ms^{-1} and from the west over Beaumont/Port Arthur (Figure 3-10a). At 300 and 1050 m agl, winds are southeasterly over Corpus Christi and north to northwesterly over Southeast Texas. At 1800 m agl, southerly and easterly winds occur over most of the domain. At 1000 CST, surface wind speeds increase to 3-4 ms^{-1} and the airflow becomes northwesterly over most of the domain (Figure 3-10b). Aloft, wind speeds are near 5 ms^{-1} and the anticyclonic circulation persists. Over Houston, winds back from northwesterly at 300 m agl to southerly at 1800 m agl. At 1600 CST, surface winds are from the south over Galveston Bay and from the west-southwest over Houston, Beaumont/Port Arthur, and southwest Louisiana (Figure 3-10c). In the evening, surface winds become weak and variable in Beaumont/Port Arthur and southwesterly elsewhere (Figure 3-10d). Winds aloft over Houston are southwesterly at 300 m agl and northwesterly at 1050 and 1800 m agl. As is evident in Figure 3-10d, the center of the high-pressure system is located northwest of Houston. The recirculating airflow around this high-pressure system suggests a strong potential for increased residence times of air pollutants in the region.

On 2 September at 0400 CST, surface winds are southerly in the Corpus Christi area and westerly over Houston and Beaumont/Port Arthur (Figure 3-11a). At 300 m agl, winds over Houston are from the west and wind speeds are very high (8–10 ms^{-1}). The 1050 and 1800 m agl wind fields show an anticyclonic circulation centered approximately over Galveston and Sabine, respectively. To the west of the circulation center, over the Houston area, winds are from the south and southeast and to the east, over southwestern Louisiana, winds are from the northwest. At 1000 CST, surface wind speeds throughout the domain increase to approximately 3–4 ms^{-1} (Figure 3-11b). Aloft, winds are westerly at 300 m agl, southwesterly at 1050 m agl, and southerly at 1800 m agl. During the afternoon, southerly flow develops throughout the domain (Figure 3-11c). Along the gulf coast, surface winds are southwesterly, and around Galveston Bay, winds are from the south and southeast. Unlike the previous day, afternoon winds are southerly throughout most of Louisiana and east Texas. Winds aloft are predominantly from the south at 300 and 1050 m agl. Above the mixed layer (1800 m agl), winds are southerly over Corpus Christi, southwesterly over Houston, and northerly over Port Arthur and Lake Charles. Southerly components dominate the wind fields at all levels at

2200 CST (Figure 3-11d). In Houston, simulated surface wind speeds are weaker than observed.

Temperature and Specific Humidity Fields

Plots of the simulated surface temperature fields for 0400, 1000, 1600, and 2200 CST are shown in Figure 3-12. The high temperatures observed during this episode are replicated in the simulated fields. On 1 September, near-surface temperatures over the Gulf are between 28 and 29°C during the night and between 29 and 30°C during the day; a diurnal variation of approximately 1°C. Inland, surface temperatures at 0400 CST are near 22°C while temperatures along the coast are between 24°C and 25°C (Figure 3-12a). During the afternoon, simulated temperatures increase to 33°C in the Houston area (Figures 3-12c). Surface temperatures decrease slowly and are still 28°C in the Houston area at 2200 CST (Figure 3-12d). On 2 September, surface temperatures at 1000 CST are more than 30°C in the Houston and Beaumont/Port Arthur areas and maximum simulated temperatures in Houston on this day reach approximately 33°C (Figures 3-13c and d).

Figures 3-14 and 3-15 show the simulated surface specific humidity fields for 1 and 2 September. On 1 September at 0400 CST, high humidities near 18 gkg^{-1} occur along the coast; elsewhere values are generally near 16 gkg^{-1}. Daytime specific humidities in the Houston and Beaumont/Port Arthur areas are between 16 and 17 gkg^{-1}. On 2 September, the specific humidity is somewhat higher with values near 17 gkg^{-1} inland and 19 gkg^{-1} over the Gulf.

Vertical Cross-Sections of Wind and Potential Temperature

Vertical cross-sections (y-z sections) of the simulated wind and potential temperature fields along east-west grid cell 75 are shown in Figures 3-16 through 3-19. During the first half of 1 September, winds are from the northwest below 800 m agl and veer to the south aloft (Figure 3-16a and b). As for 24–25 October, the onshore flow is evident in the 1600 CST section (Figure 3-16c). On 2 September, westerly winds below 600 m agl in the morning change to southerly with the onset of the sea breeze in the afternoon. The sea-breeze flow appears to extend up to approximately 1000 m agl and wind speeds are about 4–5 ms^{-1} (Figure 3-17c). In the evening, southerly winds develop at all levels (Figure 3-17d).

Comparison With Observed Data

Tables 3-5 and 3-6 summarize the daily mean simulated and observed values, the mean residuals (MRES), and mean unsigned errors (MUE) for wind direction, wind speed, u and v components, temperature, and specific humidity for the 31 August - 2 September 1993 episode at SAIMM level 1 (surface), level 6 (300 m agl), level 10 (1050 m agl), and level 12 (1800 m agl). Plots of the hourly MUE for surface wind speeds and wind directions are illustrated (Figure 3-18).

TABLE 3-5. Comparison of mean simulated and observed values for 31 August–2 September 1993.

	Level 1, 10 m agl		Level 6, 300 m agl		Level 10, 1050 m agl		Level 12, 1800 m agl	
	Sim	Obs	Sim	Obs	Sim	Obs	Sim	Obs
31 August								
Wind direction (°)	200	200	231	234	249	245	190	187
Wind speed (m s^{-1})	2.0	2.5	4.0	4.8	4.2	4.7	3.3	3.9
U-component (m s^{-1})	0.3	0.3	1.8	2.0	1.4	1.3	−0.1	−0.3
V-component (m s^{-1})	1.5	1.6	1.6	1.5	1.7	1.8	1.5	1.5
Temperature (°C)	27.9	28.0	26.0	19.7	20.2	16.0	14.4	10.1
Humidity (g kg^{-1})	17.5	18.2	15.8	15.9	12.0	11.8	9.2	9.2
1 September								
Wind direction (°C)	251	251	260	259	251	234	175	169
Wind speed (m s^{-1})	2.1	2.4	4.9	5.3	3.6	4.1	3.8	4.3
U-component (m s^{-1})	1.3	1.3	3.2	2.9	0.9	0.8	−0.9	−1.0
V-component (m s^{-1})	0.4	0.3	0.0	−0.3	−0.5	−0.5	0.6	0.5
Temperature (°C)	28.1	28.6	27.2	27.0	20.6	20.7	14.8	15.1
Humidity (g kg^{-1})	17.0	17.1	15.7	15.5	13.6	13.1	10.6	10.3
2 September								
Wind direction (°)	219	221	234	230	210	202	202	201
Wind speed (m s^{-1})	2.5	3.1	5.8	6.2	3.9	4.3	2.9	3.3
U-component (m s^{-1})	0.9	1.0	3.5	3.3	1.1	0.9	0.4	0.2
V-component (m s^{-1})	1.6	1.9	2.6	2.8	2.4	2.6	1.9	1.9
Temperature (°C)	27.9	29.0	27.0	26.6	21.1	21.4	15.4	15.8
Humidity (g kg^{-1})	17.9	17.0	16.8	17.0	13.0	12.1	9.6	9.4

TABLE 3-6. Statistical comparison of simulated and observed values for 31 August–2 September 1993.

	Level 1, 10 m agl		Level 6, 300 m agl		Level 10, 1050 m agl		Level 12, 1800 m agl	
	MRES	MUE	MRES	MUE	MRES	MUE	MRES	MUE
31 August								
Wind direction (°)	−1.6	16.7	−3.0	15.5	2.1	10.0	3.0	9.3
Wind speed (m s^{-1})	−0.5	0.6	−0.8	1.0	−0.5	0.6	−0.5	0.6
U-component (m s^{-1})	0.0	0.5	−0.2	0.8	0.1	0.4	0.1	0.4
V-component (m s^{-1})	−0.1	0.6	0.1	1.1	−0.1	0.6	0.0	0.5
Temperature (°C)	−0.2	1.3	6.3	6.7	4.2	4.7	4.3	4.5
Humidity (g kg^{-1})	−0.6	1.3	−0.1	0.6	0.3	0.6	0.0	0.3
1 September								
Wind direction (°)	−0.5	15.4	−4.0	13.7	−2.3	9.7	−0.1	8.2
Wind speed (m s^{-1})	−0.3	0.6	−0.4	1.0	−0.5	0.7	−0.5	0.6
U-component (m s^{-1})	−0.1	0.6	0.2	1.0	0.2	0.6	0.1	0.6
V-component (m s^{-1})	0.0	0.5	0.3	1.0	0.0	0.6	0.1	0.5
Temperature (°C)	−0.4	1.2	0.1	0.6	−0.1	0.4	−0.3	0.4
Humidity (g kg^{-1})	−0.2	1.1	0.2	0.3	0.6	0.8	0.3	0.4
2 September								
Wind direction (°)	−2.5	10.3	4.2	13.6	5.6	9.5	0.6	7.7
Wind speed (m s^{-1})	−0.6	0.9	−0.4	1.0	−0.4	0.5	−0.4	0.5
U-component (m s^{-1})	−0.1	0.6	0.2	0.9	0.3	0.5	0.5	0.2
V-component (m s^{-1})	−0.3	0.7	−0.2	1.1	−0.1	0.4	0.0	0.4
Temperature (°C)	−1.1	1.4	0.4	0.7	−0.3	0.5	−0.4	0.5
Humidity (g kg^{-1})	0.8	1.2	−0.2	0.4	0.8	0.9	0.2	0.3

The statistics for this episode indicate that observations are well represented in the simulated fields. Model performance for the wind fields is quite good for all days. The simulated mean wind speeds are somewhat weaker than observed at all levels; errors in the simulated wind speeds are no more than 1 ms^{-1} for any of the levels shown in Table 3-6. As indicated by the mean values as well as the errors, wind directions at the surface and aloft are also well simulated; mean unsigned errors range from 7.7 degrees (for level 12 on 2 September) to 16.7 degrees (level 1 on 31 August).

Surface temperatures are generally underestimated for level 1 (30 m agl) on all three days. Mean unsigned errors are between 1.2°C and 1.4°C. These errors could be attributed to the difference between the height at which surface temperatures are measured and the height of the first level at which temperatures are simulated, which is 30 m agl. The high errors for the upper-level temperatures on 31 August indicate that the initial temperature sounding may not have been representative of the mean temperature conditions within the domain. As for the 23–25 October episode, the specific humidities are generally better simulated aloft than at the surface. The mean unsigned errors are between 1.1 and 1.3 gkg^{-1} at the surface and less than 1 gkg^{-1} aloft.

Figure 3-18 shows the hourly variation in MUE for the surface winds on 1 and 2 September. These plots suggest that the diurnal variations in surface winds are well represented in the simulated fields. Hourly wind speed MUE is always less than 1.5 ms^{-1} and less than 1 ms^{-1} for most of the period. Maximum MUE in wind direction is 28 degrees. As expected, the highest errors in wind direction occur during periods of weak wind speeds in the early morning. On both days, errors in wind direction are also the highest during the early afternoon, from about 1200 to 1400 CST, when the sea breeze arrival causes wind direction reversals along the bay and gulf coasts.

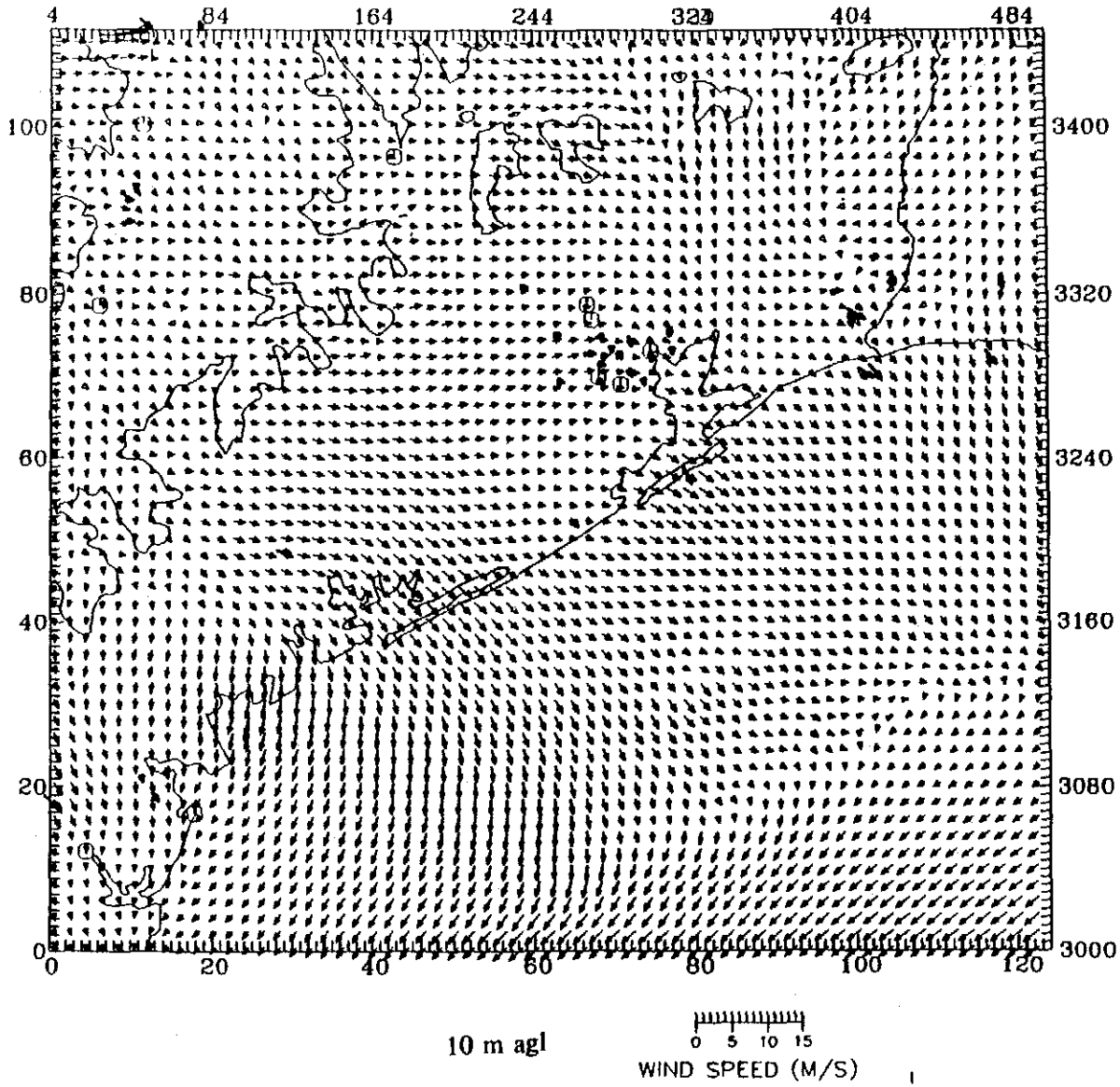

FIGURE 3-1a. SAIMM wind fields for the Southeast Texas area for 0400 CST 24 October 1992.

4 INPUT PREPARATION

The data and techniques used in preparing the UAM-V inputs for the southeast Texas modeling application are described in this section. The meteorological and air quality data were primarily provided by the TNRCC; supplemental meteorological data were obtained from the National Climatic Data Center (NCDC). To ensure the successful application of the UAM-V using the large quantity of field data available for both episodes, the data were plotted and quality assured before using them in preparing inputs.

As noted earlier, the modeling emission inventories were prepared by the TNRCC.

METEOROLOGICAL INPUTS

The UAM-V requires meteorological input files containing hourly, three-dimensional fields of winds (WIND), temperature (TEMPERATUR), water vapor concentration (H2O), vertical exchange coefficients (or diffusivities) (VDIFFUSION), and atmospheric pressure (HEIGHT). All meteorological inputs used in this application were generated using the SAIMM as described in Section 3. This section describes the procedure for converting the simulated fields to the format and vertical resolution used by the UAM-V.

The general procedure for converting the output from the SAIMM to input for the UAM-V is described by Schulhof and Douglas (1992). The SAIMM vertical layer heights were transformed from the SAIMM vertical coordinate system to the terrain-parallel, fixed-height vertical coordinate system employed in the UAM-V. The SAIMM output was linearly interpolated to the UAM-V layers. However, the vertical coordinate systems of the SAIMM and the UAM-V were defined such that the need for interpolation of the wind fields is minimized. Thus, the SAIMM wind fields are mapped almost directly to the UAM-V cell-centers 1 through 8 using SAIMM layers 1 (10 m agl), 2 (50 m agl), 4 (150 m agl), 6 (300 m agl), 8 (550 m agl), 10 (1050 m agl), 12 (1800 m agl), and 13 (2600 m agl), respectively. To minimize the potential for loss of emissions and entrainment of air of unknown composition through the model top, the O'Brien vertical velocity adjustment procedure (O'Brien, 1970), which minimizes vertical velocity at the top of the modeling domain, was invoked in preparing the UAM-V input wind fields.

The SAIMM specific humidity fields were converted to water vapor concentration in ppm by volume. Plots of the UAM-V-ready temperature, water vapor, and pressure fields are not presented in this section. The spatial and temporal variation of the temperature and humidity fields are discussed in Section 3.

The HEIGHT file defines the vertical structure of the UAM-V. This file contains the height of the layer interfaces and the atmospheric pressure for the midpoint of each layer, for each horizontal grid cell. Although the layer heights can vary in space and time, for this application they remain constant. Eight vertical layers were used, with interface heights at 20, 80, 220, 380, 720, 1380, 2120, and 3030 meters above ground level. The atmospheric pressure is used for the calculation of some chemical reaction rates and is based on SAIMM output.

The UAM-V allows for specification of wind fields, vertical exchange coefficients, and layer heights for each of the nested grids used in the simulation. Horizontal interpolation of the 4-km SAIMM fields was necessary to generate UAM-V input fields for the 16 km coarse-grid domain, and in some cases the 2-km nested grids. Note that the UAM-V reads coarse-grid temperature and humidity fields only; fields for the nested grids for these variables are calculated internally by the UAM-V. The same vertical structure was used for the coarse grid and all nested grids, and thus no HEIGHT file was specified for the nested grids.

The vertical diffusivities control the diffusion of pollutants between the UAM-V layers. In the SAIMM, the vertical diffusivities are estimated using a turbulent kinetic energy (TKE) scheme. These calculations are described briefly in the SAIMM user's guide (Kessler and Douglas, 1992) and in more detail by Ulrickson and Mass (1990). Vertical exchange coefficients exhibit a diurnal variation similar to mixing heights with maxima occurring during the afternoon. The afternoon fields are generally characterized by diffusivities that increase then decrease with height. The UAM-V layer interface at which the maximum values occur and the rate at which they decrease above the maximum may be used to infer the height of the mixed layer.

For this application, the SAIMM-generated vertical diffusivities were interpolated from the SAIMM vertical structure to the UAM-V layer interfaces and smoothed using four passes of a five-point smoothing routine. In addition, a land-use dependent minimum value was imposed at the interface between layers one and two in order to maintain a physically realistic well-mixed nocturnal boundary layer. The minimum values applied were 5 m^2s^{-1} over urban areas, 3 m^2s^{-1} over forested areas, and 1 m^2s^{-1} elsewhere.

Figures 4-1 and 4-2, at the end of this section, illustrate the vertical variation of the diffusivities for the 4-km nested grid at 1400 CST for 24 October 1992 and 1 September 1993, respectively. As expected, maximum diffusivities generally occur inland. For 24 October, the diffusivities peak at the interface between layers 4 and 5 (380 m) (Figure 4-1d) and decrease above layer 6 (1380 m) (Figure (4-1f). Similarly, on 1 September the high diffusivities are found inland and the maximum is located at the top of layer 5 (720 m) (Figure 4-2e), indicating that the simulated daytime mixing heights are somewhat higher for this episode than for the October 1992 episode.

AIR QUALITY INPUTS

Air quality inputs required by the UAM-V include initial concentrations of each of the chemical species (the AIRQUALITY file), hourly concentrations of each chemical species along the lateral boundaries of the outer, coarse-grid domain (the BOUNDARY

file), and hourly concentrations of each chemical species along the top boundary of the domain (TOPCONC). Observed air quality data for the surface, EPA-recommended continental background concentrations, and clean marine concentrations were used to set the initial and boundary concentrations.

Estimates of marine air concentrations are based on hydrocarbon samples collected off the coast of southern California (Moore et al., 1991). These air samples suggested a marine hydrocarbon concentration of around 10 ppbC. The marine hydrocarbons were split into CB-IV species using 76 percent PAR, 10 percent OLE, 3 percent ETH, and 11 percent aromatics, which were split equally between TOL and XYL. Trace amounts of FORM, ALD2, and other CB-IV species were assumed. To be consistent with this small amount of hydrocarbons, NO_x concentrations must also be small. Marine concentrations of NO2 and NO were set to 0.5 ppb and 0.0 ppb, respectively. The resulting marine air concentrations are summarized in Table 4-1. Table 4-2 summarizes the EPA-recommended default (or background) values.

TABLE 4-1. Marine air concentrations of CB-IV species (ppb).

NO	0.0	OLE	0.5000	OPEN	0.0010
NO2	0.5000	PAR	7.6000	PAN	0.0010
O3	40.0000	TOL	0.0786	PNA	0.0010
CO	200.0000	XYL	0.0688	H2O2	0.0010
ALD2	0.0500	ISOP	0.0010	HONO	0.0010
ETH	0.1500	CRES	0.0010	HNO3	0.0010
FORM	0.0500	MGLY	0.0010	NXOY	0.0001

TABLE 4-2. EPA default boundary concentrations of CB-IV species (ppb).

NO	0.0	OLE	0.3000	OPEN	0.0010
NO2	2.0000	PAR	14.9400	PAN	0.0010
O3	40.0000	TOL	0.1800	PNA	0.0010
CO	350.0000	XYL	0.0975	H2O2	0.0010
ALD2	0.5550	ISOP	0.1000	HONO	0.0010
ETH	0.5100	CRES	0.0010	HNO3	0.0010
FORM	2.1000	MGLY	0.0010	NXOY	0.0001

Initial Conditions

The AIRQUALITY file contains initial concentrations of the chemical species used in the Carbon-Bond IV chemical mechanism for the initial hour of the simulation. Where available, observed concentrations of ozone (O_3), carbon monoxide (CO), nitric oxide (NO), nitrogen dioxide (NO_2), and oxides of nitrogen (NO_x) were used to specify the initial concentrations. Surface-based observations were used in the lower 4 UAM-V layers (up to 380 m agl). Pseudo-sites were placed in areas away from monitoring sites and were assigned EPA-recommended continental background values for the land portion

of the domain. Values representative of clean marine air (as noted above) were used over the Gulf of Mexico below 380 m agl. Locations of the air quality monitoring sites for which data were available for the episode days, pseudo sites (indicated by the name BACK), and the region for which marine air concentrations were used (shaded area) are shown in Figure 4-3. Plots of the gridded initial concentrations for both episodes for ozone and NO_2 are shown in Figure 4-4.

Lateral Boundary Conditions

The BOUNDARY file contains concentrations of each of the chemical species along the lateral boundaries of the modeling domain. Concentrations along the entire southern and southern half of the eastern boundaries, for all levels, were specified using values representative of marine air. Because the areas to the north and west of the domain are primarily rural, EPA-recommended default concentrations were used for all levels and all times along these boundaries. Ozone observations for two monitoring sites (Ragley, LA and Le Bleu, LA) were averaged and used to specify the hourly boundary concentrations for the portion of the eastern boundary located over land. The observation-based values were used below the mixing height; EPA background values were used above.

Table 4-3 summarizes the observed ozone concentrations for the 23–25 October 1992 episode, averaged for Ragley, LA and Le Bleu, LA and the layer up to which they were

TABLE 4-3. Surface boundary concentrations for the portion of the eastern boundary located over land for the 23–25 October 1992 episode. Surface boundary values based on average concentrations for the Ragley, LA and Le Bleu, LA monitoring sites. "Height" column indicates the height up to which these values were assigned (based on simulated mixing heights).

	23 October		24 October		25 October	
Hour	Ozone (ppb)	Height (m)	Ozone (ppb)	Height (m)	Ozone (ppb)	Height (m)
0900	*	50	*	100	51	150
1000	46	150	53	150	64	300
1100	53	300	61	300	66	300
1200	58	550	61	550	67	550
1300	60	550	59	1050	70	550
1400	59	550	61	1050	74	1050
1500	58	1050	61	1050	79	1050
1600	52	1050	53	1050	70	550
1700	*	200	*	50	63	300
1800	*	100	*	50	49	150
1900	*	50	*	50	50	150
2000	*	50	*	50	52	150
2100	*	50	*	50	49	150

* Calculated value less than 40 ppb; background ozone concentration of 40 ppb assumed.

used. Because averaged ozone concentrations were near 4 pphm for the duration of the 1993 episode, background ozone concentrations were used for all boundaries for that episode.

Top Boundary Concentrations

The TOPCONC file contains pollutant concentrations at the top of the modeling domain. These concentrations remain constant in space and in time throughout the simulation period. No aircraft measurements were available for these episodes and, thus, EPA background concentrations were used for all species.

OTHER INPUTS

Land-Use Inputs

The UAM-V SURFACE file contains fractional coverage of each of 11 land-use categories. Land-use data are used by the UAM-V to calculate deposition rates for the chemical species and by the albedo/haze/ozone column preprocessor to estimate albedo and thus derive the photolysis rates. For this application, SURFACE files for the coarse grid and all nested grids were prepared by the TNRCC. The distribution of land-use categories for each grid is summarized in Table 4-4. Plots of the land use are shown in Figures 4-5 and 4-6.

TABLE 4-4. Distribution of land-use categories (in percent) used in the application of the UAM-V to the southeast Texas area.

	Domains			
Categories	16-km Grid	4-km Grid	2-km Grid (Houston)	2-km Grid (Beaumont/ Port Arthur)
Urban	2.6	5.0	9.9	5.6
Agricultural	24.1	26.5	46.9	21.2
Range	6.4	2.3	2.4	0.1
Deciduous Forest	4.0	3.9	4.0	3.7
Coniferous Forest	10.9	15.8	9.0	9.0
Mixed Forest	6.0	5.6	7.6	4.6
Water	43.1	35.7	16.3	35.0
Barren Land	0.6	0.6	0.8	0.3
Nonforest Wetland	2.2	4.7	3.0	20.3
Mixed Agricultural/Range	0.0	0.0	0.0	0.0
Rocky (low shrubs)	0.1	0.0	0.0	0.1

Chemistry Parameters

The CHEMPARAM file contains the list of species to be simulated and several other chemistry-related parameters including reaction rate constants, upper and lower bounds, activation energies, and reference temperatures. The chemistry parameters used for this application are those for the Carbon Bond IV (CB-IV) mechanism.

Albedo/Haze/Ozone Column and Photolysis Rates

Information about the surface albedo, atmospheric turbidity (haze), and ozone column are contained in the ALHZOZ file. The surface albedo values were derived based on the land-use data specified in the SURFACE file and range from 0.04 to 0.08. Ozone column data were estimated using NASA satellite data of daily global ozone measurements, archived by the National Space Science Data Center (NSSDC). Because values of turbidity are not well known, a value of 0.094, which is representative of rural conditions, was used throughout the domain. The RATES file contains tabulated photolysis rates or *J*-values for five key reactions: photolysis of NO_2, HCHO (two-product channels), O_3 (to form $O(^1D)$), and ALD2. Using the UAM-V light model preprocessor (SAI, 1995), rates are specified for a range of values of solar zenith angle, surface albedo, ozone column, and turbidity spanning all the conditions that may be encountered during the simulations.

5 TRACER SIMULATIONS

Inert tracer simulations are often used to evaluate the airflow patterns and assess the potential for the initial and boundary conditions to influence the simulated pollutant concentrations (e.g., ozone) in an actual simulation. For these simulations, the UAM-V is exercised in an unreactive mode (i.e., the chemistry is turned off). Simulated air parcels originating within the domain and along the lateral and top boundaries are tagged as initial condition, lateral boundary condition, and top boundary condition tracers, respectively. Advection of these tracers within, into, and out of the modeling domain is simulated using the UAM-V meteorological input fields, and the composition of each grid cell in terms of these tracers are calculated for each time step. The relative contribution of each tracer "species" indicates the potential of that tracer to influence the simulated pollutant concentrations within the grid cell in an actual simulation. The actual contribution from initial and boundary conditions can only be assessed by performing a full chemistry simulation with emissions.

For each episode, the tracer simulations were initiated at 0000 CST on the first day of the episode and run until the end of the episode period. Six tracers were used including the initial conditions, one for each of the four lateral boundaries, and for the top boundary. The tracers were assigned appropriate species names (e.g., initial conditions is IC and boundary conditions along the northern boundary is NBC). The contribution in percent of each of the species is calculated for each grid cell. Plots of the percent contribution of the initial and lateral boundary condition tracers for the surface layer are presented below for selected hours. No plots are shown for the top boundary tracers as their contribution to surface-layer concentrations were small.

23-25 OCTOBER 1992

Initial Condition Tracer

For this episode, the potential effects of the initial conditions are illustrated in Figure 5-1. This figure shows the percent contribution of the initial condition tracer (IC) for 1200 CST on 24 October, 36 hours after the simulation was initiated. As expected, most of the initial conditions have been advected out of the modeling domain, and the potential for the initial conditions to influence the simulation results in the Houston/Galveston and Beaumont/Port Arthur areas is small.

Boundary Condition Tracer

Figure 5-2 illustrates the potential contribution of each lateral boundary tracer for 1200 CST on 24 October. At this time, the northern boundary tracer (NBC) dominates the northern portion of the domain and the eastern boundary tracer (EBC) dominates the southern portion (Figure 5a and b). Potential contributions from the southern (SBC) and western boundary tracers (WBC) are small (Figure 5-2c and d). As a result of the persistent northerly flow that characterizes this episode, the northern boundary tracer (NBC) continues to be dominant on 25 October with potential contributions greater than 70 percent in Houston and the Beaumont/Port Arthur area grid cells (not shown).

31 AUGUST - 2 SEPTEMBER 1993.

Initial Condition Tracer

The contribution of IC tracer at 1200 CST on 1 September is illustrated in Figure 5-3. Relative to the boundary condition tracers, the potential contribution of the initial conditions are quite large in an area along the eastern boundary. The relatively high contribution of the IC tracer on the second day of the simulation may be attributed to the anticyclonic circulation (recirculation) that characterizes the airflow during this episode.

Lateral Boundary Tracer

The potential contribution of the lateral boundary tracers for 1200 CST 1 September is illustrated in Figure 5-4. As for the initial condition tracers, plots of the boundary tracers for this day are reflective of the anticyclonic circulation that characterizes the airflow during this episode. As indicated by Figures 5a-d, the NBC tracer dominates the northeast quadrant of the domain, the WBC tracer contributes to grid cells along the western boundary, the eastern boundary is not important, and the SBC tracer influences primarily areas over the Gulf. These plots suggest that none of the boundaries are expected to influence the simulation results significantly.

6 SUMMARY

This report summarizes the preparation of air quality and meteorological inputs for application of the UAM-V to the Southeast Texas nonattainment areas for two historical ozone episodes. Input preparation constitutes the basis of the UAM-V modeling analysis. The overall modeling study consists of evaluation of base-case model performance (statistical and graphical) and includes diagnostic and sensitivity analysis.

For this application of the UAM-V, meteorological inputs were generated using the Systems Applications International Mesoscale Model (SAIMM), a data assimilating prognostic model. To ensure accurate simulation of the thermally-driven airflows in the region (i.e, land-sea breeze circulations), a new four-dimensional data assimilation (FDDA) technique that accommodates the use of surface-based temperature and moisture data was employed. Successful application of the updated SAIMM was demonstrated using graphical and statistical analysis to compare the simulated fields with observations. Procedures for converting the SAIMM-derived meteorological fields into UAM-V-ready inputs were also described.

Inert UAM-V tracer simulations were performed to evaluate the potential influence of the initial and boundary conditions on simulated pollutant concentrations. Results indicate that (1) appropriate simulation periods were chosen for both episodes (i.e., most of the initial conditions were advected out of the modeling domain before simulation of the primary episode day); (2) persistent northerly flow showed a potentially large influence from the northern boundary for the 23-25 October 1992 episode; and (3) airflows associated with anticyclonic circulation patterns resulted in small potential influence from any of the lateral boundaries for the 31 August - 2 September 1993 episode.

REFERENCES

Anthes, R. A. 1983. Regional models of the atmosphere in middle latitudes. *Mon. Wea. Rev.*,111:1306-1335.

Anthes, R. A., E. Y. Hsie, and Y.-H. Kuo. 1987. "Description of the Penn State/NCAR Mesoscale Model Version 4 (MM4)." NCAR Technical Note (NCAR/TN282 + STR). Available from the National Center for Atmospheric Research, Boulder Colorado.

Douglas, S. G., R. C. Kessler, and J. Lester. 1992. "Preparation of Meteorological Fields for Air Quality Modeling Using Mesoscale Data Assimilation." Air and Waste Management Association Specialty Conference "Tropospheric Ozone and the Environment II," Atlanta, Georgia, November 4-7, 1991.

Douglas, S. G., N. K. Lolk, and S. Mitsutomi. 1993a. "Meteorological Modeling to Support Urban and Regional Photochemical Modeling of Los Angeles, Sacramento, and the Texas-Louisiana Gulf Coast." Air and Waste Management Association Conference, "Regional Photochemical Measurement and Modeling Studies," San Diego, November 8-12, 1993.

Douglas, S. G., G. E. Mansell, T. C. Myers, M. M. Jimenez, and D. L. Perry. 1995. "Application of UAM-V to the Northeast as Part of Phase I of the Modeling Ozone Cooperative (MOCA)." Systems Applications International, San Rafael, California (SYSAPP-95/049).

Douglas, S. G., S. B. Shepard, and J. L. Haney. 1993. "Photochemical Modeling of the Broader Sacramento Area: Base-Case Modeling Analysis." Systems Applications International, San Rafael, California (SYSAPP-93/056).

Garratt, J. R., J. C. Wyngaard, and R. J. Francey. 1982. Winds in the atmospheric boundary layer—prediction and observation. *J. Atmos. Sci.*, 39:1307-1316.

Kessler, R. C., and S. G. Douglas. 1991. A numerical study of mesoscale eddy development over the Santa Barbara Channel. *J. Applied Meteorol.*, 30(5).

Kessler, R. C., and S. G. Douglas. 1992. "User's Guide to the Systems Applications International Mesoscale Model (Version 3.0)." Systems Applications International, San Rafael, California (SYSAPP-92/072).

Mahrer, Y., and R. A. Pielke. 1977. A numerical study of the air flow over irregular terrain. *Contr. Atmos. Phys.*, 50:98-113.

Mahrer, Y., and R. A. Pielke. 1978. A test of an upstream spline interpolation technique for the advective terms in a numerical mesoscale model. *Mon. Wea. Rev.*, 106:818-830.

Moore, G. E., J. P. Killus, and G. Z. Whitten. 1991. Composition of marine air offshore of the Western United States. *J. Appl. Meteorol.*, 30(5).

Morris, R. E., R. C. Kessler, S. G. Douglas, and L. R. Chinkin. 1990. "Preliminary Modeling for the San Joaquin Valley Air Quality Study." Systems Applications International, San Rafael, California (SYSAPP-90/106).

O'Brien, J. J. 1970. Alternative solutions to the classical vertical velocity profile. *J. Atmos. Sci.*, 39:2701-2711.

SAI. 1995. "User's Manual for Variable Grid UAM (UAM-V) Preprocessor and Utility Programs." Systems Applications International, San Rafael, California (SYSAPP-95/033).

SAI, Sonoma Technology Inc., Earth Tech, Alpine Geophysics, and A. T. Kearney. 1995. *Gulf of Mexico Air Quality Study, Final Report*, three volumes. U.S. Department of the Interior, Minerals Management Service, Gulf of Mexico OCS Region, New Orleans, Louisiana (OCS study MMS-95-0038, 0039, 0040).

Schulhof, R. R., and S. G. Douglas. 1992. "User's Guide for the MM2UAM Software. Version 1.0." Systems Applications International, San Rafael, California.

Stauffer, D. R., and N. L. Seaman. 1990. Use of four-dimensional data assimilation in a limited-area mesoscale model. Part I: Experiments with synoptic-scale data. *Mon. Wea. Rev.*, 118:1250-1277.

Stauffer, D. R., N. L. Seaman, and F. S. Binkowski. 1991. Use of four-dimensional data assimilation in a limited-area mesoscale model. Part II: Effects of data assimilation within the planetary boundary layer. *Mon. Wea. Rev.*, 199:734-754.

Ulrickson, B. L., and C. F. Mass. 1990. Numerical investigation of mesoscale circulations over the Los Angeles Basin. Part I: A verification study. *Mon. Wea. Rev.*, 118:2138-2161.

SYSAPP-95/067

Final Report

APPLICATION OF UAM-V FOR THE HOUSTON/GALVESTON AND BEAUMONT/PORT ARTHUR NONATTAINMENT AREAS FOR TWO MULTI-DAY OZONE EPISODES

VOLUME II: UAM-V MODEL PERFORMANCE EVALUATION

ICF KAISER

Systems Applications International

September 1995

Final Report

APPLICATION OF UAM-V FOR THE HOUSTON/GALVESTON AND BEAUMONT/PORT ARTHUR NONATTAINMENT AREAS FOR TWO MULTI-DAY OZONE EPISODES

VOLUME II: UAM-V MODEL PERFORMANCE EVALUATION

30 September 1995

Prepared for

Texas Natural Resource Conservation Commission
12100 Park 35 Circle
Austin, TX 78753

Prepared by

Nina K. Lolk
Hans P. Deuel
Jay L. Haney
Sharon G. Douglas

Systems Applications International
101 Lucas Valley Road
San Rafael, CA 94903
415-507-7100

Contents

List of Figures v
List of Tables xi
Acknowledgments xiii

1 INTRODUCTION 1-1
Background 1-1
Overview of the Study 1-1
Modeling Grid Specification 1-2
Simulation Periods 1-4

2 DIAGNOSTIC AND SENSITIVITY ANALYSIS 2-1
23–25 October 1992 2-1
31 August–2 September 1993 2-7

3 MODEL PERFORMANCE EVALUATION 3-1
23–25 October 1992 3-2
31 August–2 September 1993 3-6

4 SUMMARY AND RECOMMENDATIONS 4-1

References R-1

APPENDIX A: TIME-SERIES PLOTS OF OBSERVED AND SIMULATED OZONE CONCENTRATIONS FOR THE DIAGNOSTIC AND SENSITIVITY SIMULATIONS FOR THE 23-25 OCTOBER 1992 AND 31 AUGUST - 2 SEPTEMBER 1993 EPISODES

APPENDIX B: TIME-SERIES PLOTS COMPARING SIMULATED AND OBSERVED NO, NO_2, AND CO CONCENTRATIONS FOR THE BASE CASE SIMULATIONS

Figures

1-1 Southeast Texas UAM-V modeling domain 1-2

1-2 Locations of ozone nonattainment areas in the inner nested grids . . . 1-3

2-1 Locations of air quality monitoring sites for the 23–25 October 1992 episode in the Southeast Texas UAM-V modeling domain 2-15

2-2 Locations of air quality monitoring sites for the 23–25 October 1992 episode in the Houston subdomain 2-16

2-3 Locations of air quality monitoring sites for the 31 August – 2 September 1993 episode in the Southeast Texas UAM-V modeling domain 2-17

2-4 Locations of air quality monitoring sites for the 31 August – 2 September 1993 episode in the Houston subdomain 2-18

2-5a Twenty-four hour backward particle paths culminating at the GALC and TLMC monitoring sites at 1700 CST, 24 October 1992 2-19

2-5b Twenty-four hour backward particle paths culminating at the H11H and WORA monitoring sites at 1200 CST, 25 October 1992 2-20

2-5c Twenty-four hour backward particle paths culminating at the H07H and S43S monitoring sites at 1300 CST, 25 October 1992 2-21

2-6 Maximum simulated ozone concentration for the middle 4-km grid for 23–25 October 1992: initial simulation 2-22

2-7 Maximum simulated ozone concentration for the middle 4-km grid for 23–25 October 1992: double biogenic VOC emissions 2-25

2-8 Maximum simulated ozone concentration for the middle 4-km grid for 23–25 October 1992: mixing heights decreased by 25 percent 2-28

2-9a Twenty-four hour backward particle paths culminating at the H11H and H07H monitoring sites at 1500 CST, 1 September 1993 2-31

2-9b Twenty-four hour backward particle paths culminating at the HCFA and S43S monitoring sites at 0600 CST, 1 September 1993 2-32

2-9c Twenty-four hour backward particle paths culminating at the S43S and PAWC monitoring sites at 1500 CST, 2 September 1993 2-33

2-9d Twenty-four hour backward particle paths culminating at the KTZA monitoring sites at 1700 CST, 2 September 1993 2-34

2-10 Maximum simulated ozone concentration for the middle 4-km grid for 31 August - 2 September 1993: initial simulation 2-35

2-11 Maximum simulated ozone concentration for the Houston and Beaumont/Port Arthur subdomains for 31 August - 2 September 1993 2-38

2-12 Maximum simulated ozone concentration for the middle 4-km grid for 31 August - 2 September 1993 2-44

2-13 Difference in maximum simulated ozone concentration for the middle 4-km grid for 31 August - 2 September 1993 2-47

2-14 Maximum simulated ozone concentration for the middle 4-km grid for 31 August - 2 September 1993: effective mixing heights increased by 25 percent 2-50

2-15 Observed and SAIMM simulated surface temperatures for Aldine: 31 August - 2 September 1993 2-53

2-16 Observed and SAIMM simulated surface temperatures for Beaumont: 31 August - 2 September 1993 2-56

2-17 Observed and SAIMM simulated surface specific humidity for Aldine: 31 August - 2 September 1993 2-59

2-18 Observed and SAIMM simulated surface specific humidity for Beaumont: 31 August - 2 September 1993 2-62

2-19 Observed and SAIMM simulated surface winds for Aldine: 31 August - 2 September 1993 2-65

2-20 Observed and SAIMM simulated surface winds for Beaumont: 31 August - 2 September 1993 2-68

2-21 Observed and SAIMM simulated planetary boundary layer for Aldine: 31 August - 2 September 1993 2-71

2-22 Observed and SAIMM simulated planetary boundary layer for Beaumont: 31 August - 2 September 1993 2-74

2-23 Comparison of hourly mean unsigned errors for SAIMM simulations Run 1 and Run 2: surface temperature 2-77

2-24 Comparison of hourly mean unsigned errors for SAIMM simulations Run 1 and Run 2: surface specific humidity 2-78

2-25 Comparison of hourly mean surface mean vector wind errors for SAIMM simulations Run 1 and Run 2 2-79

2-26 Maximum simulated ozone concentration for the middle 4-km grid on 31 August - 2 September 1993: alternate SAIMM fields 2-80

2-27 Differences in maximum simulated ozone concentration for the middle 4-km grid on 31 August - 2 September 1993: alternate SAIMM fields minus base-case SAIMM fields 2-83

3-1 Maximum simulated ozone concentrations in the Southeast Texas full domain. Base case simulation for 23 October 1992 3-13

3-2 Maximum simulated ozone concentrations in the Southeast Texas full domain. Base case simulation for 24 October 1992 3-14

3-3 Maximum simulated ozone concentrations in the Southeast Texas full domain. Base case simulation for 25 October 1992 3-15

3-4 Maximum simulated ozone concentrations in the Southeast Texas sub-domain. Base case simulation for 23 October 1992 3-16

3-5 Maximum simulated ozone concentrations in the Southeast Texas sub-domain. Base case simulation for 24 October 1992 3-17

3-6 Maximum simulated ozone concentrations in the Southeast Texas sub-domain. Base case simulation for 25 October 1992 3-18

3-7 Maximum simulated ozone concentrations in the Southeast Texas Beaumont/Port Arthur subdomain. Base case simulation for 23 October 1992 3-19

3-8 Maximum simulated ozone concentrations in the Southeast Texas Beaumont/Port Arthur subdomain. Base case simulation for 24 October 1992 3-20

3-9 Maximum simulated ozone concentrations in the Southeast Texas Beaumont/Port Arthur subdomain. Base case simulation for 25 October 1992 3-21

3-10 Scatter plot of simulated and observed ozone concentrations in the Southeast Texas full domain. Base case simulation for 23 October 1992 3-22

3-11 Scatter plot of simulated and observed ozone concentrations in the Southeast Texas full domain. Base case simulation for 24 October 1992 3-23

3-12 Scatter plot of simulated and observed ozone concentrations in the Southeast Texas full domain. Base case simulation for 25 October 1992 3-24

3-13 Time series plot of simulated and observed ozone concentrations in the Southeast Texas full domain 3-25

3-14 Scatter plot of simulated and observed NO concentrations in the Southeast Texas full domain, 23 October 1992 3-35

3-15 Scatter plot of simulated and observed NO concentrations in the Southeast Texas full domain, 24 October 1992 3-36

3-16 Scatter plot of simulated and observed NO concentrations in the Southeast Texas full domain, 25 October 1992 3-37

3-17 Scatter plot of simulated and observed NO_2 concentrations in the Southeast Texas full domain, 23 October 1992 3-38

3-18 Scatter plot of simulated and observed NO_2 concentrations in the Southeast Texas full domain, 24 October 1992 3-39

3-19 Scatter plot of simulated and observed NO_2 concentrations in the Southeast Texas full domain, 25 October 1992 3-40

3-20 Scatter plot of simulated and observed CO concentrations in the Southeast Texas full domain, 23 October 1992 3-41

3-21 Scatter plot of simulated and observed CO concentrations in the Southeast Texas full domain, 24 October 1992 3-42

3-22 Scatter plot of simulated and observed CO concentrations in the Southeast Texas full domain, 25 October 1992 3-43

3-23 Maximum simulated ozone concentrations in the Southeast Texas full domain, 31 August 1993 3-44

3-24 Maximum simulated ozone concentrations in the Southeast Texas full domain, 1 September 1993 3-45

3-25 Maximum simulated ozone concentrations in the Southeast Texas full domain, 2 September 1993 3-46

3-26 Maximum simulated ozone concentrations in the Southeast Texas Houston subdomain, 31 August 1993 3-47

3-27 Maximum simulated ozone concentrations in the Southeast Texas Houston subdomain, 1 September 1993 3-48

3-28 Maximum simulated ozone concentrations in the Southeast Texas Houston subdomain, 2 September 1993 3-49

3-29 Maximum simulated ozone concentrations in the Southeast Texas Beaumont/Port Arthur subdomain, 31 August 1993 3-50

3-30 Maximum simulated ozone concentrations in the Southeast Texas Beaumont/Port Arthur subdomain, 1 September 1993 3-51

3-31 Maximum simulated ozone concentrations in the Southeast Texas Beaumont/Port Arthur subdomain, 2 September 1993 3-52

3-32 Scatter plot of simulated and observed ozone concentrations in the Southeast Texas full domain, 31 August 1993 3-53

3-33 Scatter plot of simulated and observed ozone concentrations in the Southeast Texas full domain, 1 September 1993 3-54

3-34 Scatter plot of simulated and observed ozone concentrations in the Southeast Texas full domain, 2 September 1993 3-55

3-35 Time series plot of simulated and observed ozone concentrations in the Southeast Texas full domain, 31 August – 2 September 1993 . . . 3-56

3-36 Scatter plot of simulated and observed NO concentrations in the Southeast Texas full domain, 31 August 1993 3-65

3-37 Scatter plot of simulated and observed NO concentrations in the Southeast Texas full domain, 1 September 1993 3-66

3-38 Scatter plot of simulated and observed NO concentrations in the Southeast Texas full domain, 2 September 1993 3-67

3-39 Scatter plot of simulated and observed NO_2 concentrations in the Southeast Texas full domain, 31 August 1993 3-68

3-40 Scatter plot of simulated and NO_2 ozone concentrations in the Southeast Texas full domain, 1 September 1993 3-69

3-41 Scatter plot of simulated and observed NO_2 concentrations in the Southeast Texas full domain, 2 September 1993 3-70

3-42 Scatter plot of simulated and observed CO concentrations in the Southeast Texas full domain, 31 August 1993 3-71

3-43 Scatter plot of simulated and CO ozone concentrations in the Southeast Texas full domain, 1 September 1993 3-72

3-44 Scatter plot of simulated and observed NO_2 concentrations in the Southeast Texas full domain, 2 September 1993 3-73

Tables

2-1 Original and modified (effective mixing height reduced by 25 percent) K_v profiles for a grid cell in Houston area 2-5

2-2 Original and modified (effective mixing height reduced by 25 percent) K_v profiles for a grid cell in Beaumont/Port Arthur area 2-6

2-3 Original and modified (effective mixing height increased by 25 percent) K_v profiles for a grid cell in Houston area 2-13

2-4 Original and modified (effective mixing height increased by 25 percent) K_v profiles for a grid cell in Beaumont/Port Arthur area 2-6

3-1 Initial simulation performance statistics for the October 1992 episode 3-11

3-2 Initial simulation performance statistics for the August–September episode 3-12

ACKNOWLEDGMENTS

The following SAI technical staff are acknowledged for their contributions to the project (in alphabetical order): Zitian Guo, A. Belle Hudischewskyj, Thomas C. Myers, Daniel R. Sprenkel, and Shiang Y. Wu.

Editorial and clerical support was provided by Andrew Alden, Rita L. Beacock, Sandy J. Cristensen, Cristi-Ann Jackson, and Jo Ann Moennighoff.

1 INTRODUCTION

BACKGROUND

As mandated by the Clean Air Act Amendments of 1990, air quality planning agencies for ozone nonattainment areas designated as serious or above must perform photochemical modeling to evaluate ozone attainment strategies and demonstrate attainment of the National Ambient Air Quality Standard (NAAQS). The Houston/Galveston area is designated "severe-17" with an attainment date of 2007, while the Beaumont/Port Arthur area is a "serious" area with an attainment date of 1999. The Texas Natural Resource Conservation Commission (TNRCC) has recently applied the current regulatory version of the Urban Airshed Model (UAM) to these areas using routinely available air quality and meteorological data for historical episodes. Because of the complex meteorological conditions influencing the production and transport of ozone in these areas, the TNRCC concluded that the current regulatory version of the model, applied using routinely collected data, was inadequate for simulating episodes for ozone planning purposes. Recognizing the need for supplemental air quality, meteorological, and emission inventory data for adequately simulating episodes in these nonattainment areas, the TNRCC sponsored a small supplemental field program in the summer of 1992 and a more comprehensive program during the summer of 1993 known as the Coastal Oxidant Assessment for Southeast Texas (COAST) program.

In addition to the efforts made in collecting supplemental air quality, meteorological, and emission inventory data for photochemical modeling, the TNRCC requested and was granted permission by the EPA to apply the variable-grid version of the UAM, known as UAM-V, for episodes occurring during 1992 and 1993, using supplemental data collected during the field programs, for the purpose of developing the State Implementation Plan (SIP) for ozone. In addition to its variable nested-grid feature, the UAM-V directly accepts three-dimensional meteorological fields (i.e., winds, temperatures) developed from the application of a data-assimilating prognostic meteorological model; a necessary approach for accurate simulation of the complex three-dimensional structure of the land-/gulf-breeze circulation patterns affecting ozone production and transport in the area. The TNRCC is applying the UAM-V for four ozone episodes (16–19 August 1993, 6–11 September 1993, 23–25 October 1992, and 31 August - 2 September 1993).

OVERVIEW OF THE STUDY

The primary objective of this study was to provide the TNRCC with base-case modeling inputs for two historical ozone episodes, 23–25 October 1992 and 31 August - 2 September 1993, that can be used for future-year attainment-demonstration modeling. The overall study consisted of several tasks: (1) evaluation and quality assurance of

aerometric data and (2) development of meteorological and air quality inputs, and (3) application of UAM-V and model performance evaluation.

The input preparation methodologies and resulting model inputs for the two episode periods are detailed in the companion report by Lolk et al. (1995). This document describes the application of the UAM-V for the two episodes. Diagnostic analysis of the model inputs and results of sensitivity simulations designed to examine the response of the model to changes in the inputs are discussed in Section 2. Model performance is summarized in Section 3. Recommendations for further analysis are provided in Section 4.

MODELING GRID SPECIFICATION

The UAM-V modeling domain for the southeast Texas area as illustrated in Figure 1-1 consists of multiple nested grids with varying resolution. The outer (coarse) grid

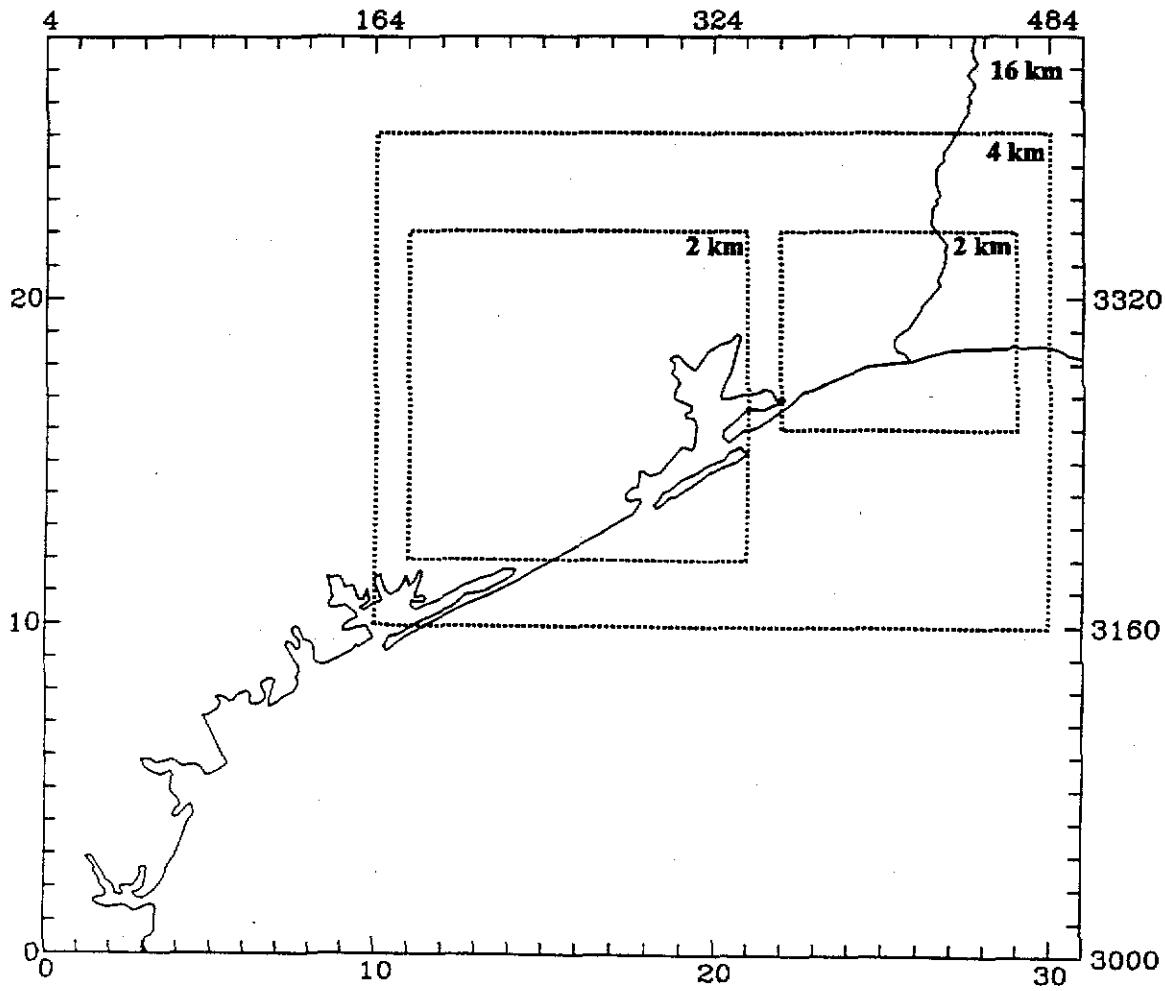

FIGURE 1-1. Southeast Texas UAM-V modeling domain. Inner boxes indicate locations of nested grids.

encompasses the Houston/Galveston and the Beaumont/Port Arthur nonattainment areas as well as the Corpus Christi, Victoria, and Austin urban areas, and a portion of southwestern Louisiana. The origin of the modeling domain is 4 km Easting and 3000 km Northing in Zone 15 Universal Transverse Mercator (UTM) coordinates. The outer grid consists of 31 grid cells in the west-east direction and 28 grid cells in the south-north direction with a horizontal resolution of 16 km. A middle domain, with 4-km resolution, encompassing the nonattainment areas and the area in between, consists of 80 grid cells in the west-east direction and 60 grid cells in the south-north direction. Two inner domains with 2 km horizontal resolution focus on the Houston/Galveston and Beaumont/Port Arthur areas, respectively (Figure 1-2). The first (Houston) consists of 80 grid cells in the west-east direction and 80 grid cells in the north-south direction and the second (Beaumont/Port Arthur) consists of 56 grid cells in the west-east direction and 48 grid cells in the south-north direction. In the vertical, the UAM-V domain consists of eight vertical layers with interfaces at 20, 80, 220, 380, 720, 1380, 2120, and 3030 meters above ground level.

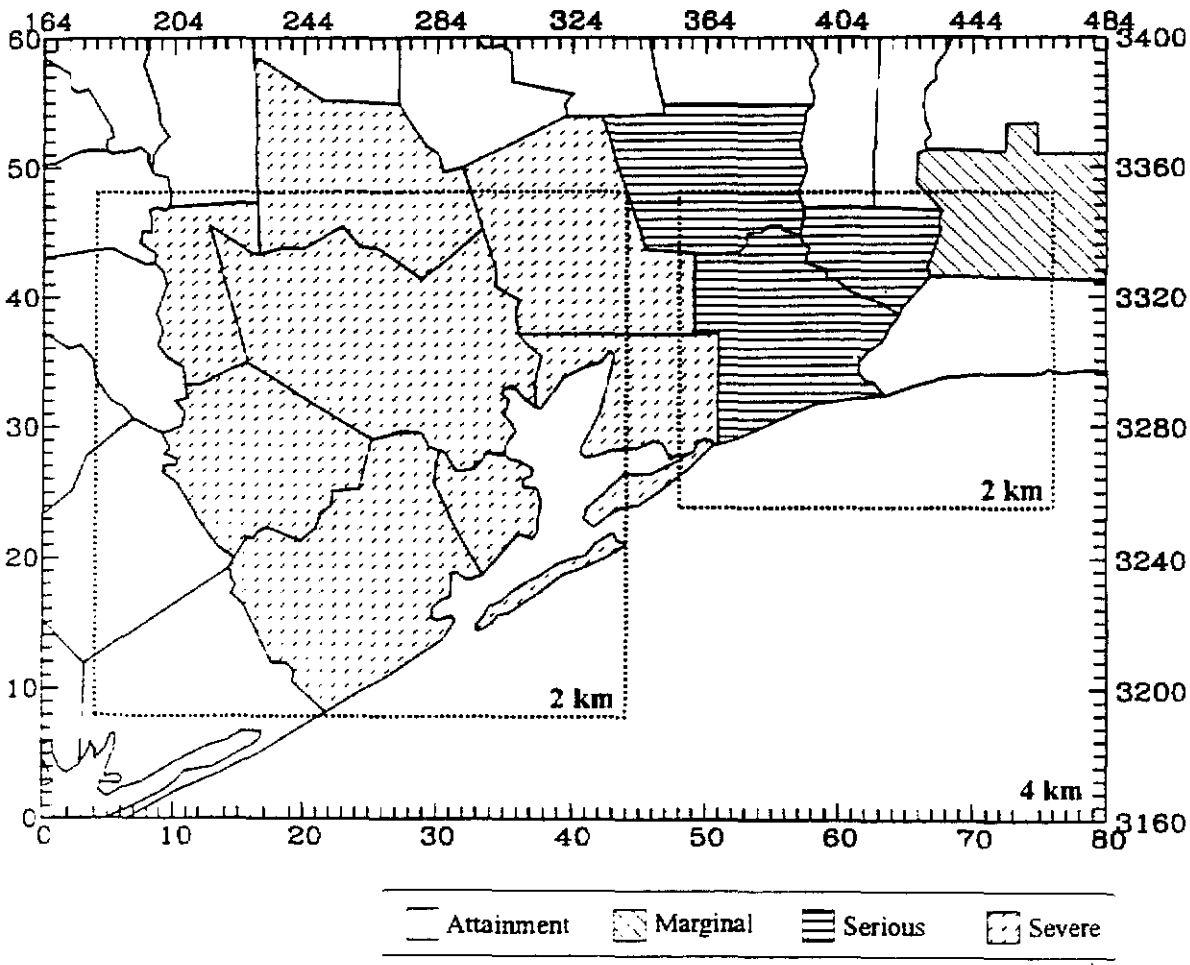

FIGURE 1-2. Locations of ozone nonattainment areas in the inner nested grids.

SIMULATION PERIODS

Two multiday ozone episodes have been selected for this application of UAM-V for the Houston/Galveston and Beaumont/Port Arthur nonattainment areas: 23-25 October 1992 and 31 August - 2 September 1993. In each case, the first day of the simulation period represents a start-up day, used to limit the influence of the initial conditions (which are not well known) on the simulation of the primary episode days. The selection of episodes from 1992 and 1993 was guided by the magnitude and temporal and spatial distribution of observed ozone concentrations as well as the availability of supplemental data.

2 DIAGNOSTIC AND SENSITIVITY ANALYSIS

The objectives, procedures, and results of the UAM-V diagnostic and sensitivity analysis for two Southeast Texas modeling episodes, 23–25 October 1992 and 31 August - 2 September 1993, are described in this section. Diagnostic analysis was used to examine the effects of uncertainty (especially with regard to the assumptions invoked during the input preparation process) and to identify possible deficiencies in the model inputs. Sensitivity analysis was used to investigate the sensitivity of the model to the various model inputs and to ensure that the response of the model to changes in the inputs is physically realistic. Following the preparation of inputs and initial application of the UAM-V, a series of diagnostic and sensitivity simulations was performed for each episode. The results of these simulations were examined using a variety of graphical and statistical analysis products including (1) time-series plots of the observed and simulated pollutant concentrations, (2) contour plots showing isopleths of simulated pollutant concentrations, and (3) model performance statistics. For this modeling study, a limited number of diagnostic and sensitivity simulations were performed with the primary objective of evaluating and understanding model sensitivity to uncertainties and assumptions invoked in the preparation of the meteorological inputs.

The sections below describe, for both episodes, the conceptual model of meteorological and air quality conditions encountered during the episodes, the results of the initial simulation, and the results of the diagnostic and sensitivity analysis.

For reference, plots indicating the locations of the Southeast Texas area air quality monitoring sites are provided in Figures 2-1 through 2-4.

23–25 OCTOBER 1992

Conceptual Model

While northerly winds aloft increased throughout this episode as an upper-level high-pressure system moved southeastward along the coast, surface winds in the Houston/Galveston (HG) and Beaumont/Port Arthur (BPA) areas remained weak and variable. The region was under the influence of high pressure (weak synoptic pressure gradients) and several flow reversals occurred near the surface. Southeasterly winds during the daytime on 23 October were followed by northwesterly winds on 24 October. Surface winds changed direction again in the afternoon on 24 October, with the onset of the gulf breeze in the late afternoon. As a result of the northwesterly surface winds and the late onset of the gulf breeze, high ozone concentrations were observed to the southeast of Houston, in Texas City and at Galveston. The peak observed ozone concentration for this day was 198 ppb and was measured at Galveston. On 25 October,

early-morning southwesterly winds followed by southeasterly winds in the afternoon shifted the maximum ozone concentrations farther to the north, near the Baytown area. The peak observed ozone concentration in Houston on this day was 157 ppb and occurred at H07H. Similarly, exceedances of the federal ozone standard on 25 October in the Beaumont/Port Arthur area of 137 and 125 ppb (measured at the WORA and S43S monitoring sites, respectively) were most likely due to stagnating surface winds. Maximum surface temperatures were near 30°C in Houston and Beaumont and near 27°C in Galveston.

To illustrate the transport potential of the airflow patterns for this episode, two-dimensional, 24-hour backward particle paths terminating at the location and time of the observed peak ozone concentration are presented in Figure 2-5. The backward particle paths ending at 1700 CST on 24 October at the GALC and TLMC monitoring sites suggest a potential contribution from recirculation of ozone and precursor pollutants on this day (Figure 2-5a). Backward particle paths from the observed ozone peaks in the HG and BPA areas on 25 October (at 1300 CST and WORA at 1200 CST), indicate very stagnant conditions during the 12 hours leading up to the time of the peaks (Figure 2-5b and c).

In summary, the backward particle paths for this episode suggest that ozone exceedances in the HG and BPA areas were caused by the buildup and recirculation of local emissions due to stagnating surface winds. Transport from one nonattainment area to another is not indicated by the surface-layer trajectories nor the persistent upper-level winds.

Initial Simulation

The initial simulation for the 23–25 October 1992 episode utilized the plume-in-grid (P-i-G) treatment and the two 2-km inner grids. Seventy point sources were selected (by the TNRCC) for P-i-G treatment based on NO_x emission rates and source location. Plots of the simulated maximum ozone concentrations for the middle grid are presented in Figure 2-6. Time-series plots comparing observed and simulated ozone concentrations for the initial simulation are presented in Section 3. Simulated ozone concentrations for all three days are significantly underestimated at many monitoring sites, particularly in the HG area, indicating deficiencies either in the meteorological or emissions inputs. The maximum simulated ozone concentration for 23 October (Figure 2-6a) is 83 ppb and is located approximately 40 km to the north of Baytown, whereas the observed peak of 112 ppb was measured in Beaumont (at the BMTC monitoring site). As for the previous day, simulated maximum ozone concentrations for 24 October (Figure 2-6b) are lower than observed in both the HG and BPA areas. However, the characteristics of the simulated ozone concentration patterns for this day agree well with the observed concentrations; the simulated peak in the middle (4 km) nested grid is 107 ppb and is located over the gulf, southwest of Sabine Pass. The simulated peak concentration on 25 October (Figure 2-6c) is 98 ppb and is located approximately 20 km southeast of the HNWA monitoring site. Two exceedances were recorded in the BPA area on 25 October, but the simulated maximum in the BPA 2 km grid (not shown) is only 106 ppb.

The initial simulation for this episode represents the base-case simulation and is described in more detail in the following section. Two diagnostic/sensitivity simulations were performed to examine the effects of input uncertainty on the simulated ozone concentrations and to examine the possible cause of the underestimation in the initial simulation.

Diagnostic and Sensitivity Simulations

Diagnostic and sensitivity simulations involving changes to the emissions and meteorological inputs were performed for the 23–25 October 1992 episode. Because a majority of the diagnostic and sensitivity simulations performed for this study were meteorology-related and the meteorological fields were generated using 4 km resolution, the 2-km inner grids were not used in these simulations. The effect on simulated ozone concentrations of using the inner high-resolution grids were examined as part of the diagnostic and sensitivity analysis for the second episode.

Emissions-Related Simulations

Possible reasons for the significant underestimation of domain-wide ozone concentrations for this episode included uncertainties or deficiencies in the emissions inventory. Examination of the simulated oxides of nitrogen (NO_x) concentrations indicate fairly good agreement with the observed values. Measurements of volatile organic compound (VOC) concentrations for this episode were inadequate for evaluation of simulated VOC concentrations. However, comparison of VOC emissions for the two episodes indicate that biogenic VOC emissions for October 1992 are about half of those estimated for September 1993. Although this is not counterintuitive given the differences corresponding to the episode dates, it is well known that there are significant uncertainties (using current algorithms) regarding the effects of temperature and sunlight on biogenic emissions. Thus, the first diagnostic simulation for this episode involved doubling the biogenic VOC emissions to test the response of the simulated ozone concentrations to uncertainties in the biogenic emission estimates.

Plots of the simulated maximum ozone concentrations for the double biogenic VOC simulation for the middle (4 km) grid are shown in Figure 2-7. Time-series plots comparing the observed and simulated ozone concentrations for this simulation and the initial simulation are shown in Appendix A. The simulated ozone concentrations are higher for most monitoring sites and overall model performance improves significantly, but the simulated peak on 24 October (Figure 2-7b) at Galveston is still only 102 ppb. The maximum simulated concentrations in the middle (4 km) grid increase from 107 to 145 ppb for 24 October and from 98 to 131 ppb for 25 October with the higher biogenic emissions. Ozone concentrations for 25 October (Figure 2-7c) are still significantly underestimated in the Baytown area, where the two highest observed concentrations of 157 and 148 ppb were observed on this day.

Meteorology-Related Simulations

To examine the effects of uncertainties in the vertical-exchange-coefficient inputs on the simulated ozone concentrations, a UAM-V sensitivity simulation was performed using modified vertical exchange coefficients (or K_vs). Modification of the vertical exchange coefficients alters the mixing characteristics and, thus, the effective mixing height. Because simulated ozone concentrations were underestimated for the initial simulation, the K_vs were modified such that the effective mixing heights are reduced by 25 percent. In the SAIMM, the mixing height is defined as the height at which the value of K_v drops to 10 percent of its maximum value. The reduction in effective mixing height was achieved by shifting the vertical profile of K_v such that the estimated mixing height for each hour and each grid cell was reduced by 25 percent. The altered K_vs were then interpolated to the UAM-V layer interface heights using the standard procedure for converting SAIMM fields into UAM-V format (see Section 4 of Volume I of this report).

The original and modified K_v profiles for 1400 CST for all three days and two locations (Houston and Beaumont/Port Arthur) are shown in Tables 2-1 and 2-2. The decrease in effective mixing height is achieved by a more rapid decrease in K_v values with height. For example, the effective mixing height for the Houston area on 23 October, has been reduced from approximately 1400 m to 1050 m. The shape of the K_v profile is altered but the higher values near the ground will have little effect on the already well-mixed layers.

Plots of the resulting simulated maximum ozone concentrations are presented in Figure 2-8. Time-series plots comparing the observed and simulated ozone concentrations for this simulation and the initial simulation are shown in Appendix A. As expected, simulated ozone concentrations increase throughout the domain. Simulated peaks in the middle (4 km) grid are increased by 16, 8, and 11 ppb for 23, 24, and 25 October, respectively. The concentration patterns are relatively unchanged and model performance is not significantly improved.

In summary, the improvement in model performance that is gained by using the modified K_V fields is relatively small compared to the effect of doubling the biogenic VOC emissions. In light of the relatively poor model performance for this episode, additional diagnostic and sensitivity simulations should be performed. These should include simulations to test the sensitivity of the model to uncertainties in the various emissions components as well as the boundary conditions. In addition, further examination of uncertainties in the meteorological inputs should be pursued. One possible diagnostic simulation involves running the SAIMM with the upper-air data for the H04H wind profiler site omitted from the FDDA objective analysis fields. Compared to the data for the Lake Charles NWS radiosonde, the wind data for the H04H site are characterized by high wind speeds and strong vertical wind shear. Use of these data in the SAIMM simulation may have enhanced the advection and mixing of pollutants and may have contributed to the lower than observed simulated ozone concentrations.

TABLE 2-1. Original and modified (effective mixing height reduced by 25 percent) K_v profiles for a grid cell in Houston area, 1400 CST.

SAIMM Level	Original (m^2s^{-1})	Modified (m^2s^{-1})
23 October 1992		
1	51	158
2	43	158
3	193	159
4	239	158
5	170	157
6	163	155
7	158	154
8	159	159
9	153	79
10	160	6
11	8	0
12	0	0
13	0	0
24 October 1992		
1	46	162
2	31	141
3	165	123
4	198	105
5	235	93
6	254	77
7	152	62
8	97	38
9	59	12
10	19	0
11	0	0
12	0	0
13	0	0
25 October 1992		
1	28	32
2	15	35
3	117	40
4	66	45
5	55	50
6	39	60
7	26	71
8	27	64
9	51	24
10	78	9
11	22	0
12	0	0
13	0	0

TABLE 2-2. Original and modified (effective mixing height reduced by 25 percent) K_v profiles for a grid cell in Beaumont/Port Arthur area, 1400 CST.

SAIMM Level	Original (m^2s^{-1})	Modified (m^2s^{-1})
23 October 1992		
1	44	175
2	53	158
3	147	149
4	179	141
5	217	134
6	239	126
7	162	117
8	136	124
9	115	87
10	133	2
11	2	0
12	0	0
13	0	0
24 October 1992		
1	44	175
2	53	158
3	147	149
4	179	141
5	217	134
6	239	126
7	162	117
8	136	124
9	115	87
10	133	2
11	2	0
12	0	0
13	0	0
25 October 1992		
1	43	125
2	42	120
3	135	116
4	160	114
5	132	112
6	132	104
7	117	94
8	111	61
9	88	6
10	8	1
11	0	0
12	0	0
13	0	0

31 AUGUST–2 SEPTEMBER 1993

Conceptual Model

The meteorological conditions for this episode are characteristic of the most frequently occurring weather type associated with ozone episodes in the Southeast Texas area. A high pressure system centered over southeast Texas during this episode resulted in light and variable surface winds, high temperatures, and suppressed vertical mixing. Light and variable winds on the first day of the episode, followed by westerly wind components on the middle and last days of the episode caused ozone and precursor concentrations to build up and subsequently to be advected eastward. No exceedances of the federal ozone standard were observed in Southeast Texas on this day. On 1 September, exceedances were observed at the H11H and H07H (Baytown) monitoring sites with maximum concentrations of 164 and 121 ppb, respectively. Another exceedance of 137 ppb occurred southeast of Houston at the Smith Point monitoring site. On 2 September, the area of high ozone concentrations continued to move eastward. Two exceedances were recorded on this day, one at Stowell (131 ppb) at 1300 CST and another at the S43S Beaumont monitoring site (139 ppb), two hours later at 1500 CST.

Backward particle paths for the afternoon of 1 September, suggest that the time of maximum observed ozone concentration in Baytown (1500 CST) was preceded by 24 hours of relatively weak and variable surface winds in the Houston area (Figure 2-9a). This may have allowed precursor emissions and ozone concentrations to build up, particularly in the ship channel area, and winds from the west-northwest during the 8-10 hours leading up to the time of the peak, may have carried pollutants eastward to the locations of high observed ozone concentrations east of Houston (e.g., H11H, SPTC, H07H, and STWC). Twenty-four hour forward particle paths for UAM-V layer 6 (720-1380 m agl) initiated at the S43S monitoring site at four-hour intervals on 1 September suggest persistent advection of pollutants over the gulf to the southeast of the BPA area (Figure 2-9b). This is consistent with relatively high observed concentrations at Sabine (105 ppb) for this day.

Backward particle paths terminating at the S43S and PAWC monitoring sites in the Beaumont/Port Arthur area, at which the two highest ozone concentrations for 2 September were observed, suggest a potential contribution from transported ozone originating in areas east of Galveston Bay where high ozone concentrations were observed the day before (e.g., SPTC and STWC) (Figure 2-9c). Similarly, Figure 2-9d illustrates the potential contribution from overnight elevated transport of pollutants originating in the Baytown area to the near-exceedance at the KTZA site in northern Jefferson County.

In summary, the particle path analysis for this episode suggests that transported ozone and precursor pollutants from the Houston/Galveston nonattainment area likely contributed to high observed ozone concentrations in the Beaumont/Port Arthur area on 2 September.

Initial Simulation Results

For the initial simulation of this episode, the UAM-V was run with P-i-G and all the nested grids. Plots of the maximum simulated ozone concentrations for the middle grid are shown in Figure 2-10. Time-series plots comparing the observed and simulated ozone concentrations for this episode are presented in Section 3. While simulated ozone concentrations for this episode are somewhat overestimated, the spatial and temporal characteristics of the observed ozone concentration patterns are replicated. The peak simulated ozone concentration for 31 August (Figure 2-10a) is 123 ppb and occurs approximately 40 km north and east of the H10H monitoring site. The peak observed concentration was 96 ppb, measured at H07H. In the BPA area, simulated ozone concentrations are also generally higher than observed; but the simulated peak is located very close to the observed peak. Simulated maximum ozone concentrations for 1 September (Figure 2-10b) are higher than observed throughout much of the domain. The simulated peak in the HG area is 166 ppb; this compares favorably in magnitude with the observed peak of 164 ppb but it is located northwest of the monitoring site at which the peak was observed and is higher than observed peaks in that area. The location of the simulated peak is near the H04H monitoring site, about 20 km northwest of H11H, where the observed peak occurred. On 2 September, maximum ozone concentrations are well-simulated in both the HG and BPA areas (Figure 2-10c). The simulated and observed peaks in the HG area are 139 and 115 ppb, respectively. In the BPA area, the high simulated ozone concentrations occur farther inland than indicated by the observations.

Note that the plots of the simulated concentrations for the 4-km middle grid include the simulation results for the 2-km inner grids and that significant smoothing of the high resolution results may occur due to the representation of the results using 4 km resolution. The results for each of the high resolution grids are discussed in Section 3.

Diagnostic and Sensitivity Simulations

The diagnostic and sensitivity simulations for the 31 August - 2 September 1993 episode examined the specification of certain UAM-V simulation parameters and the effects of uncertainties in the meteorological inputs on simulated ozone concentrations. Two simulations were performed to examine the response of the model to different UAM-V simulation parameters. One simulation examined the use of the inner high-resolution grids and another simulation provided information about the effects of using the P-i-G treatment. The meteorology-related diagnostic/sensitivity simulations examined the effects of (1) increasing the effective mixing heights (through modification of the K_v profiles) and (2) using alternate SAIMM-derived inputs.

Simulation Parameters

The first simulation, which entailed running the UAM-V without the 2-km inner grids, examined the effects of using higher resolution in areas with high emission density and also served as the control simulation for the subsequent meteorological diagnostic/sensitivity simulations. The results of this simulation are discussed in terms

of two subdomains corresponding to the inner 2 km grids. Plots of the simulated maximum ozone concentrations for this simulation for the subdomains are shown in Figure 2-11. Time-series plots comparing the observed and simulated ozone concentrations for this simulation and the initial simulation are shown in Appendix A. A comparison of the simulation results (compare Figure 2-11 with Figure 3-26 through 3-31) indicates that the simulated maximum ozone concentrations both increase and decrease as a result of using the 2 km inner grids. Within the HG subdomain, maximum ozone concentrations for 31 August and 1 September (Figures 2-11a and b) decrease by 3 and 1 ppb, respectively and increase for 2 September by 1 ppb (Figure 2-11c) without the 2-km inner grids. Within the BPA subdomain, maximum ozone concentrations decrease by 5 ppb for 31 August (Figure 2-11d) and increase by 7 and 8 ppb for 1 and 2 September, respectively (Figures 2-11e and f). Thus, for this episode, the sensitivity of the simulated ozone concentrations to horizontal grid resolution is somewhat greater for the BPA subdomain than for the HG subdomain. The concentration patterns are altered slightly; use of the 2 km grids generally improves model performance.

Plots of simulated maximum ozone concentrations for the simulation without P-i-G are shown in Figure 2-12. Time-series plots comparing the observed and simulated ozone concentrations for this simulation and the control simulation are shown in Appendix A. This simulation was run without the 2 km nested grids. Comparison of results for this simulation and the control simulation indicates that the effects of adding the P-i-G treatment are evident throughout the domain and that the simulated peaks change only slightly. Figure 2-13 illustrates the difference in the maximum simulated ozone concentrations arising from the use of the P-i-G treatment. Positive differences indicate that the simulated maximum ozone concentrations are higher with the use of the P-i-G treatment. Figures 2-13a through 2-13c indicate that, with P-i-G, simulated maximum ozone concentrations are higher near source locations in Texas City and in the Beaumont/Port Arthur area. This results from the more realistic injection of point source emissions into the grid that is achieved using the P-i-G treatment (without P-i-G, NO_x emissions are injected directly into the whole grid cell in which the point source is located, and this results in artificial ozone titration over a wider area than the actual plume). Downwind of the source locations, the calculated daily maximum ozone concentrations are generally lower with P-i-G. Deviations from this pattern in the effects of P-i-G are noted: (1) increases away from the source locations (e.g, on 1 September in the Beaumont/Port Arthur area and in western Louisiana) may be due to displacement of the NO_x plume into a VOC-rich area such that ozone production is enhanced and (2) decreases in ozone without accompanying increases at the source locations in the Baytown area for 31 August and 2 September may be the result of high plume-heights such that surface ozone concentrations near the sources are not affected. Note that the differences for 1 September may in part be due to differences in the emissions inventories. An error in the mobile emissions inventory was discovered after the simulation without P-i-G was performed and the correction was incorporated in the inventory used for the P-i-G simulation.

Meteorology-Related Simulations

Similar to the 1992 episode, a diagnostic/sensitivity simulation was performed for the 1993 episode to examine the effect on the simulated ozone concentrations of uncertainties in the specification of the K_vs. Because ozone concentrations were generally overestimated in the initial simulation, the K_v profiles were modified to reflect a 25 percent increase in effective mixing height. Tables 2-3 and 2-4 show the original and modified K_v profiles for all three days. Note that following the shift of the K_v profile, constant values were assigned below the lowest modified layer. Time-series plots comparing the observed and simulated ozone concentrations for this simulation and the control simulation are shown in Appendix A. The maximum simulated ozone concentrations (Figure 2-14) decrease for all three days: from 120 to 115 ppb for 31 August, from 179 to 157 ppb for 1 September, and from 146 to 131 ppb for 2 September. The location of the simulated peak for 1 September is shifted southeastward to a location just south of the observed peak as a result of the K_v modification. The greatest differences occur in the Houston area on 1 September with decreases in the maximum simulated ozone concentrations of approximately 10-15 percent.

The second diagnostic/sensitivity simulation utilized alternate meteorological fields. Initial application of the SAIMM to the Southeast Texas modeling domain utilized a recently developed data assimilation technique for incorporation of surface-based temperature and moisture data into the SAIMM simulations. As documented in Volume I of this report, the new data assimilation technique resulted in good model performance. To test the sensitivity of the UAM-V simulations to the improved data assimilation technique, the SAIMM was run without incorporation of surface temperature and moisture data.

The resulting alternate meteorological inputs are characterized by cooler surface temperatures and, perhaps more importantly, lower mixing heights. Figures 2-15 through 2-22 compare the simulated and observed surface-level temperature, specific humidity, and wind vectors, and show the PBL heights for the two different simulations with (RUN 1) and without (RUN 2) assimilation of surface temperature and moisture data, for two sites, Aldine (HALC) and Beaumont (BMTC). Not surprisingly, these plots indicate that improved model performance is achieved for RUN 1 in terms of the diurnal profiles of surface temperature (Figures 2-15 and 2-16) and specific humidity (Figures 2-17 and 2-18). In general, if the surface temperature and moisture data are omitted, the SAIMM-simulated surface temperatures are higher than observed during the night and lower than observed during the day. Changes in the simulated wind vectors (Figures 2-19 and Figures 2-20) are slight, perhaps due to the relatively strong nudging coefficients applied for the wind nudging. The most notable changes occur in the simulated PBL heights (Figures 2-21 and 2-22). Daytime maximum PBL heights for both the HALC and BMTC monitoring sites are 20-30 percent higher when surface temperature data are assimilated.

Figures 2-23 and 2-24 illustrate the hourly variation in mean unsigned error[1] for surface temperature and surface specific humidity for each day of the simulation period. Again, due to the fairly flat diurnal profiles, the RUN 2 simulation results are characterized by larger errors during the time of day when minimum and maximum values are observed. Figure 2-25 shows the hourly mean surface vector wind errors[2] for the two simulations. In general, the differences in mean wind vector errors for the two simulations are small. This suggests that, with the particular set of simulation parameters that were utilized for this application of the SAIMM, assimilation of surface temperature and moisture represents neither a benefit nor a disbenefit to the simulated surface wind fields.

UAM-V model performance for the simulation using the SAIMM meteorological fields without surface temperature and moisture data is generally degraded compared to the initial simulation. Time-series plots comparing the observed and simulated ozone concentrations for this simulation and the control simulation are shown in Appendix A. Figure 2-26 shows the simulated maximum ozone concentrations for the 4-km middle grid. On 31 August, the simulated peak increases from 120 to 130 ppb and the peak is shifted about 40 km to the southeast as a result of using the alternate SAIMM fields. Similarly, on 1 September, the peak increases from 179 to 194 ppb and is shifted to the southeast, though not as far as for the first day. On the last day, the location of the peak moves from the BPA area to the HG area, and the downwind plume (to the north of Houston) is enhanced.

Figure 2-27 illustrates the difference in maximum simulated ozone concentration that results from omitting surface temperature and moisture data in the SAIMM simulation. Differences are predominantly positive for the episode and are generally larger and more widespread in the Houston area. Large positive changes occur in the Baytown area 31 August and 1 September. The most notable occurrence of negative changes in over the bay on 31 August. On 2 September, large positive changes occur to the eat (downwind) of the BPA area.

The response of the model in the HG and the BPA areas to the alternate SAIMM fields is somewhat different. For the Houston subdomain, the maximum simulated ozone concentrations for the first, second and third episode days increase by 10, 15, and 13 ppb, respectively. In the BPA subdomain, the corresponding changes are 1, 2, and less than 1 ppb, respectively. The response of the UAM-V to the alternate SAIMM fields is believed to be mostly due to changes in the effective mixing heights. The UAM-V responded as expected to changes in the K_vs, therefore it is noteworthy that the simulated concentrations are more responsive to the alternate meteorological fields in the HG area

$$\textit{Mean Unsigned Error} = \frac{\sum_{i=1}^{N} |S_i - O_i|}{N}$$

$$\overline{|\Delta V|} = \frac{1}{I \cdot J} \sum_{i=1}^{I} \sum_{j=1}^{J} [(u_{i,j}^{f} - u_{i,j}^{o})^2 + (v_{i,j}^{f} - v_{i,j}^{o})^2]^{1/2}$$

than in the BPA area. This indicates that the effects of the surface temperature nudging vary across the domain.

In summary, use of the alternate SAIMM fields results in higher simulated site-specific peaks and degraded model performance, particularly in the HG area. Thus for this episode, the inclusion of surface temperature and moisture data in the SAIMM simulation leads to better episode-specific fields and thus, better replication of the spatial and temporal ozone concentration patterns for this episode.

TABLE 2-3. Original and modified (effective mixing height increased by 25 percent) K_v profiles for a grid cell in the Houston area, 1400 CST.

SAIMM Level	Original (m^2s^{-1})	Modified (m^2s^{-1})
31 August 1993		
1	67	67
2	149	67
3	202	67
4	235	67
5	271	67
6	289	67
7	300	179
8	292	276
9	79	296
10	2	140
11	0	2
12	0	0
13	2	1
1 September 1993		
1	52	522
2	128	52
3	189	52
4	232	52
5	283	52
6	312	52
7	334	52
8	346	210
9	340	328
10	310	344
11	5	320
12	0	27
13	2	1
2 September 1993		
1	50	50
2	125	50
3	186	50
4	229	50
5	283	50
6	313	50
7	338	50
8	355	199
9	356	329
10	247	355
11	7	284
12	0	31
13	4	2

TABLE 2-4. Original and modified (effective mixing height increased by 25 percent) K_v profiles for a grid cell in Beaumont/Port Arthur area, 1400 CST.

SAIMM Level	Original (m^2s^{-1})	Modified (m^2s^{-1})
31 August 1993		
1	51	51
2	126	51
3	185	51
4	226	51
5	276	51
6	302	51
7	323	51
8	211	212
9	147	319
10	146	190
11	4	147
12	0	11
13	1	0
1 September 1993		
1	47	47
2	111	47
3	159	47
4	193	47
5	234	47
6	256	47
7	275	47
8	197	193
9	137	274
10	34	173
11	0	54
12	0	0
13	3	2
2 September 1993		
1	48	48
2	115	48
3	168	48
4	206	48
5	253	48
6	281	48
7	303	48
8	315	192
9	198	299
10	143	277
11	5	158
12	0	12
13	4	2

3 MODEL PERFORMANCE EVALUATION

Before the UAM can be used to assess the effectiveness of ozone attainment strategies it must be demonstrated that the model acceptably replicates each historical ozone episode (i.e., a base-case simulation is achieved). This requires a careful and comprehensive evaluation of model performance. In this section we present the results of the base-case simulation and provide a detailed summary of model performance.

Model performance for each ozone episode was assessed using graphical and statistical analysis. While the focus of this evaluation was ozone, the simulation of other species for which observed data are available (NO_2, NO, and CO) was also examined.

Graphical analysis products included (1) time-series plots of observed and simulated pollutant concentrations, (2) contour plots showing isopleths of simulated pollutant concentrations and, where available, observed surface-layer concentrations, and (3) scatter plots comparing the simulated and observed concentrations.

Statistical analysis of the model results included the calculation of a number of statistical measures of bias including the mean residual, mean unsigned error, mean relative error (normalized bias), mean unsigned relative error (gross error), and the root mean square error. Their definitions are as follows:

$$\textit{Mean Residual} = \frac{\sum_{i=1}^{N} (S_i - O_i)}{N}$$

$$\textit{Mean Unsigned Error} = \frac{\sum_{i=1}^{N} |S_i - O_i|}{N}$$

$$\textit{Mean Relative Error} = \frac{\sum_{i=1}^{N} (S_i - O_i)/O_i}{N}$$

$$\textit{Mean Unsigned Relative Error} = \frac{\sum_{i=1}^{N} |S_i - O_i|/O_i}{N}$$

$$\textit{Root Mean Square Error} = \sqrt{\frac{\sum_{i=1}^{N} (S_i - O_i)^2}{N}}$$

where O_i is the ith observation, S_i is the ith simulated value, and N is the number of observed or simulated values.

A lower bound of 6 pphm, per EPA guidance (EPA, 1991), was used for calculating the mean relative error and the mean unsigned relative error; the relative error was not computed for observation and simulation pairs when the observed value is less than the lower bound. This was done to avoid excessive weighting of the relative means by low values and to avoid dividing by zero.

In addition to these basic measures of bias, the unpaired accuracy of the peak concentration and the average accuracy of the peak concentration (paired in space but unpaired in time) were computed. The unpaired accuracy of the peak concentration is defined as:

$$\textit{Unpaired Accuracy of the Peak Concentration} = \frac{(S_{\max} - O_{\max})}{O_{\max}}$$

where the maxima are taken over all locations and times (the location and time of the maximum simulated value does not have to be the same as the site and time of the observed maximum).

The average accuracy of the peak concentration is defined as:

$$\textit{Average Accuracy of the Peak Concentration} = \frac{\sum_{i=1}^{N} \frac{(S_{i,\max} - O_{i,\max})}{O_{i,\max}}}{N}$$

where the maximum simulated and observed concentrations are paired in space but not in time.

In the calculation of these statistical measures, weighted interpolation of the simulated values in the four grid cells surrounding a monitoring site was performed to provide collocated pairs of simulated and observed values.

The resulting statistical performance measures were compared with the general ranges provided in the UAM guidance document (EPA, 1991) for unpaired highest prediction accuracy, normalized bias, and gross error.

23-25 OCTOBER 1992

Statistical Analysis

Statistics comparing the simulated and observed ozone concentrations for each of the episode days are given in Table 3-1. The performance statistics are presented for three

regions of the modeling domain: (1) the full domain, interpolated to a 4 km grid spacing by incorporating the Houston/Beaumont/Port Arthur 4 km interior domain; (2) the Houston/Galveston 2 km subdomain (HG), and (3) the Beaumont/Port Arthur 2 km subdomain (BPA).

In all cases and for all days, the signed measures of peak accuracy are negative, indicating that the model underestimates the peak ozone concentrations. This is irrespective of whether the peak simulated and observed maxima are considered unpaired in time (average accuracy of the peak), or unpaired in both time and space (unpaired accuracy of the peak).

For 23 October, the unpaired accuracy of the peak and the average accuracy of the peak indicate that the area-wide simulated maxima and, in particular, the simulated maxima at the monitoring sites, are (on average) significantly underestimated.

The accuracy parameters for 24 October indicate that the overall peak intensity in the BPA domain (-2.0%) is well simulated, but that the site-specific peak accuracy is significantly underestimated (−30.3%). Within the HG subdomain, as well as the full domain, site-specific model performance, as indicated by the average accuracy parameter, is better than for 23 October, while the underestimation of the overall maximum increases.

The peak concentrations are similarly underestimated for 25 October.

A comparison of the normalized bias, a signed measure of model performance resolved in both time and space, versus the normalized gross error, which is unsigned, gives a direct measure of the relative preponderance of overestimation to underestimation. For all three episode days and for all grid resolutions and domains, the magnitudes of these two measures are nearly equal. This indicates that the differences between simulated and observed ozone concentrations are nearly uniformly of the same sign. Consequently, the dominant deficiency in the present simulation is an underestimation of the ozone concentrations.

Analysis of Domain-Wide Simulated Concentration Patterns

A comparison of the maximum simulated ozone concentrations throughout the modeling domain compared with the maximum observed concentrations for the sites within the domain gives insight into domain-wide differences in simulation accuracy. Figures 3-1 through 3-3 compare simulated and observed maximum ozone concentrations for the entire modeling domain at 16 km grid resolution, over all hours, for each of the three modeling days, respectively. Similarly, Figures 3-4 through 3-6 give the same information for the HG subdomain, while Figures 3-7 through 3-9 show the BPA subdomain.

Figure 3-1 shows that the observed maximum for 23 October occurs in the Beaumont area, while the simulated maximum occurs near the northwestern portion of the domain, with a secondary maximum of nearly equal magnitude slightly north of Houston. Domain-wide ozone concentrations are simulated to be on the order of 40 to 60 ppb. By

the second day of the episode (Figure 3-2) the simulated peak is located over the Gulf between the Houston and the Beaumont/Port Arthur urban areas, whereas the observed maximum is in Galveston. Area-wide simulated ozone concentrations have increased somewhat. The final day of the episode (Figure 3-3) shows a simulated peak north of Corpus Cristi (the observed peak is in Houston), and domain-wide ozone concentrations are on the order of 70 ppb.

For the HG subdomain, the maximum simulated ozone concentration of 84 ppb occurs in the northeastern corner of the subdomain for the first day of the episode (Figure 3-4), in contrast to an observed maximum of 108 ppb located to the northwest of Houston. Domain-wide ozone concentrations are again in the 40 to 60 ppb range. The simulated ozone concentrations for 24 October in the HG subdomain (Figure 3-5) are characterized by domain-wide ozone concentrations in the range of 60 to 70 ppb, with a subdomain simulated maximum of 107 ppb. The observed maximum at Galveston is not well simulated, and site-specific peaks in the Houston area are generally underestimated by approximately 20 ppb. The plot of the maximum simulated ozone concentrations for the final episode day for the HG subdomain (Figure 3-6) shows a peak of 101 ppb to the northwest of Houston, in contrast to the observed maximum of 157 ppb measured at the H07H monitoring site, located just east of Houston.

The BPA subdomain has an observed peak of 112 ppb for 23 October, and a simulated maximum ozone concentration of 76 ppb (Figure 3-7). Simulated area-wide ozone concentrations vary from 40 to 70 ppb. The simulated maximum for the second episode day for this subdomain (Figure 3-8) is 110 ppb, in contrast to the observed maximum of 112 ppb. Area-wide simulated concentrations range from 40 to 100 ppb. For the final episode day (Figure 3-9) the simulated maximum for this subdomain is located between the two secondary observed maxima. The primary observed maximum of 137 ppb is underestimated.

From the above analysis it is clear that the initial simulation poorly reproduces both the magnitude and location of the observed peak ozone concentrations.

Analysis of Site-Specific Simulated Concentrations

The dynamics of ozone evolution, and the quality of the simulation with respect to non-peak observations, are addressed through examination of scatter plots. These plots compare the simulated and observed ozone concentrations for each hour of the simulation period at each monitoring site. Figures 3-10 through 3-12 show scatter plots of the simulated and observed ozone concentrations for each hour of 23, 24, and 25 October, respectively. These figures indicate that, as noted above, the peak ozone concentrations are significantly underestimated. However, for less extreme ozone concentrations, the data are somewhat more closely clustered, indicating an even distribution of over- and under-estimated concentrations.

Time-series plots for the base-case simulation of 23–25 October are provided in Figure 3-13. In these plots, the solid line represents a distance-weighted interpolation of the simulated values in the four grid cells surrounding the monitoring site. The dashed lines represent the highest and lowest values in the nine grid cells surrounding the monitoring

site. The shaded area, therefore, represents the range of simulated ozone concentrations within one grid cell of the monitoring site.

Figure 3-13 illustrates that only the coarsest features of the dynamics of the evolution of the mid-day ozone peak are qualitatively captured. That is, the initial rise in the observed ozone coincides temporally with the simulated rise in the ozone concentration, and the peak of the observed and simulated ozone profiles temporally nearly coincide. However, there are a number of serious systematic discrepancies in addition to those noted above.

The air quality data analysis performed as part of this modeling study indicated the presence of ozone titration at a number of the observation sites. The initial simulation, while capturing the dynamics of this titration rather effectively, seems to overestimate the removal of ozone during the evening, as well as the duration of high concentrations of ozone titrants (e.g., NO_x). For a majority of the sites exhibiting this effect (H11H, HWAA, HALC, TLMC, C35C, HOEA, H04H, H03H, HCFA, PAWC, H08H, H07H, L005), the simulated results indicate that the ozone levels do not recover after this titration, while the observations indicate that the concentrations rise again within a few hours, and remain somewhat elevated throughout the night. Possible explanations for this systematic discrepancy between the observed and the simulated concentrations include:

1. Emission inventory overestimation of NO_x, or underestimation of VOC's for this time period;

2. Poor model performance in simulation of VOC's, *vide. infra*; and

3. Inaccuracies in the meteorological inputs.

One and three are addressed directly in the diagnostic and sensitivity analysis. Model performance for oxides of nitrogen (NO_x) can be compared directly with observations. While simulation results are available for volatile organic compounds (VOC's), observational data are not. Figures 3-14 through 3-16 show scatter plots for nitrogen oxide (NO) for each of the three days, respectively, while Figures 3-17 through 3-19 show similar plots for nitrogen dioxide (NO_2). The simulation of NO_2 on 23 October is quite good, while the simulated concentrations for 24 and 25 October are systematically slightly higher than observed. Model performance with respect to NO is fair, with the exception of 25 October, which has significantly higher simulated concentrations than observed. The observed NO concentrations for this day are significantly lower than the observations for the previous two days, a feature not captured by the simulation. Whether or not this feature is represented in the emission inventory requires further scrutiny. NO_2 observations show similar distributions over the three days, despite that the episode is from Friday to Sunday. Time-series plots comparing simulated and observed concentrations of NO and NO_2 are presented in Appendix B.

Finally, Figures 3-20 through 3-22 show scatter plots for simulated and observed carbon monoxide (CO) hourly concentrations. The model results underestimate the observed CO concentrations. As CO is relatively inert, this indicates that either CO emissions are underestimated in the modeling inventory, or CO concentrations are not simulated well

due to uncertainties in the meteorological inputs. In particular, changes in the mixing height can dilute or concentrate surface level emissions across the board. This possibility is addressed directly in the diagnostic and sensitivity simulation analysis. A time-series plot comparing simulated and observed CO concentrations is presented in Appendix B.

Summary of Model Performance

The EPA recommended values for acceptable model performance (EPA, 1991) are: normalized bias within ± 15 percent, normalized gross error less than 35 percent, and unpaired accuracy of the peak within ± 20 percent. Consequently, in nearly all cases model performance for the 23–25 October 1992 episode does not meet EPA's statistical criteria (c.f., Table 3-1). The magnitude of the daily simulated maximum concentrations are significantly lower than those observed, and the peak simulated concentrations are not well spatially collocated with the observed peak concentrations. The simulation of the temporal dynamics of ozone evolution, while qualitatively capturing the expected diurnal behavior, overestimates the removal of ozone in the evening.

31 AUGUST–2 SEPTEMBER 1993

Statistical Analysis

The performance statistics for the base-case (or initial) simulation of this episode are summarized in Table 3-2. The performance statistics are presented for three regions of the modeling domain: (1) the full domain, interpolated to a 4 km grid spacing by incorporating the Houston/Beaumont/Port Arthur 4 km interior domain, (2) the Houston/Galveston 2 km subdomain (HG), and (3) the Beaumont/Port Arthur 2 km subdomain (BPA).

The unpaired accuracy of the peak for the three episode days and for each of the subdomains provides a direct measure of the accuracy of the simulated peak, irrespective of temporal or spatial restriction. For 31 August and 1 September peak concentrations are overestimated in both the HG and BPA areas. The unpaired accuracy of the peak is significantly higher for the BPA subdomain (46.5% and 28.5%, respectively) than for the HG subdomain (28.5% and 9.8%, respectively). This is in contrast to the last day of the episode, for which the peak in the Beaumont region is well simulated (−0.4%), while the Houston area maximum is again overestimated (23.3%). It should also be noted that the differences in values of the simulated maximum concentration in the Houston subdomain over those for the full domain on 1 and 2 September are only in part attributable to the higher grid resolution employed by the UAM-V for this subregion *(vide supra)*.

The average accuracy of the peak compares the simulated and observed peak ozone concentrations for each air quality monitoring site, irrespective of timing. For the first day of the episode in the Houston area, the average accuracy of the peak shows that the peak concentrations are on average slightly underestimated (−7.7%), while in the Beaumont/Port Arthur region, the peak concentrations are overestimated (25.4%). For 1 September, the site-specific peak ozone concentrations are overestimated for the two

subdomains, as well as for the entire domain. The overestimation in the Houston subregion (42.4%) is significantly worse than that in the Beaumont/Port Arthur domain (10.0%). For the final day of the episode, the site specific peaks are slightly underestimated throughout the modeling domain.

These two criteria indicate that the Houston area peak ozone concentrations are well simulated for 31 August and 2 September, but are significantly overestimated on 1 September. The Beaumont/Port Arthur area peak concentrations are overestimated on the first day of the episode, but are well represented by the simulated peaks for the subsequent days.

This comparison can be coupled with an analysis of the normalized bias and the normalized gross error, which compare model performance on a site specific and time-resolved basis. A smaller absolute value of the normalized bias than the normalized gross error indicates that there is a distribution of both over- and under-estimated values at some sites for some times. If the absolute magnitudes of these two values are nearly equal, and both are positive, then the observed values are uniformly overestimated. On the other hand, if the absolute magnitudes are nearly equal but the normalized bias is negative, then the observed values are uniformly underestimated. Consequently, these two measures for 31 August indicate that, for values above the cutoff concentration of 60 ppb, all site-specific values are underestimated in the HG subdomain (normalized bias of −40.4%, but normalized gross error or 40.4%), and overestimated in the BPA subdomain (normalized bias and normalized gross error of 29.6%). The normalized bias (HG: 34.8%, BPA: 8.3%) and normalized gross error (HG: 47.3%, BPA: 16.1%) for 1 September show that there is a preponderance of overestimation at the sites, but there is some underestimation. Finally, for 2 September, the Houston area is predominately underestimated (normalized bias of −12.7% and normalized gross error of 21.3%), while the distribution of over- and under-estimation among the sites on an hourly basis for the Beaumont/Port Arthur region is nearly even (normalized bias of 0.6% and normalized gross error of 16.9%).

For the full domain, the normalized gross error for the first two days (36.1% and 37.7%, respectively), normalized bias for the second day (26.8%), and the unpaired accuracy of the peak for the first day (27.8%) are outside the EPA recommended guidelines for acceptable model performance. Details of this comparison are provided through examination of spatial and temporal characteristics of the simulated ozone concentrations.

Analysis of Domain-Wide Simulated Concentration Patterns

Figures 3-23 through 3-25 compare simulated and observed peak maximum ozone concentrations for the full modeling domain at 16 km grid resolution, for the three modeling days, respectively. Similarly, Figures 3-26 through 3-28 provide the same information for the HG subdomain, while Figures 3-29 through 3-31 show the BPA subdomain.

Figure 3-23 shows that for the full domain, the simulated maximum of 123 ppb occurs to the northeast of Houston; this is consistent with the observed ozone concentration

patterns. The simulated maximum for 1 September for the full domain (Figure 3-24) occurs over the Gulf (along the eastern boundary), in an extension of the Beaumont/Port Arthur area plume to the southeast. Simulated ozone concentrations for both days in outlying areas of the domain range from 50 to 70 ppb. The simulated maximum for the final day (Figure 3-25) again occurs near Houston, while the observed maximum is located in Beaumont. Area-wide maximum concentrations show a gradient from 50 ppb in the southwest portion of the domain to 100 ppb in the northeast portion of the domain. This gradient reproduces the distribution of maximum observed ozone concentrations.

The HG subdomain has a simulated maximum ozone concentration of 123 ppb in the northeastern corner of the domain on 31 August (Figure 3-26); area-wide simulated ozone concentrations range from 50-70 ppb to the southwest (upwind) of Houston, and from 90-100 ppb range to the northeast (downwind) of Houston. The simulated concentration patterns for 1 and 2 September (Figures 3-27 and 3-28) are generally consistent with the observations. For these days, the simulated maximum concentrations are located to the northeast of the observed maximum concentrations by approximately 17 and 28 km, respectively. However, maximum ozone concentrations in the Houston urban area are significantly overestimated.

The BPA subdomain for 31 August (Figure 3-29) has a 123 ppb simulated ozone maximum nearly collocated with the observed maximum. Domain wide simulated concentrations are low (60 ppb) to the south and high (100 ppb) to the north of Beaumont. This captures the southwest-to-northeast gradient in the observed peaks. For 1 September, the simulated (152 ppb) and observed (118 ppb) maximum ozone concentrations in this subdomain (Figure 3-30) are laterally offset from one another. However, the simulated maximum concentrations in the locale of the observation sites are generally within 20 ppb of the observed values. Area wide maximum simulated ozone concentrations are generally higher than observed. The magnitudes of the simulated and observed maximum ozone concentrations for the final day of the episode in the BPA subdomain (Figure 3-31) agree well, although they are not collocated. Relative to the observation, the high simulated concentrations are shifted to the northeast.

Analysis of Site-Specific Simulated Concentrations

Scatter plots for the simulated and observed ozone concentrations for each air quality monitoring site and each hour of the day are presented in Figures 3-32 through 3-34 for the three episode days, respectively. These plots compare the observed ozone concentration with the concentration simulated at the monitor site. The y=x line represents where the data points would fall if there were a perfect correlation between observed and simulated site-specific ozone concentrations. The scatter plot for 31 August (Figure 3-32) shows a systematic overestimation of small magnitude. The magnitude of this overestimation increases on 1 September (Figure 3-33) for all concentrations. The last day of the episode shows much better clustering of the observed and simulated data (Figure 3-34), with only a slightly higher preponderance of overpredictions among the lower observed concentrations.

Time-series plots illustrating the site specific evaluation of the temporal evolution of observed and simulated ozone concentrations for monitoring sites throughout the modeling domain are shown in Figure 3-35. In these plots, the solid line represents a distance-weighted interpolation of the simulated values in the four grid cells surrounding the monitoring site. The dashed lines represent the highest and lowest values in the nine grid cells surrounding the monitoring site. The shaded area, therefore, represents the range of simulated ozone concentrations within one grid cell of the monitoring site. The qualitative diurnal profile of ozone evolution is well represented at a majority of the sites, with the exception of HMCA, HLAA, HCQA, HCFA, and HWAA, where the presence of a nighttime simulated secondary peak each day is not supported by the data. As these sites are all collocated within a 15 km radius in Houston, it is likely that the same phenomena (e.g., recirculation of pollutants back into the Houston area or a feature of the emission inventory) give rise to the discrepancy in each case. Ozone concentrations for two other sites (KTZA and S42S) are not well simulated for the first two days of the episode. For the majority of the remaining data, the discrepancy between observations and simulated results falls into two categories: 1) quantitative disagreement, e.g., overprediction of the magnitude of the maximum ozone concentration on 1 September, and 2) improper simulation of ozone titration events.

The NO_x induced mid day titration of ozone on 31 August, discussed in the air quality data analysis performed as part of this modeling study, is poorly captured at a number of sites (e.g., BMTC, GALC, CRSC, H07H, H04H, H03H, H01H, HLAA, and S43S), and elucidates a possible deficiency in the emissions inventory of ozone titrants. As is evidenced in Figures 3-36 through 3-41, simulation of NO is quite good (Figures 3-36 through 3-38) while NO_2 is somewhat overestimated (Figures 3-39 through 3-41). A detailed analysis of the temporal evolution of these precursors is recommended in order to understand the relative dominance of NO_x or VOC limiting processes on ozone production. Time-series plots of simulated and observed concentrations of NO and NO_2 are presented in Appendix B.

Figures 3-42 through 3-44 show scatter plots of simulated and observed CO concentrations for the three episode days. High observed concentrations are generally underestimated, while low observed concentrations are slightly overestimated for the first two days. For 2 September, CO concentrations are generally simulated well, although most of the high observed concentrations are underestimated. Time-series plot of simulated and observed CO concentrations is presented in Appendix B.

Summary of Model Performance

While the performance statistics for this episode are not outside the EPA recommended ranges by as wide a margin as those for the 1992 episode, the simulation shows a preponderance of overpredictions, particularly on 1 September. The last day of the episode is well within EPA recommended simulation guidelines on all criteria, while the first episode day has mixed results, as described above. The maxima for all days are overestimated. The primary systemic inaccuracy is an overestimation of the magnitude of the maximum ozone concentration at each monitoring site on 1 September. Features of the simulation, such as NO_x titration of ozone, are discussed above, and specific emissions inventory concerns raised by this discussion should be examined. The

sensitivity of the simulation to changes in meteorological inputs was examined in Section 2.

TABLE 3-1. Initial simulation performance statistics for the October 1992 episode.

	23 October 1992			24 October 1992			25 October 1992		
	Full Domain[a]	Houston[b]	Beaumont/ Port Arthur[b]	Full Domain[a]	Houston[b]	Beaumont/ Port Arthur[b]	Full Domain[a]	Houston[b]	Beaumont/ Port Arthur[b]
Observed Maximum (ppb)	112	108	112	198	198	112	157	157	137
Simulated Maximum (ppb)	85	84	75	107	107	110	98	101	106
Unpaired Accuracy of the Peak (%)	−23.7	−22.1	32.6	−45.8	−45.7	2.0	−37.7	−35.5	−22.7
Average Accuracy of the Peak (%)	−47.6	−62.2	−40.9	−27.8	−37.6	−30.3	−23.0	−31.8	−29.8
Normalized Bias (%)	−51.1	−65.3	−48.5	−41.5	−51.4	−41.0	−32.1	−42.7	−33.8
Normalized Gross Error (%)	51.6	65.3	48.5	42.4	51.7	41.0	35.9	43.9	35.7

[a] 4 km grid resolution
[b] 2 km grid resolution

95067.31

TABLE 3-2. Initial simulation performance statistics for the August-September 1993 episode.

	31 August 1993			1 September 1993			2 September 1993		
	Full Domain[a]	Houston[b]	Beaumont/ Port Arthur[b]	Full Domain[a]	Houston[b]	Beaumont/ Port Arthur[b]	Full Domain[a]	Houston[b]	Beaumont/ Port Arthur[b]
Observed Maximum (ppb)	96	96	84	164	164	118	139	115	139
Simulated Maximum (ppb)	123	123	123	166	180	152	139	142	139
Unpaired Accuracy of the Peak (%)	27.8	28.5	46.5	1.4	9.8	28.5	0.3	23.3	−0.4
Average Accuracy of the Peak (%)	2.0	−7.7	25.4	31.3	42.4	10.0	−6.9	−8.6	−5.8
Normalized Bias (%)	−6.4	−40.4	29.6	26.8	34.8	8.3	−2.7	−12.4	0.6
Normalized Gross Error (%)	36.1	40.4	29.6	37.7	47.3	16.1	16.9	21.3	16.9

[a] 4 km grid resolution
[b] 2 km grid resolution

95067.31

4 SUMMARY AND RECOMMENDATIONS

Application of the variable-grid Urban Airshed Model (UAM-V) to the southeast Texas area included: (1) preparation of meteorological and air-quality inputs for UAM-V (emissions and land-use inputs were provided by the TNRCC); (2) application of the modeling system to the simulation of the 23–25 October 1992 and 31 August–2 September 1993 ozone episode periods; (3) a limited diagnostic and sensitivity analysis to examine the effects of uncertainty in the model inputs on the UAM-V simulation results; and (4) the evaluation of model performance for the episodes through comparison of the simulated pollutant concentrations with observed data.

The primary objective of this model application study was to provide the TNRCC with base-case modeling inputs for the two historical ozone episodes. The diagnostic analysis was limited by schedule and resource constraints. Thus, while a reasonable base-case simulation was achieved for the 31 August–2 September 1993 episode, acceptable model performance was not obtained for the 23–25 October 1992 episode.

Model performance for 31 August–2 September 1993 is characterized by good agreement between the simulated and observed ozone concentrations for the first and last days of the episode; simulated ozone concentrations for the middle day (1 September) are higher than observed, especially within the Houston/Galveston (HG) area. Transport of ozone (and precursor pollutants) from the HG area to the Beaumont/Port Arthur (BPA) area during the simulation period is indicated by the simulation. Agreement between the simulated and observed concentrations within the BPA area is especially good for 2 September. Model performance with respect to oxides of nitrogen (NO_x) is also reasonable; the timing and magnitude of the observed concentrations are generally represented in the simulation. Sensitivity simulations performed for this episode examined the effects of horizontal resolution, use of the P-i-G treatment for NO_x emissions from elevated point sources, and uncertainty in the meteorological inputs. Use of a high (2 km) resolution grid over the HG and BPA areas was beneficial with respect to model performance while the application of the P-i-G treatment had little effect on the ability of the model to reproduce the surface-level ozone concentrations. The sensitivity analysis also indicated that assimilation of surface temperature and moisture data in preparing the meteorological inputs was beneficial for this episode.

Simulated ozone concentrations for the 23–25 October 1992 episode period are significantly lower than observed in both the HG and BPA areas. Diagnostic/sensitivity simulations performed for this episode indicate some sensitivity of the simulated ozone concentrations to specification of the vertical exchange coefficients (simulated ozone concentrations increase when the effective mixing height is reduced) and greater sensitivity to the specification of biogenic hydrocarbon emissions (doubling of these emissions resulted in higher ozone concentrations throughout the domain and improved model performance).

Given the differences in model performance for the two episodes, a detailed comparison of the inputs for the two episodes in terms of characteristics (e.g., emissions totals, timing and extent of the land-/gulf-breeze circulation) as well as quality (e.g., representativeness and quantity of data; ability of the inputs to represent, given the limitations of the data and input preparation methodologies, the relevant features of the historical ozone episodes) might be used to further identify the causes of the model performance deficiencies. Additional analyses to assess and quantify the effects of uncertainty and further evaluate the modeling system for use in future control-strategy evaluation might include:

- An assessment of the effects of the boundary condition specification (in particular, use of the EPA-recommended default boundary condition concentrations for the October episode, given the seasonal differences between this and most episodes for which the EPA guidance was developed);

- Additional evaluation of the meteorological inputs for the October episode. (As noted earlier in this report, assimilation of wind profiler data for the Houston area monitoring site contributed to high wind speeds aloft and possibly to the low simulated ozone concentrations for this episode. Additional quality assurance of these data is warranted);

- Further evaluation of the magnitude and spatial and temporal distribution of the emission inventory components including a comparison (on a per capita basis) with emissions for other similar urban areas and an examination of the VOC-to-NO_x ratio with respect to data collected during the 1992 and 1993 field programs;

- Use of UAM-V process analysis to further evaluate the inputs and examine in more detail certain features of the simulations; and

- Additional sensitivity testing of the model features (e.g., whether the use of the P-i-G treatment affects the response of the model to emission reductions).

REFERENCES

EPA. 1991. *Guideline for Regulatory Application of the Urban Airshed Model.* U.S. Environmental Protection Agency (EPA-450/4-91-013).

Lolk, N. K., Z. Guo, H. P. Deuel, J. L. Haney, and S. G. Douglas. 1995. "Application of UAM-V for the Houston/Galveston and Beaumont/Port Arthur Nonattainment Areas for Two Multi-Day Ozone Episode." Systems Applications International, San Rafael, California (SYSAPP-95/054).